Geochemical study of xenoliths from the Navajo Volcanic Field; Arizona, New Mexico, and Utah

by

Patrick D. Mattie

A Thesis Submitted in Partial Fulfillment of the Requirements for
Master of Science in Geochemistry
November, 1996

New Mexico Institute of Mining and Technology
Socorro, New Mexico, USA

Abstract

The Navajo Volcanic Field offers a unique area to study mafic xenoliths due to an abundance of dikes and diatremes with associated crustal xenoliths. Mafic xenoliths in kimberlite pipes and minette diatremes in the Navajo Volcanic Field are of four lithologic types, in order of decreasing abundance: garnet granulite, amphibolite, pyroxene granulite, and gabbro. Mafic xenoliths from 3 kimberlites and 3 minettes define eight geochemical groups, of which Groups I and III occur only in Moses Rock dike (gabbros) and Red Mesa pipe (amphibolites), respectively. With these two exceptions, there is no correlation of chemical groups with xenolith or host-rock lithology, geographic location, or degree of xenolith alteration or metamorphism.

Group I (n=8) with high Mg numbers (0.7-0.8) and high CaO/TiO2(20-60) and low TiO2 (<0.5wt%), shows only slight chondrite-normalized LREE enrichment, and a strong subduction zone component (SZC) (depletion in Nb and Ta relative to neighboring incompatible elements) and positive Sr, Ba, Eu, and K (SBEK) anomalies on primitive mantle normalized spidergrams. Group II (n=5) with intermediate CaO/TiO2 (10-20) and TiO2 (0.5-0.9 wt%) has flat to LREE depleted patterns, a SZC and SBEK anomalies. Group III (n=3) with very high CaO/TiO2 (40-60) and low TiO2 (< 0.5 wt%) has nearly flat REE patterns, a very prominent SZC and large SBEK anomalies. Group IV (n=5) with low CaO/TiO2 (<8) and variable TiO2 (1 -1.7 wt%) shows significant LREE enrichment (100 x chondrites), a variable SZC, and small or absent SBEK anomalies. Group V (n=2) with CaO/TiO2 =10-20 and Ti =0.5-0.7 wt%, shows flat to slightly LREE-enriched patterns, a small SZC, and small SBEK anomalies. Group VI (n=2) with CaO/TiO2=10%and TiO2 =0.7-1.1wt% shows flat to slightly LREE depleted patterns (10x chondrite) and variable Ta-Nb depletion. Group VII has CaO/TiO2=5-10 and TiO2=0.6-1.5 with LREE enriched (30-80x Chondrite) patterns and small to no Ta-Nb depletion. Group VII has abundances of CaO/TiO2 > 40 and TiO2< 0.3 wt %, with a

depletion of middle REE and strong positive Eu anomalies on chondrite normalized REE plot, and a Ta-Nb depletion.

Rapid variation in compatible elements within each group and the common SBEK anomalies favor a cumulus origin for most or all of the mafic xenoliths. Incompatible element distributions (SZC, high Th/Ta and Th/Yb) suggest the igneous protoliths came from a variably enriched mantle wedge, for which Nd and Sr isotope data (Wendlandt, et al., 1993 & 1996) suggest an Early Proterozoic age. Similarity of incompatible element distributions in the xenoliths and in exposed Early Proterozoic mafic rocks in the Southwest support this interpretation. There is no evidence in the xenolith population for post-Proterozoic mafic crustal underplating. These observations are consistant with a continental lower crust that formed by a complex process within a heterogeneously enriched mantle wedge within a subduction environment.

Acknowledgments

I would like to give my thanks to everyone that helped me through this project. This includes my family most especially who through their support and unshakable faith never allowed me to doubt that I would finish. I would also like to thank the graduate students at New Mexico Tech, whose diversity was almost as great as their camaraderie. Special thanks to Jeff Klein who helped me forget about my thesis. For assistance in the field thanks to Steve Semkin and W.R. Van Schmus. For assistance in the office I thank the New Mexico Tech Argon Lab, especially Rich Esser, Matt Hielzer, and Bill McIntosh. Warm thanks to Patci Mills and Connie Apache in the E&ES Department office for execptional help with unyielding bureaucratic paperwork. Particular appreciation goes to my committee Jane Selverstone and Philip Kyle, both of whom were indispensable. Finally, my sincere gratitude to my advisor Kent C. Condie who showed me much more of the Southwest that I could have ever imagined. This project could not have been accomplished without the cooperation of the Navajo Nation and funding by NSF Grant #EAR-9316406 to Kent Condie. The XRF lab at New Mexico Tech was partially funded by NSF Grant EAR-9316467.

Table of Contents

List of Figures

List of Tables

This thesis is accepted on behalf of the faculty
of the Institute by the following committee:

Advisor

November 18, 1996

Date

I release this document to the New Mexico Institute of Mining and Technology.

Student's Signature

11/18/96

Date

CHAPTER 1: INTRODUCTION

Many mafic xenoliths have mineral assemblages and textures consistent with amphibolite to granulite grade metamorphism. It has been argued that mafic granulite and amphibolite facies xenoliths are likely to have crystallized at pressures and temperatures found in the lower crust (Ehrenberg and Griffin, 1979; Broadhurst, 1986; Rundick, 1992). Xenoliths thus provide a means to sample a cross section of an otherwise inaccessible region of the earth's crust. Although the nature of such a process creates some difficulties in deciphering stratigraphic relationships, knowledge of the composition and age of such a mafic lower crust is important in enhancing our understanding of both the origin and growth of the continental crust.

The Navajo Volcanic Field (NVF) in the Four Corners Area contains abundant xenolith-bearing volcanic necks and kimberlite dikes which provide ideal locations for the collection of xenoliths. With cooperation from the Navajo Nation, a suite of over 250 xenolith samples have been collected from six localities including Shiprock, Mitten Rock, The Thumb, Red Mesa Dike, Moses Rock Dike, and Garnet Ridge Dike. Of these, eighty-eight xenoliths were selected for the purposes of this study.

1.1 Xenoliths and the Lower Crust

Traditionally, the continental crust has been separated into two chemically different parts: the granodioritic upper crust and a mafic lower crust. The upper crust reaches to about 10 km in depth. The lower crust comprises about 10-30 km in depth or about 75% of the total crust (Taylor and McClennan, 1985). Yet, the lower crust is most poorly known. It is generally accepted that the continental crust is intermediate (andesitic) in composition (Taylor and McClennan, 1985). Estimates of the composition of the upper continental crust are based largely on a variety of approaches including sampling of Precambrian shields, weighted chemical compositions of stratigraphic sections, crustal xenolith populations, and bulk chemical compositions of

terrigenous sediments (Condie, 1993). However, to calculate the composition of the lower crust, xenoliths and exposed sections of the deep crust are the only means available. Exposed sections of the deep crust are a direct way to sample a cross-section of the lower crust. But, they are rare, usually occurring only in continental collisonal belts (Rudnick and Taylor, 1987; Rudnick, 1992; Kay et al., 1992; Percival et al., 1992). Also, it is unclear whether or not they are chemically undisturbed by the deformation and metamorphism accompanying uplift of these deep sections of continental crust (Rudnick, 1992). Crustal xenoliths on the other hand, are common in many alkaline basalts and kimberlites. Xenoliths are entrained within a host magma as it ascends rapidly through the crust to the surface. They usually remain undisturbed chemically and mineralogically by this entrainment in the host magma and as the magma cools the xenolith is sealed in a protective shell that adds to the preservation potential of the xenolith. Ultramafic xenoliths have been studied for years and much of what we know about the Earth's upper mantle comes from ultramafic xenolith research. It is now being recognized that mafic xenoliths are the most feasible method for sampling the lower crust.

1.2 Crustal History of the Southwestern U.S.

Studies of the crust in the southwestern U.S. suggest that it is comprised of accreted terranes that have been added during the early and middle Proterozoic (Condie, 1992; Karlstrom and Bowring, 1988). Four crustal provinces are recognized in the Proterozoic of southwestern U.S., of which two (Yavapai and Mazatzal) may be included within the Colorado Plateau (Condie, 1992; Karlstrom and Bowring, 1988). The terranes that comprise these crustal provinces include mainly rocks with geochemical affinities to modern oceanic arcs (Condie, 1992).

1.3 Purpose

The parental material for the mafic xenoliths may have formed in several ways, including magmatic underplating, partial melting of the lower crust, or intrusive

events in the lower or middle portions of the crust. In this study, a detailed major and trace element investigation of the mafic xenoliths was conducted by X-ray fluorescence (XRF) and instrumental neutron activation analysis (INAA) and by petrographic methods. Results from this study will be combined with P-T data obtained from mineral equilibria studies by electron microprobe conducted at the University of New Mexico by Dr. Jane Selverstone. The combined results will provide data that will be used to study the origin of the xenolith suite as well as shed light on the stratigraphic relationships among the different xenolith types. With help from rare earth element (REE) data, it should be possible to look back through the metamorphic alteration occurring in the lower crust to provide information on the source of the xenoliths. Many questions are associated with the formation of continental crust including the role of underplating in the lower crust and delamination of lower mafic material during continental arc collisions. From the results of this study, we should be able to understand better the evolution of the continental crust in this region as well as shed light on the problem of how oceanic arcs are made into continental crust.

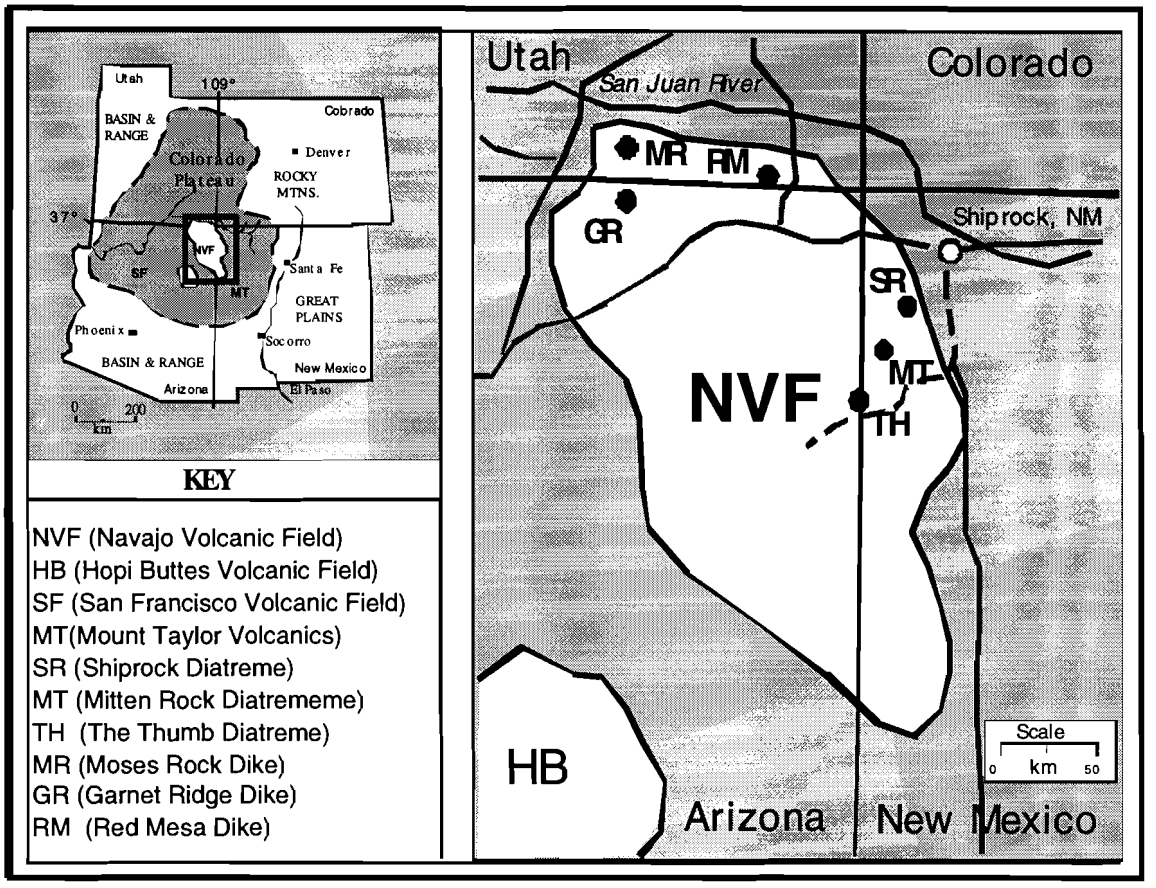

Fig. 1.1. Location Map for the Navajo Volcanic Field and xenolith hosts.

Fig. 1.2. Picture of the Shiprock Diatreme. Located near Shiprock, NM. (Picture taken facing northeast). Note the distinctive minette morphology.

1.3 Geology of the Four Corners Area

The Four Corners area lies at the junction between the states of Arizona, Colorado, New Mexico and Utah and covers the southern edge of the Colorado Plateau (fig 1.1). The Colorado Plateau is bounded by the Rocky Mountains to the north and east, the Basin and Range province to the west and south, and the Rio Grande Rift to the east. The Colorado Plateau is a stable platform with an average crustal thickness of 35-45 km and contains numerous north to northeast-trending monoclines of Laramide age (Woodward, 1973; McGetchin, et al. 1977; Laughlin et al., 1986 Laughlin and Charles, 1992). Significant geologic features in the southern Colorado Plateau province include the Navajo, Hopi, San Francisco, and Mt. Taylor volcanic fields, the Monument Uplift, the Comb Ridge monocline and the Grand Canyon Basin. This diversity in surfacial geologic features, as Gregory (1917) attests in the first detailed study of the Four Corners area geology, masks the relative uniform Paleozoic and Mesozoic sedimentary strata that covers most of the area. These strata include formations that can be traced throughout most of the region (Haynes et al., 1972; O'Sullivan and Beikman, 1963; Baars,1973; O'Sullivan and Green, 1973; O'Sullivan and Craig, 1973; Young, 1973; Northrop, 1973; Gregory, 1917).

The Navajo Volcanic Field

The Navajo volcanic field, located in the Four Corners area, consists of numerous mid-Tertiary minette and kimberlitic dikes and volcanic necks(fig 1.1) (Haynes et al., 1972; O'Sullivan and Beikman, 1963; Williams, 1936; Laughlin and Charles, 1992). Volcanism, dike, and sill emplacement in the Navajo volcanic field occurred at 28-19 Ma based on K-Ar dates from phlogopites in minettes and fission track dating of apatite and zircon (Laughlin and Charles, 1992; Laughlin, et al 1986; Naeser, 1971). Although many of the diatremes in the volcanic field have been described as kimberlites (Naeser, 1971; McGetchin and Silver, 1972; McGetchin, et al., 1973; McGetchin, et al, 1977; and Laughlin, et al, 1986), Roden (1981) has reclassified these rocks as

serpentinized ultramafic breccias (SUM) based on chemical and mineralogical differences from classic kimberlites. For geological descriptions herein, the serpentinized ultramafic breccias are referred to as kimberlite. Abundant xenoliths are associated with the minette and kimberlite diatremes and include ultramafics, meta-volcanics, granitoids, medium to high grade metamorphic rocks, and unaltered sedimentary fragments of the Paleozoic and Mesozoic country rock (Ehrenberg and Griffin, 1979; McGetchin et al., 1977; McGetchin and Silver, 1972; Williams, 1936; Gregory, 1917).

Shiprock, Mitten Rock, and The Thumb

Shiprock, Mitten Rock and the Thumb are diatremes situated between the San Juan Basin to the east and the Red Rock monocline to the west (figs 1.1,1.2, &1.3) (Delaney, 1987; Delaney and Pollard, 1981; O'Sullivan and Beikman, 1963; Williams, 1936).

The Shiprock diatreme crops out in the Mancos Shale on the Four Corners platform which is underlain by Paleozoic and Mesozoic sedimentary strata 1,000 m thick (Delaney, 1987; Delaney and Pollard, 1981). Shiprock is composed of minette and minette-tuff breccia, emplaced ~31 Ma during mid-Tertiary volcanic activity (Semken, 1992; Laughlin et al., 1986; Naeser, 1971; Williams, 1936; Gregory, 1917). Granitoid and shallow sedimentary xenoliths are abundant at Shiprock. Some granitoid xenoliths were noted up to 1-2 m in size. Yet, despite the relative abundance of granitoid xenoliths, xenoliths of other rock types are scarce.

Mitten Rock diatreme is located approximately 13 km southwest of Shiprock along the eastern side of the Mitten Rock monocline (fig 1.3) (Naeser, 1971;O'Sullivan and Beikman, 1963; Williams, 1936). It is also ~31 Ma in age and is composed of felsic minette that crops out in the exposed Cretaceous Mancos Shale (Naeser, 1972; Williams, 1936). Xenoliths are abundant within the minette matrix that weathers to a vesicular rock (McGetchin et al.,1977). Overall the mafic xenoliths are predominant

with a lesser amount of granitoid xenoliths. The mafic xenoliths are small, averaging 4-10 cm in diameter. Xenoliths of other rock types are rare.

The Thumb diatreme is located along the eastern side of the Red Rock monocline approximately 20 km southeast of Shiprock and in line with Mitten Rock (fig 1.3)(McGetchin et al., 1977; O'Sullivan and Beikman, 1963; Williams, 1936). The Thumb crops out in the Jurassic Morrison Formation and is composed of a biotite-rich minette that is more magnesian than the typical minette of the Navajo Volcanic field (McGetchin et al., 1977; Williams, 1936). Xenoliths of all types are abundant and many ultramafic and high-pressure crustal xenoliths can be found (Erhenberg and Griffin, 1982; McGetchin et al., 1977; Williams, 1936). Sizes of xenoliths vary from 5-7 cm to >30 cm in diameter. On average, xenoliths are between 10-15 cm in size.

Red Mesa Diatreme

The Red Mesa dike is located 4 km northwest of Red Mesa and 1 km north of the Arizona-Utah state line (fig 1.4). The Red Mesa dike is a kimberlite (SUM) emplaced within the cross-bedded Navajo Sandstone (Haynes, et al., 1972). Extensive weathering has formed a large circular depression of approximately 75 m in diameter and left a large array of xenolith types in the depression. Many types of xenoliths occur in the Red Mesa dike including metasediments, granitoids, granulites, amphibolites, quartzites and even hydrocarbon-rich limestone from the Paradox Formation. On average the xenoliths vary from 2 cm to 30 cm in diameter, and no large granitoids occur at this location.

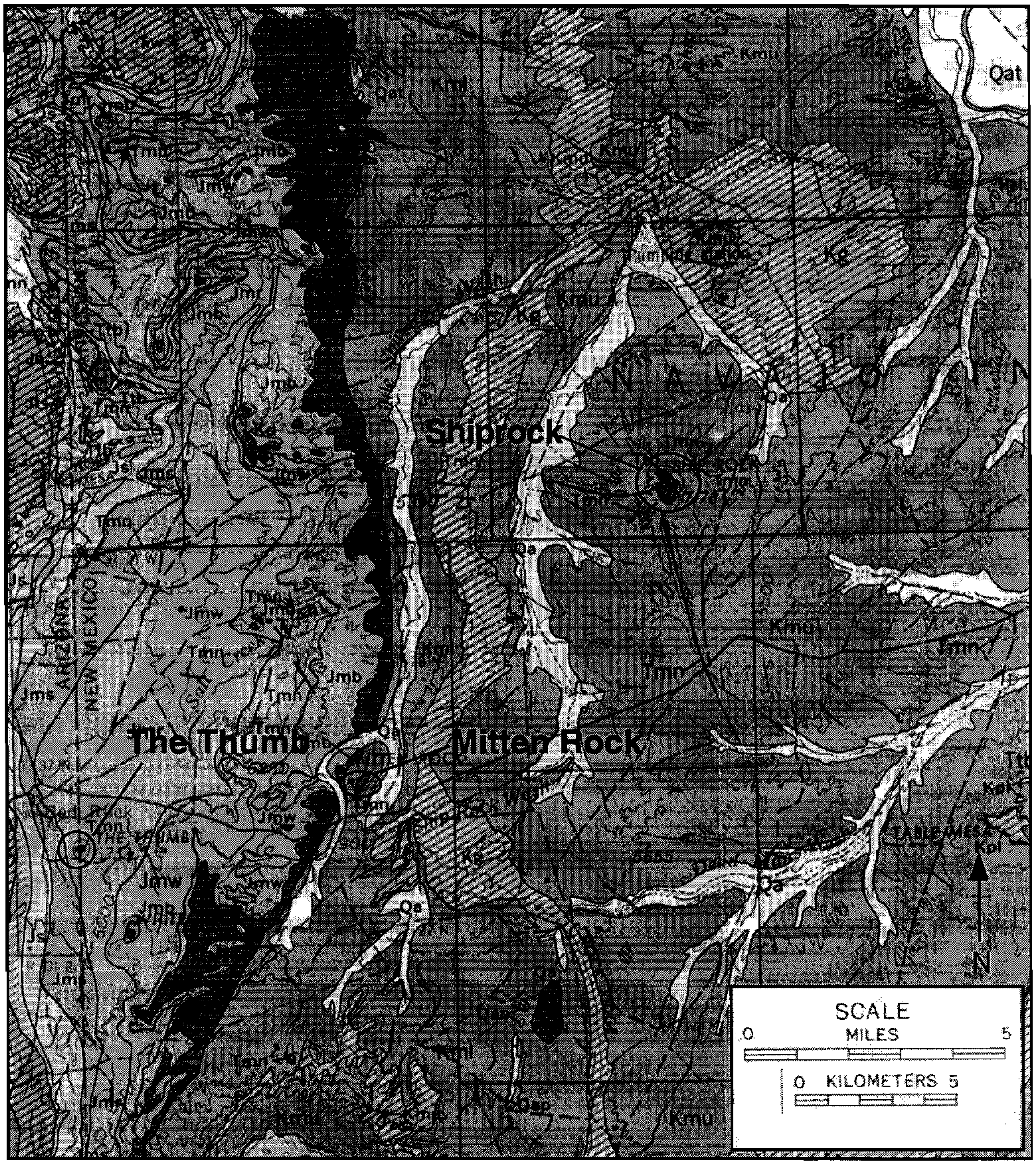

Fig. 1.2. Geologic Map of four corners area of New Mexico, Arizona, Utah, and Colorado. Located are minette dikes. (ref USGS Geologic Map I-345)

Garnet Ridge and Moses Rock

Garnet Ridge and Moses Rock dikes are kimberlitic (SUM) intrusive bodies located between the Monument uplift and Comb Ridge monocline (McGetchin, 1972; McGetchin et al., 1973). Moses Rock dike is crescent-shaped and is located 8 km southeast of Mexican Hat, Utah and approximately 3 km west of the Comb Ridge monocline (fig 1.4) (McGetchin et al., 1977; McGetchin et al., 1973; Haynes et al., 1972; McGetchin and Silver, 1972). The Comb Ridge monocline forms the eastern boundary of the Monument Uplift and has several kimberlitic dikes occurring in close proximity along the length of its axis. Moses Rock dike has been described as a kimberlite-bearing breccia-filled intrusion that crops out in the Permian Cutler Formation (McGetchin and Silver, 1972; McGetchin et al., 1973). Xenoliths of all types are abundant, including metasediments, granitoids, metagabbro, amphibolite, and eclogites (McGetchin et al., 1977; McGetchin and Silver, 1972). Xenoliths vary in size from 2 cm to >2 m; generally the mafic and ultramafic xenoliths occur as fragments 5 cm to 30 cm in diameter (McGetchin and Silver, 1972).

Garnet Ridge dike is located south of Moses Rock along the Comb Ridge monocline, approximately 8 km south of the Arizona-Utah state line and 12 km south west of Mexican Water, Arizona (fig 1.4) (O'Sullivan and Beikman, 1963). Garnet Ridge dike has been described as a kimberlite-bearing breccia-filled intrusion (SUM) occurring in the Jurassic age Summerville Formation (McGetchin et al., 1973; McGetchin and Silver, 1972; O'Sullivan and Biekman, 1963). Xenoliths include metasediments, granitoid, gabbro, amphibolite, and garnet granulites. The relative proportions of each xenolith type are similar to Moses Rock. Xenoliths vary in size from 2 cm to >2 m in diameter.

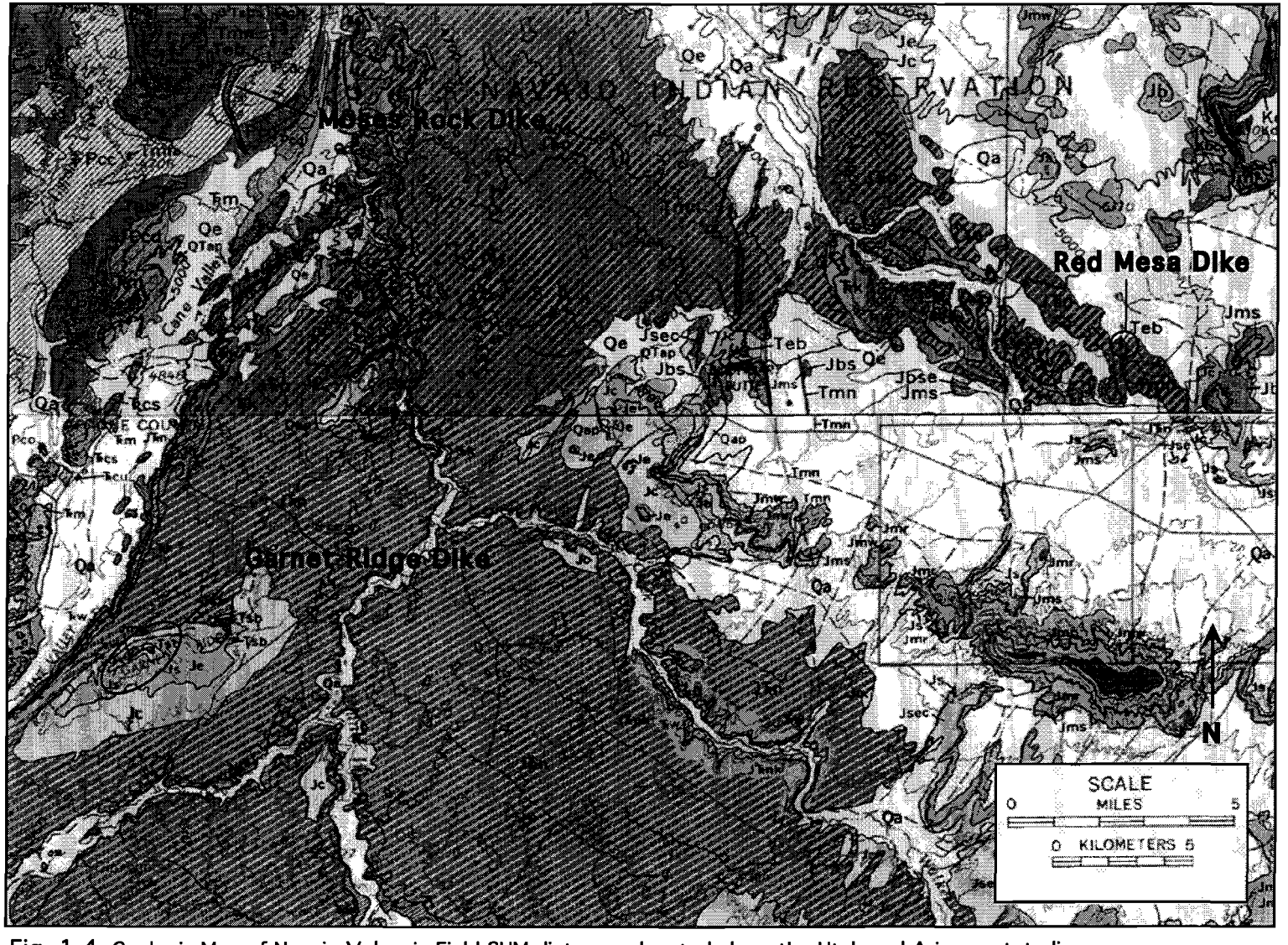

Fig. 1.4. Geologic Map of Navajo Volcanic Field SUM diatremes located along the Utah and Arizona state line. (ref. USGS Maps I-345 and I-629)

CHAPTER 2: THE CRUSTAL XENOLITH SUITE

2.1 Introduction

Over 250 xenoliths were collected from the Navajo Volcanic Field. The xenolith samples were divided in the field based on hand sample descriptions into five broad groups: 1) metasediments; 2) felsic granulites; 3) mafic granulites; 4) amphibolites; and 5) granitoids. Samples selected for this study include all of the samples orginally described as amphibolite and mafic granulite. A total of 73 samples were chosen for chemical analysis by X-ray fluorescence (XRF). All 73 samples were prepared for analysis as described in Appendix A.

2.2 Petrography

Fourty xenolith samples were examined in thin section. Criteria used for thin section selection included: 1) mineral assemblages useful for microprobe analysis; 2) representative distribution over primary geochemical populations; and 3) selection of anomalous geochemical samples for identification of trace mineralogy. The 73 xenolith samples can be divided into four broad groups based on hand sample and petrographic investigation of relic textures and modal estimates of the mineralogy: 1) garnet granulites; 2) pyroxene granulites; 3) amphibolites; and 4) gabbos. Brief petrographic descriptions for each of the groups are listed in Table II and detailed individual descriptions for the thin sectioned samples are listed in Appendix B.

Garnet Granulites

The garnet granulite xenoliths are the most abundant petrographic group of mafic xenoliths, comprising 22 of the 40 samples thin sectioned and 34 of the 73 total mafic xenolith samples. The primary mineralogy consists of garnet, clinopyroxene, plagioclase, ilmenite, ± amphibole ± orthopyroxene ± rutile (Fig. 2.1). Most of the granulite xenolith population has undergone some degree of alteration. Alteration minerals include clinozoisite, hornblende, muscovite, biotite, rutile, and ilmenite. Retrograde reactions are evidenced by very fine-grained material along grain boundaries and intragranular cracks in samples from the minette diatremes. Partial replacement of clinopyroxene and garnet by secondary hornblende and white mica, and complete alteration of plagioclase to clinozoisite or epidote are observed in most of the granulite samples from the kimberlite hosts. The garnet granulite group can be further divided into sub-groups based on differences in texture and primary mineralogy. These sub-groups are listed in Table 2.1 with a brief description of the distiguishing characteristics of each. These differences cannot be distinguished by hand sample alone, thus only the thin section samples are divided into sub-groups.

TABLE 2.1. Garnet Granulite Subgroups

Group	Sample	Major Minerals	Description
IA	RM56, RM53 MR44	gar+cpx+plag	large garnets, relic cpx, and secondary hbl common
IB	MR57, GR45	gar+cpx+hbl+plag	primary hbl; large garnets; epidote alteration
IC	MR60 TH46	gar+cpx+opx+plag	cpx-opx exsolution lamellae; coarse grained; no primary hbl; secondary amph replacing cpx; garnet fractures filled with white mica
ID	MR50, MR66 TH39	gar+cpx+plag	large garnets; no hbl; ± rutile; TH39 unaltered
IE	MR46	plag+cpx+opx+hbl + gar	biotite, rutile, ilmenite, present, not completely granoblastic
IF	GR11, GR13 GR21, MR45 MR52, RM47 RM60	gar+cpx+plag	garnet pseudomorphed by muscovite; hbl replacing cpx; white mica and clino-zoisite replacing plag.
IG	MT20, TH38 TH41	plag-cpx-gar	garnets are fragmented and altered to fine grained black material

*gar=garnet; plag=plagioclase;cpx=clinopyroxene; opx= orthopyroxene; hbl= hornblende

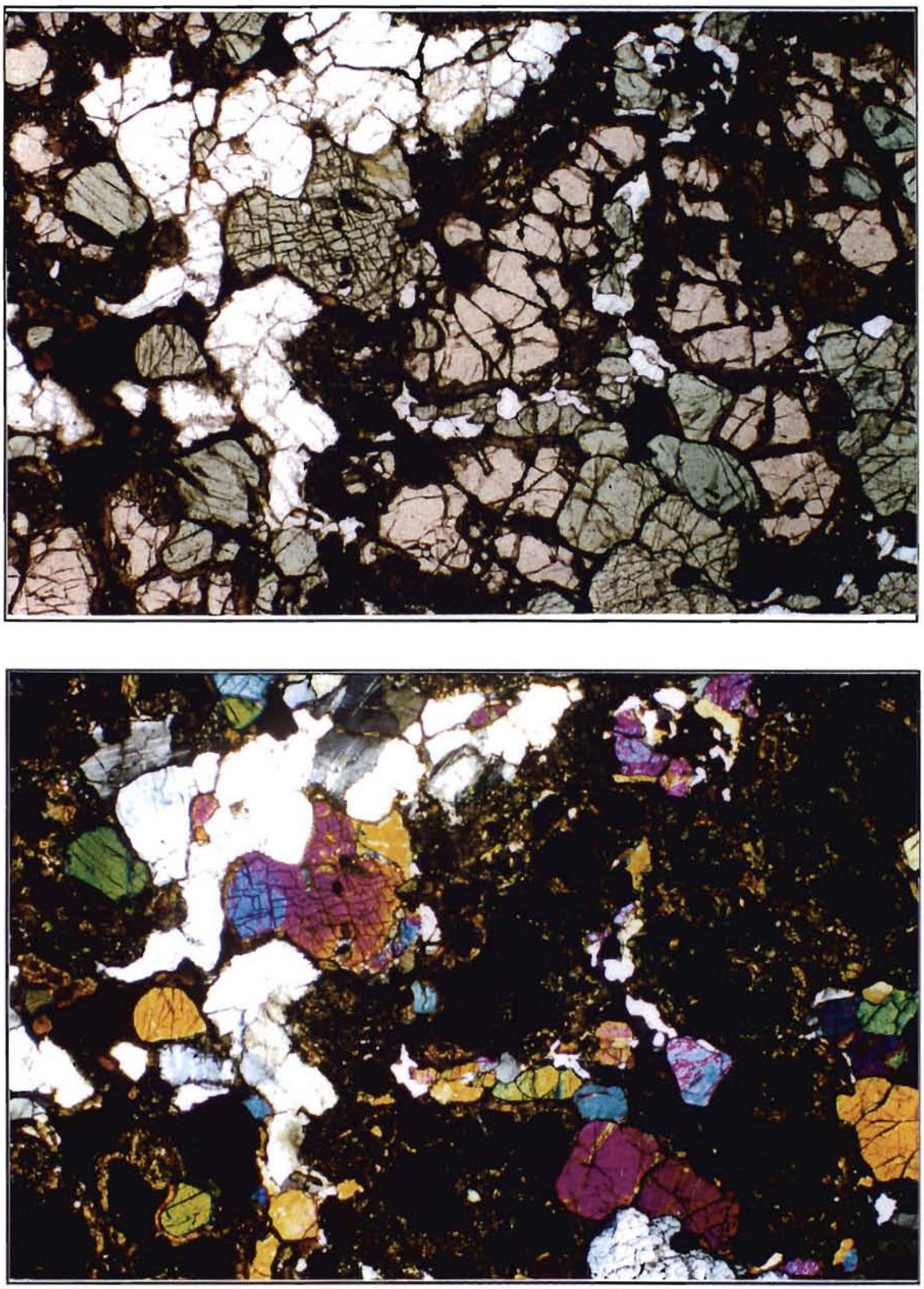

Fig. 2.1. Thin section Picture of Garnet Granulite (TH39) at 5x. Top: plane polarized light; bottom: crossed polarized light. Primary mineralogy: Garnet, clinopyroxene, plagioclase. Note: fine grained dark intergranular material.

Pyroxene Granulites

Pyroxene granulites are represented by 4 thin sectioned xenoliths and 10 of the 73 samples. The pyroxene granulites are characterized chiefly by plagioclase, clinopyroxene, and hornblende (Fig. 2.2). Alteration minerals include green amphibole, clinozoisite, biotite, and oxides. The pyroxene granulites have a medium-grained granoblastic texture. Replacement of clinopyroxene and hornblende by secondary green amphibole and biotite is observed in both the minette and kimberlite diatremes. Retrograde reactions are evidenced by very fine-grained material along grain boundaries and intragranular cracks in samples from minette diatremes.

Amphibolites

The amphibolites are represented by 7 thin sections and 20 of the 73 samples. The amphibolites have a primary mineralogy of hornblende and plagioclase ± clinopyroxene ± biotite (Fig. 2.3). Samples are commonly layered with the long axis of the hornblende lying within the foliation. Secondary alteration is evident in all of the samples. Most commonly, plagioclase is completely altered to clinozoisite and hornblende to biotite. Other alteration minerals include muscovite and ilmenite. No garnet was observed in any of the amphibolite samples although it has been found in amphibolites from Moses Rock and other areas in the NVF (Selverstone, unpublished data; Wendlandt, 1993; Smith et al., 1994; Broadhurst, 1986). A relic clinopyroxene occurs in TH34.
Sample RM62 is medium grained with not foliation of the hornblende grains creating a texture unlike the rest of the amphibolites. Due to the small population of amphibolites thin sectioned it was left in the same group, but may actually belong to a separate sub-group.

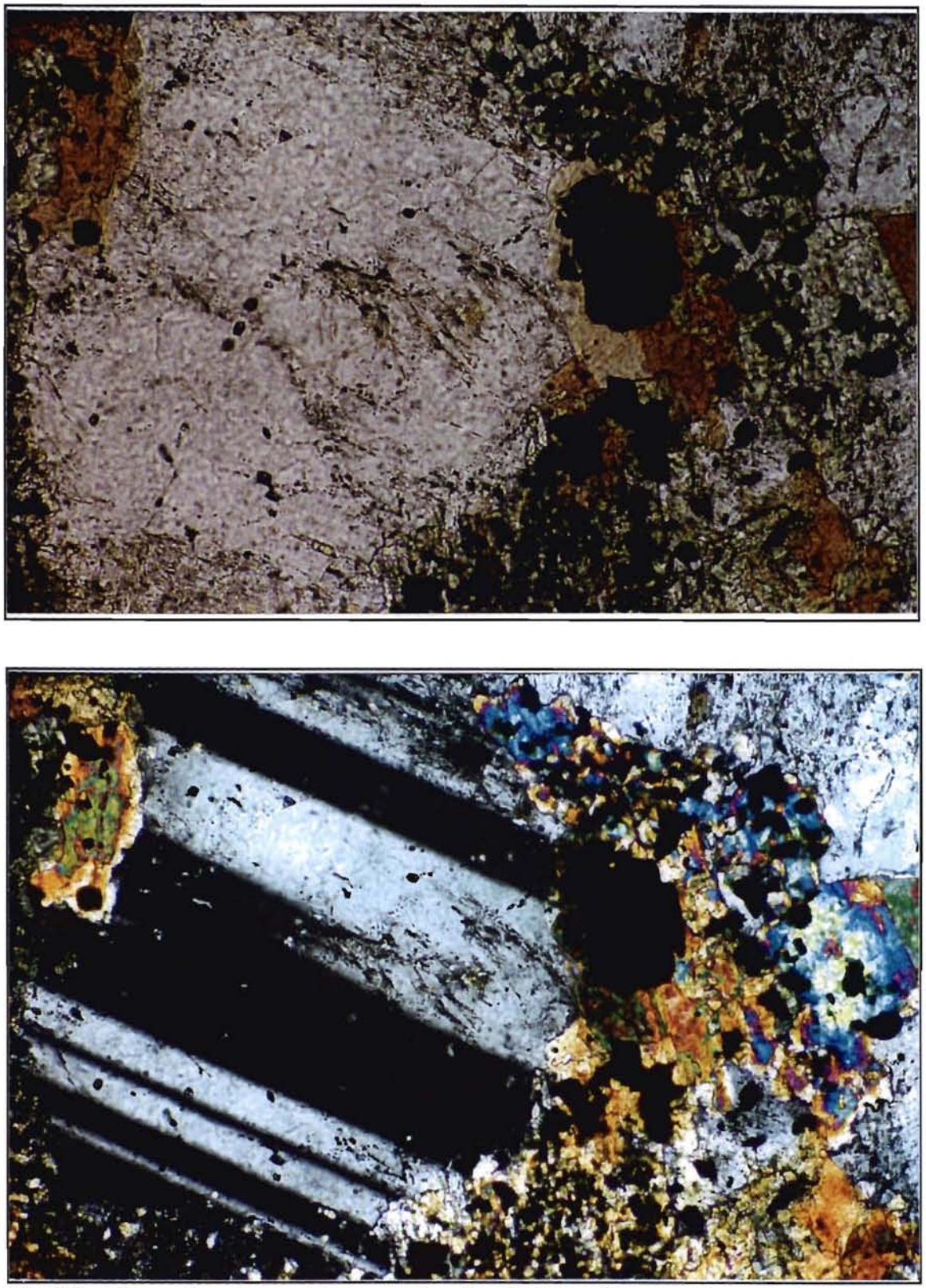

Fig. 2.2. Thin section picture of Pyroxene Granulite (MT14) at 20x. Top: plane polarized light; bottom: crossed polarized light. Primary mineralogy: clinopyroxene and plagioclase. Note: fine grained clinozoisite and epidote alteration material.

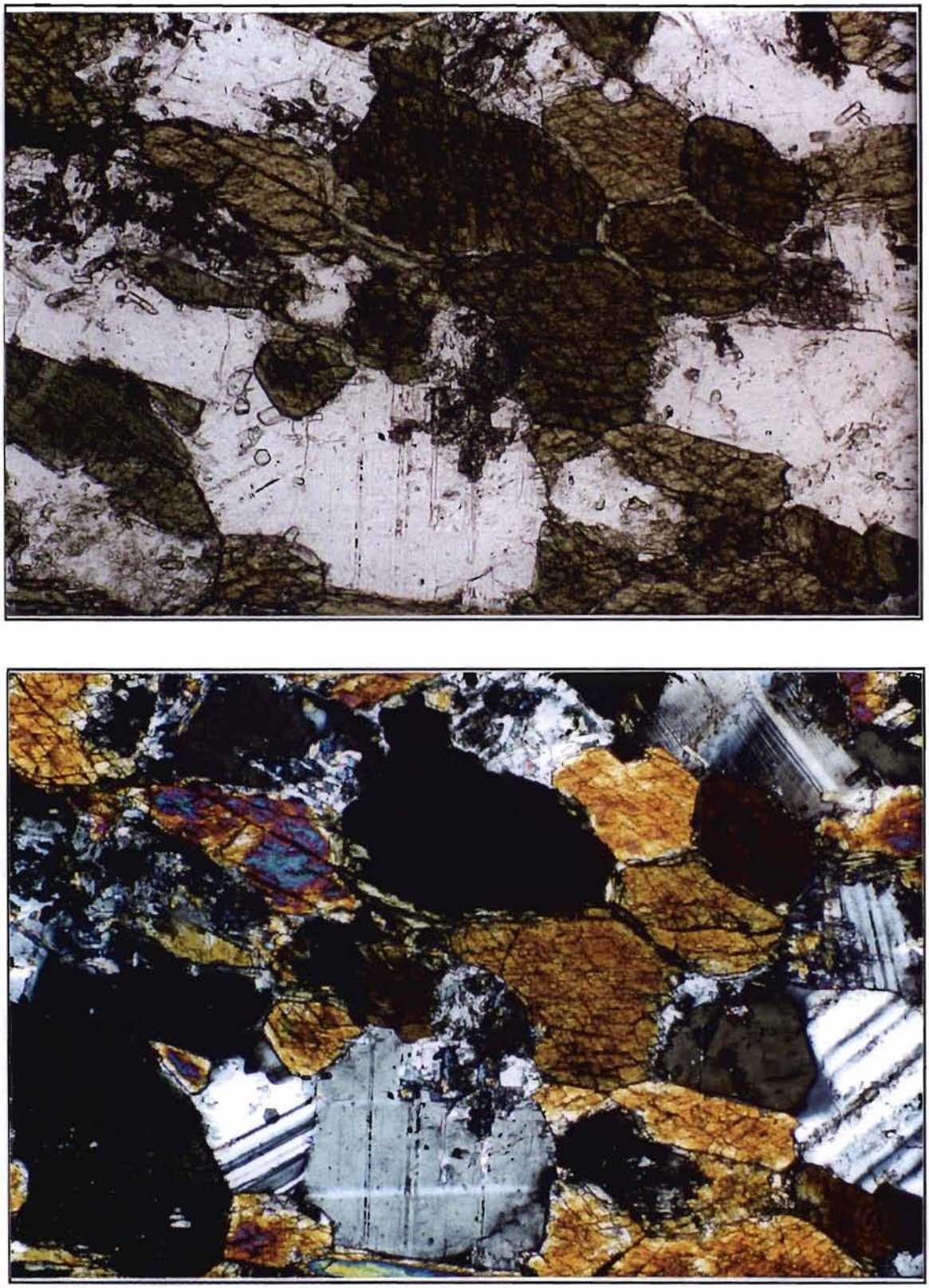

Fig. 2.3. Thin section picture of amphibolite (RM42) at 10x. Top: plane polarized light; bottom: crossed polarized light. Primary mineralogy: hornblende and plagioclase. Note: realtively unaltered apparence of hornblende and plagioclase.

The gabbro group is represented by 7 thin sections and 9 of the 73 total xenolith samples. The gabbro group is defined by a primary mineralogy of plagioclase, clinopyroxene, orthopyroxene, ± biotite (Fig 2.4). A distinctive texture of interlocking plagioclase grains resembling an sub-ophitic or intergranular igneous texture is evident in all of the gabbro samples. The igneous texture is preserved and is distinct to this group. In most cases the plagioclase shows varing degrees of alteration to clinozoisite. Plagioclase varies from fine- to medium-grained. Orthopyroxene grains are altered to clinopyroxene and in some cases to amphibole. Pyroxene grains tend to be rather large and porphyroblastic. Apart from minor differences in alteration and, in one case, the presence of primary oxides, the gabbros are the most homogeneous petrographic group.

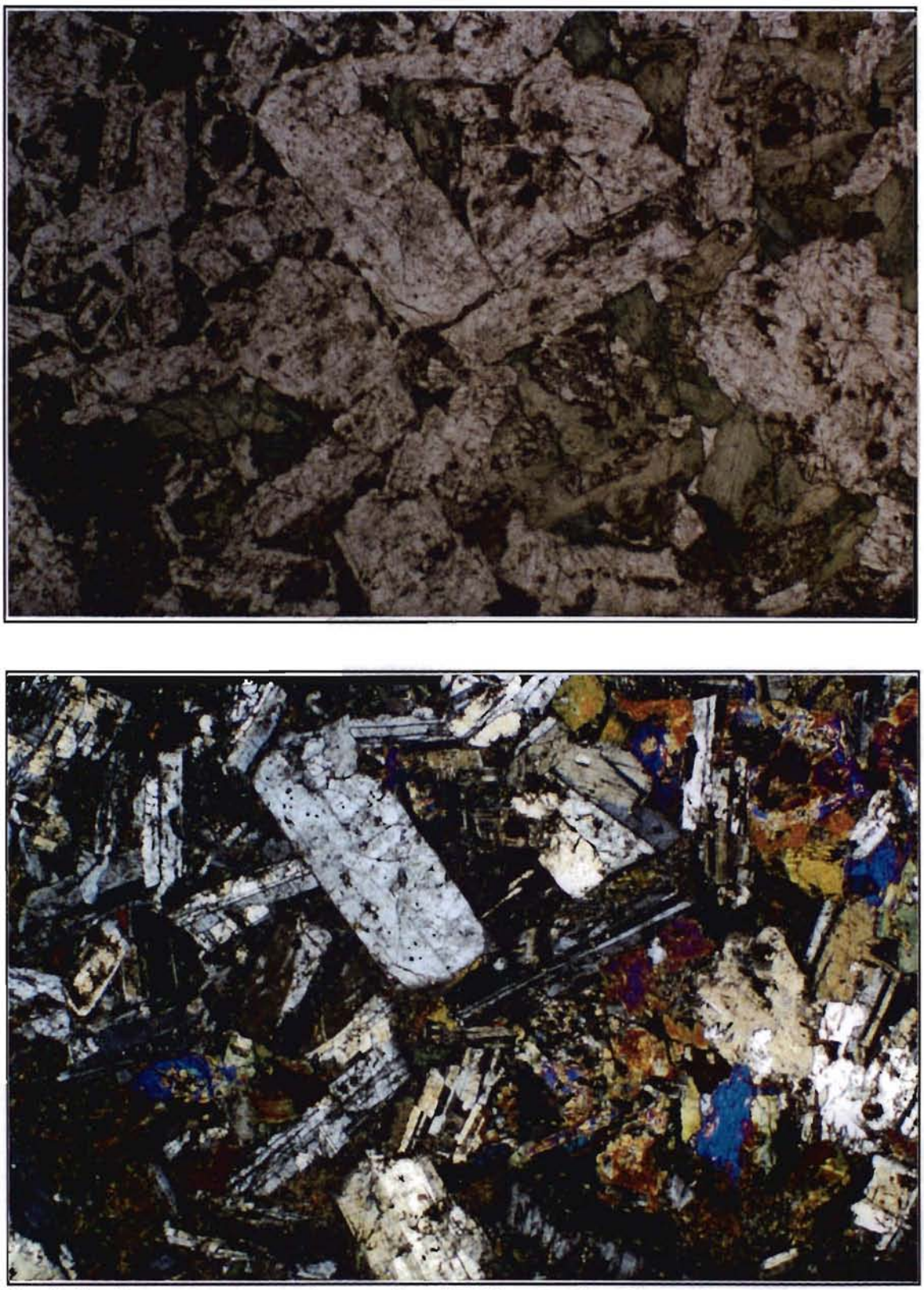

Fig. 2.4. Thin section picture of metagabbro (MR39) at 5x. Top: plane polarized light; bottom: crossed polarized light. Primary mineralogy: clinopyroxene, plagioclase. Note: preserved igneous texture.

Group	Sample	Major Minerals	Description
Garnet Granulites **n=34**	GR11* GR13* GR21* GR23 GR26 GR45* MR44* MR45* MR46* MR50* MR51 MR52* MR53 MR54 MR55 MR57* MR58* MR59 MR60* MR61 MR63 MR64* MR66* MT20* RM47* RM53* RM56* RM60* TH37 TH38* TH39 TH41* TH44 TH46*	gar+cpx+plag ±hbl±opx	large garnets, relic cpx, and secondary hlb common. Alteration minerals include white mica, clinozoisite, epidote, and amphibole.
Pyroxene Granulites n=10	MR78 MR83 RM44 RM49* RM64 MT13 MT14* MT15 MT22* MT27*	cpx+plag+hbl	relic cpx, medium grained triple junctions abound.
Amphibolite n=20	GR41 GR46 MR49 MR81 MT24* MT28* RM36 RM42* RM43* RM46* RM48 RM51 RM54 RM57 RM58 RM59 RM62* SR22 SR25 TH34*	hbl+plag+cpx	foliated; hbl altering to biotite common; plag alters to clinozoisite
Gabbro n=8	MR34* MR37* MR38* MR39* MR40* MR71 MR85 MR86* RM41*	plag+cpx+opx±bio	distinctive intergranular plagioclase texture; plag altering to clinozoisite

*Indicates thin sectioned sample (gar=garnet; plag=plagioclase;cpx=clinopyroxene; opx= orthopyroxene; hbl= hornblende)

Alteration

All of the samples showed varying degrees of alteration, from slightly in samples from Mitten Rock and the Thumb, to extremely common in sample from the kimberlite dikes (Figs. 2.1, 2.2, 2.3). The dark, fine- grained material observed along the grain boundaries in the Thumb xenolith suite may be analogous to kelyphite rims described by Rudnick (1992) as evidence of decompression melting in xenoliths. None of the xenoliths from the kimberlite dikes shows this type of alteration; rather, the majority appear to show the same metasomatic alteration as described by Broadhurst (1986) and Ehrenberg and Griffin (1979). Several explanations for the observed differences between the alteration found in minette diatremes versus kimberlite dikes have been postulated by various authors (Rudnick, 1992; Broadhurst, 1986; Ehrenberg and Griffin, 1979). Alteration in the kimberlite pipes from associated host-derived fluids during transport is the most popular theory (Rudnick, 1992; Ehrenberg and Griffin, 1979). Broadhurst (1986), however, suggested that there may have been two hydration events, one of which occurred in situ in the crust. Alteration reactions described by Broadhurst (1986) as evidence of a multi-stage hydration are evident in most of the kimberlite xenolith population collected in this study.

2.3 Whole Rock Composition

All 73 mafic xenolith samples collected from the Navajo Volcanic Field (NVF) were analyzed for major and trace elements by X-ray fluorescence (XRF). Twenty-five mafic xenolith samples were analyzed for trace and rare earth elements (REE) by instrumental neutron activation analysis (INAA) . Appendix D contains the major and trace element results for the xenolith population analyzed. All analyses were made at New Mexico Institute of Mining and Technology. Sample powders were prepared as described in Appendix A and Appendix C contains a detailed description of analytical methods for both INAA and XRF.

Data Evaluation

The data for the mafic xenoliths were evaluated by plotting on bivariate graphs. Variation diagrams using major and trace elements were constructed to identify chemically distinct populations in an attempt to identify possible source differences. Xenolith samples were first plotted according to sample locality. There is no corelation observed between geographical location and major and minor element chemistry. Next, xenolith samples were plotted according to rock type (i.e. garnet-granulite, amphibolite, pyroxene-granulite, & gabbro). Only the gabbros, of which 8 of 9 come from Moses Rock dike, have a distinct chemical and mineralogic composition. However, the remainder of the lithologic groups do not match geochemically or in geographical distribution. Chemically, the xenolith population cannot be subdivided on the basis of major element or many trace element distributions. This may be the result of remobilization of these elements during metamorphism or alteration. Only when considering the less mobile high field strength elements (HFSE) and rare earth elements (REE) can systematic variations be seen. As a result, the mafic xenolith population has been divided into 8 distinct geochemical groups based on incompatible trace elements and REE distributions.

Geochemical Populations

The eight geochemical groups are listed in Table 2.3. Each group has distinctive trace element abundances as listed in Table 2.3 and described in detail in the following sections. Group I contains all the gabbros from the Moses Rock dike. They are the most distinct group chemically and petrographically. Group I (n=8) with high Mg numbers (0.7-0.8) and high CaO/TiO_2 and low Ti, shows only slight chondrite-normalized LREE enrichment, a strong depletion in Nb and Ta relative to neighboring incompatible elements and positive Sr, Ba, Eu, and K (SBEK) anomalies on primitive mantle normalized spidergrams(Table 2.3). Group II mafic xenoliths are garnet granulite and amphibolite samples from Moses Rock, Red Mesa, and Garnet Ridge kimberlite diatremes (Table 2.3). Group II (n=5) with intermediate CaO/TiO_2 and Ti has flat to LREE depleted patterns, Ta-Nb depletions and SBEK anomalies. Group III mafic xenoliths are amphibolites from the Red Mesa diatreme (Table 2.3). Group III (n=3) with very high CaO/TiO_2 and low Ti and Zr has nearly flat REE patterns and a very prominent Ta-Nb depletions and large SBEK anomalies (Table 2.3). Group IV mafic xenoliths are composed of amphibolites, garnet granulites and pyroxene granulites from Garent Ridge, Red Mesa, Shiprock, and the Thumb. Group IV (n=5) with low CaO/TiO_2 and variable Ti shows significant LREE enrichment (100 x chondrites), variable Ta-Nb depletion, and small or absent SBEK anomalies. Group V xenoliths are garnet granulites from Moses Rock and Red Mesa diatremes. Group V (n=2) xenoliths have low CaO/TiO_2 and Ti, show slight HREE depletion, Ta-Nb depletion, and small positive SBEK anomalies. Group VI xenoliths are garnet granulites and pyroxene granulites from Garnet Ridge and Mitten Rock diatremes. Group VI (n=2) xenoliths have a slight enrichment in LREE relative to HREE, variable Ta-Nb depletions, and positive SBEK anomalies. Group VII (n=5) xenoliths are all garnet granulites from Garnet Ridge, Moses Rock, Red Mesa, and the Thumb diatremes. They have low CaO/TiO_2 , variable Ti, enrichment in LREE relative to HREE, and variable positive

SBEK anomalies and Ta-Nb depletion. Group VIII (n=2) xenoliths are garnet granulites from Moses Rock diatreme and they have high CaO/TiO2, low Ti, a concave upwards REE distribution, with positive Eu anomalies, large SBEK anomalies, and Ta-Nb depletion. The remaining samples could not be separated into separate populations. They were only analyzed for major and trace elements by XRF, which does not provide the resolution necessary to group them in existing or other geochemical groups. These samples include garnet granulites, pyroxene granulites, and amphibolites from all six sampling localities (Table 2.4).

Table 2.3. Geochemical Groups of mafic xenoliths from the Navajo Volcanic Field

Group	*Samples*	*Discriminative Observations*
GROUP I **n=8**	*Gabbro* MR34,MR37,MR38, MR39,MR40,MR71, MR85 ,MR86	CaO/TiO2 =(20-60); TiO2= (<0.5%); Mg#=(0.7-0.8); slightly enriched LREE; Ta-Nb depletion; and positive Sr,Ba,Eu, & K anomalies.
GROUP II **n=5**	*Garnet Granulite* MR50,MR66, RM56 *Amphibolite* GR21,RM58	CaO/TiO2 =(10-20); TiO2=(0.5-0.9%); LREE depleted; Ta-Nb depletion; and positive Sr,Ba,Eu, & K anomalies.
GROUP III **n=3**	*Amphibolite* RM46,RM51,RM62	CaO/TiO2 =(40-60); TiO2= (<0.5%); flat REE patterns; Ta-Nb depleted
GROUP IV **n=5**	*Garnet Granulite* TH39 *Pyroxene Granulite* RM49 *Amphibolite* GR41, RM59, SR25	CaO/TiO2=(<8); TiO2=(1-1.7%); significant LREE enrichment (100x chondrite); and variable Ta-Nb depletions.
GROUP V **n=2**	*Garnet Granulite* MR57, RM53	CaO/TiO2=(10-20); TiO2=(0.5-0.7%); slight HREE depletion (5x chondrite); Ta-Nb depleted.
GROUP VI **n=2**	*Garnet Granulite* GR45 *Pyroxene Granulite* MT14	CaO/TiO2=(10); TiO2=(0.7-1.1%); flat to slightly LREE depleted patterns (10x chondrite); variable Ta-Nb depletions
GROUP VII **n=5**	*Garnet Granulite* GR13, MR46, MR52, RM60, TH44	CaO/TiO2=(5-10); TiO2=(0.6-1.5); LREE enriched (30-80x Chondrite); small to no Ta-Nb depletions
GROUP VIII **n=2**	*Garnet Granulite* MR45, MR54	CaO/TiO2=(>40); TiO2=(< 0.3); depletion of middle REE; strong positive Eu anomalies on chondrite normalized REE plot; Ta-Nb depletion.

TABLE 2.4. Ungrouped mafic xenolith samples from the Navajo Volcanic Field

	Samples	*Discriminative Observations*
n=40	***Garnet Granulite*** GR11,GR23, GR26,MR44,MR51, MR53,MR54,MR55, MR58,MR59,MR61, MR63, MR64,MT20, RM47, TH37, TH38, TH41,TH46	largest population of xenoliths; CaO/TiO2= (2-40); TiO2=(.1-2.5%)
	Pyroxene Granulite MR78,MR83,MT13 MT15,MT22,MT27, RM44, RM64	
	Amphibolite GR46,MR49,MR81 MT24,MT28,RM36 RM41,RM42,RM43 RM48,RM54,RM57 SR22,TH34	

Major Element Chemistry

The majority of the Navajo Volcanic Field mafic xenoliths fall within the range of 44-57 % SiO_2 and 2-12 % MgO consistent with mafic to intermediate compositions (Fig.2.5 and Appendix D.1). CaO and Al_2O_3 vary from 4-16 % and 11-24 %, respectively (Fig. 2.5 & Appendix D.1). Both Na_2O and K_2O values range between 1-6 %, and P_2O_5 varies from <0.2 to 1 % (Fig. 2.5 & Appendix D.1). SiO_2 shows negative correlation with MgO but, in general, the mafic xenoliths show poor correlations of major elements on bivariate plots (Fig. 2.5). The NVF xenoliths range from quartz to nepheline normative (Figure 2.7 & Table D.4). The majority of the samples have CIPW normative that plots in the hypersthene, olivine, diopside field which would classifiy them as olivine tholeiite according to Thompson (1984) (Figure 2.7). On an AFM

diagram the majority of the NVF mafic xenolith population plots within the calc-alkaline field (Fig. 2.6).

Group I mafic xenoliths have low TiO_2 (<0.4%), low Fe_2O_3 (<10%) and high Al_2O_3 (>16%)(Figs. 2.5 & 2.8). Group II mafic xenoliths have high MgO (6-10%), low SiO_2 (45-49%), and high CaO (10-13%) (Fig. 2.5). Group III xenoliths have major element abundances that are characterized by low TiO_2 (0.1-0.35), high Al_2O_3 (17-22%), high CaO (13-15%), and low Na_2O (approx. 1%) relative to the NVF mafic xenolith population (Figs. 2.5 & 2.8). Groups I and III mafic xenoliths have the lowest TiO_2 values in the xenolith population and when TiO_2 is used in any major element ratio, these two groups are distinct (Table 2.3, Fig. 2.8). Group IV mafic xenoliths have major element abundances that are characterized by low CaO (approx. 6%), low Al_2O_3 (<16%), and high K_2O (1-4%) relative to the NVF mafic xenolith population. Group V has major element distributions characterized by low K_2O and MgO, (<0.5) and (5-6%) respectively, high Na_2O (3-4%) and intermediate values for the remainder of the major elements (Fig. 2.5). Group VI has a high MgO content (7-9%) and low $Al2O_3$ (13-14%) (Fig. 2.5). Group VII has generally intermediate major element values compared with the other NVF mafic xenolith groups and is not distinct on any of the major element bivariate plots (Fig. 2.5). Group VIII is quite distinct in major element abundances. Group VIII has the highest SiO_2 values (54-55%), and lowest MgO and Fe_2O_3, (2-3%) and (5-6%) respectively (Fig 2.5).

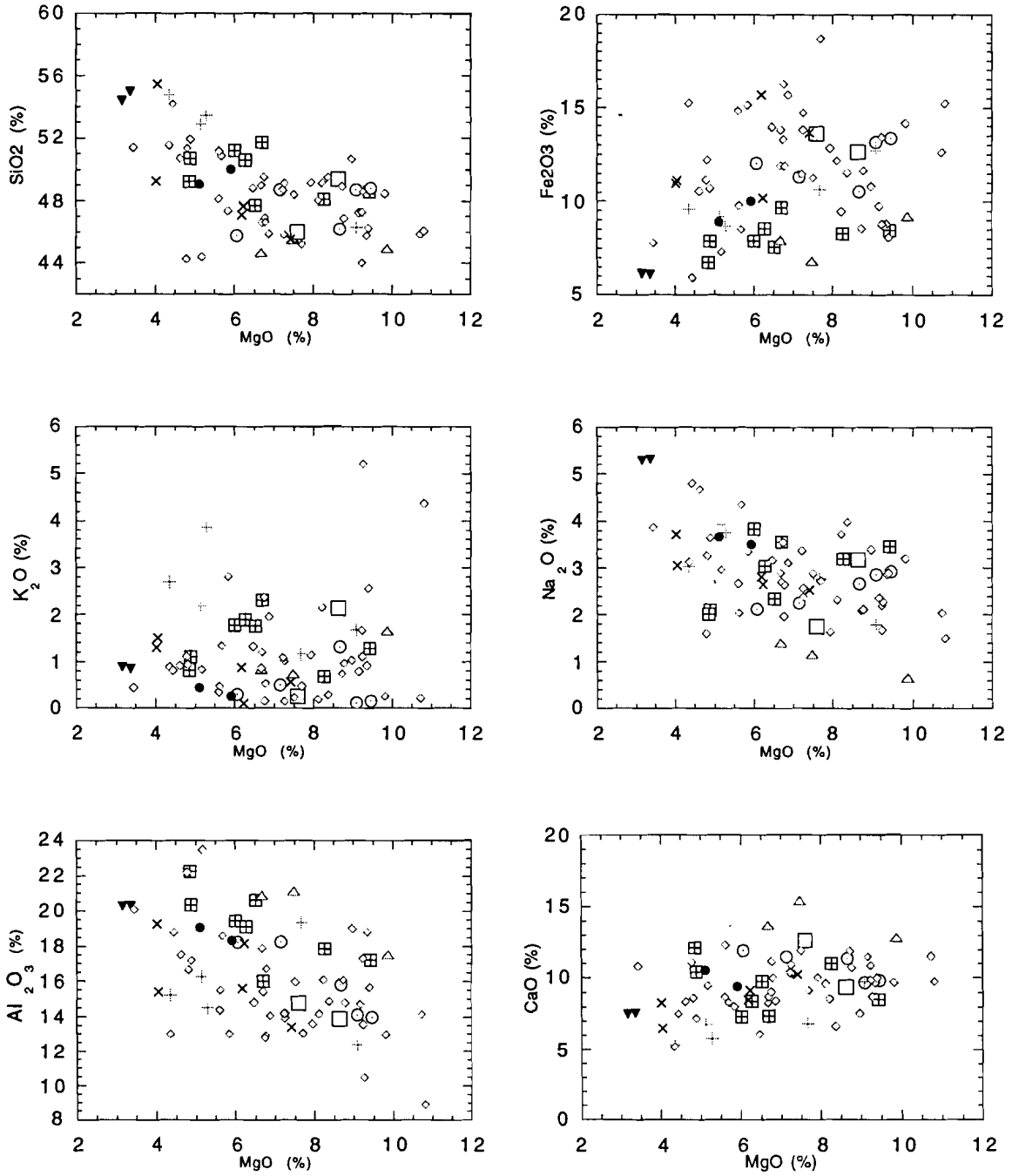

Fig.2.5. Major element plots for the Navajo Volcanic Field mafic xenolith suite. Symbols are defined as follows: Group I = crossed boxes; Group II = dotted circle; Group III = open triangles; Group IV = plus; Group V = solid dots; Group VI = open squares; Group VII = X's; Group VIII = inverted solid triangles; Ungrouped samples = open diamonds. All samples are mafic to intermediate in composition.

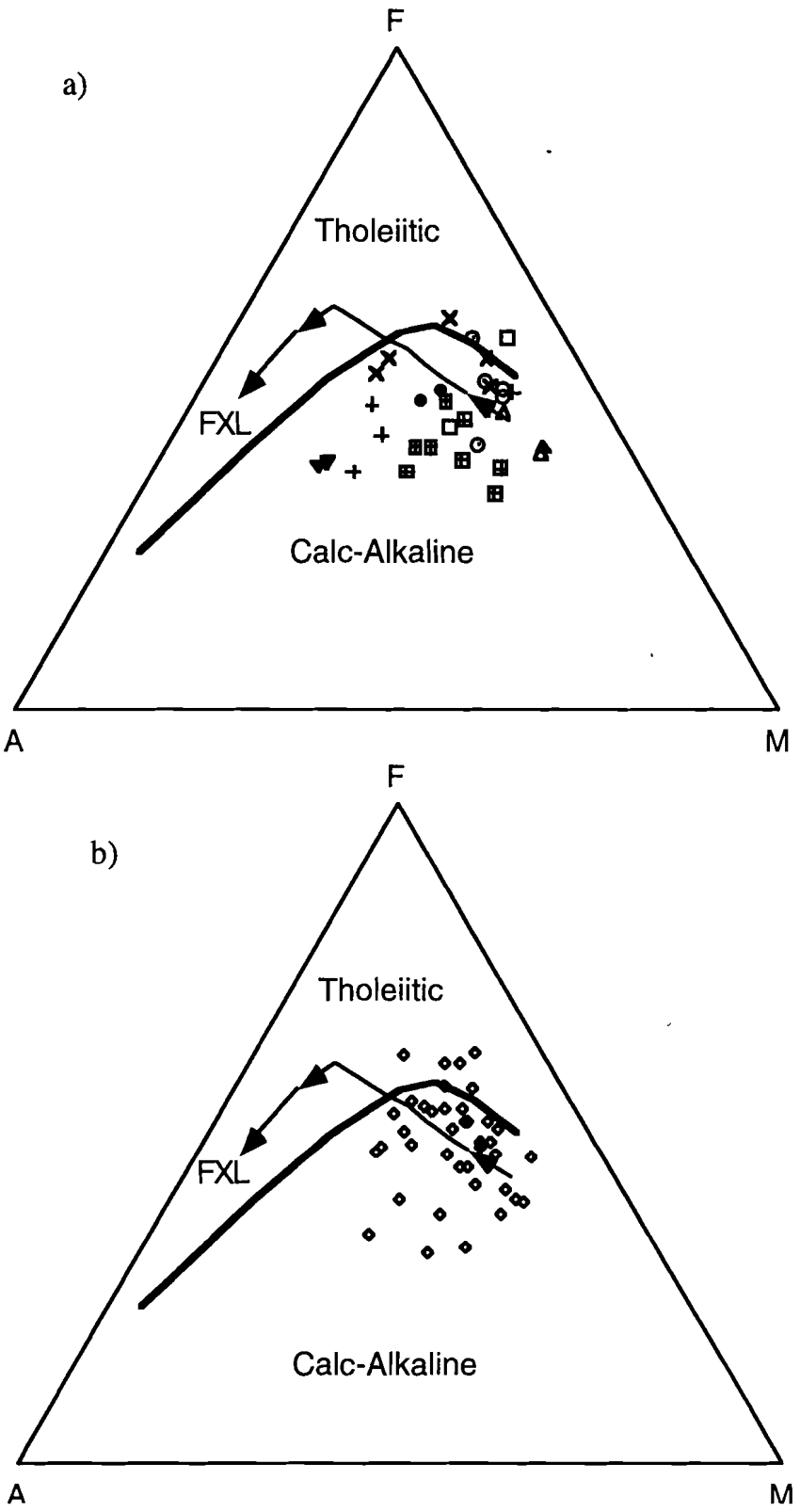

Fig. 2.6. AFM Diagrams for the NVF Xenoliths; Symbols are the same as in Fig. 2.5; a) AFM Plot NVF geochemical groups b) ungrouped NVF mafic xenoliths; Solid line divides between Tholetiitic and Calc-alkaline fields (after Kuno, 1968); FXL trend calculated from MIXNFRAC program (Nielson) using hypothetical basaltic composition as parent composition; Total Fe calcualted from (Fe2O3 * 0.8998).

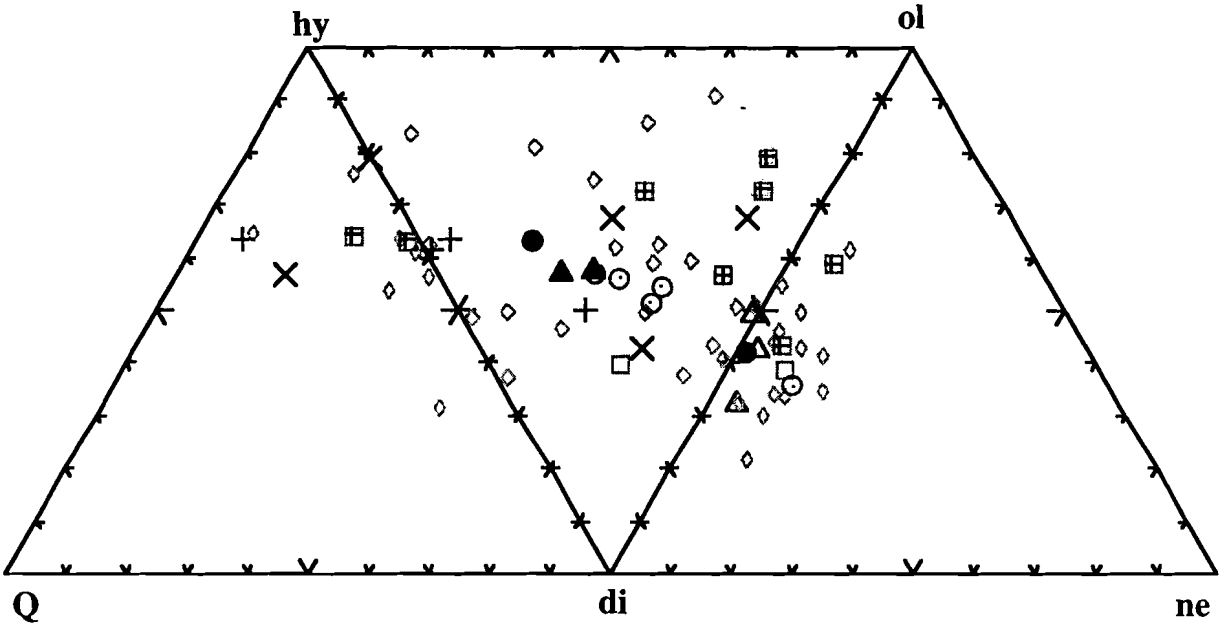

Fig. 2.7. Quartz (Q)-hypersthene (hy)-diopside (di)-olivine (ol)-nepheline (ne) plot of NVF xenoliths. Symbols are the same as in Figure 2.5. Samples trend from nepheline normative to quartz normative.

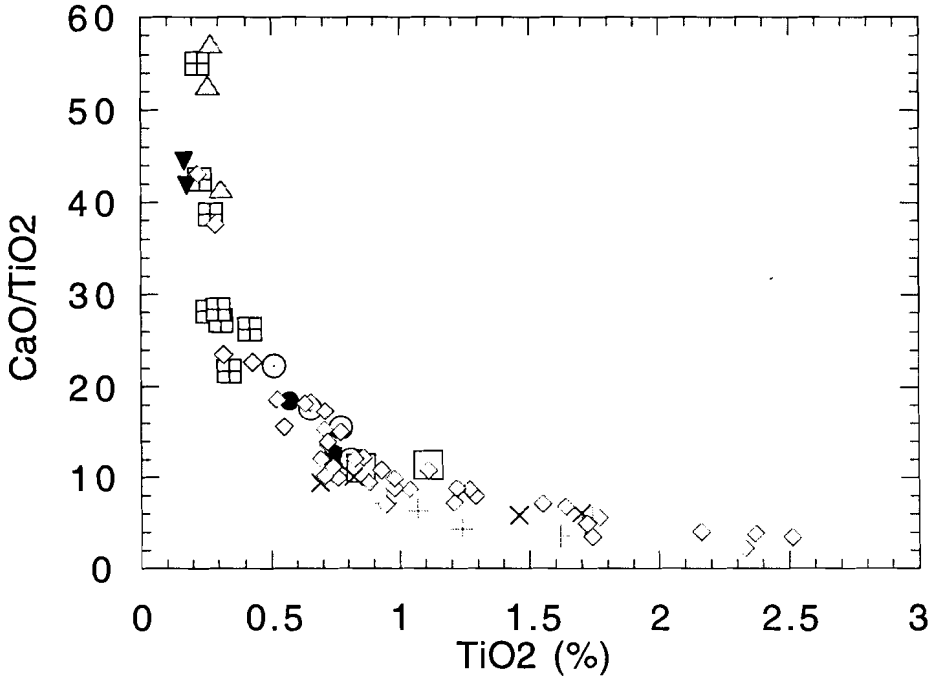

Fig. 2.8. CaO/TiO_2 vs TiO_2 for the NVF mafic xenoliths. Symbols are the same as in Figure 2.5. Groups I, III, & VIII show the highest CaO/TiO2 and lowest TiO2 values.

Incompatible Element Distributions

Incompatible elements vary over a wide range of values for the NVF mafic xenolith population (Appendix D.2 & D.3), which can best be observed on primitive-mantle normalized spider diagrams (Fig. 2.9). The xenoliths show enrichments of large ion lithophile elements (LILE) relative to high field strength elements (HFSE), with LILE abundances ranging from 1 to 100X primitive mantle values (Fig. 2.9). The LILE and HFSE show variable distributions, which do not correlate with lithology, geographic location, host material, or metamorphic grade (Table 2.3 & 2.4, Fig. 2.9). The variable enrichments in LILE may be the result of remobilization of these elements during metamorphism or alteration. Mafic xenoliths in Groups I, II, III, V, VI, & VIII have variable LILE contents showing relative enrichments in Ba, K and Sr on primitive mantle normalized diagrams (PM-n)(Fig. 2.9 SBEK anomalies). Group IV shows only small positive Ba and K anomalies on a PM-n diagram (Fig. 2.9). Group VII is the most variable with two of the five samples showing positive Sr, Ba, Eu, and K anomalies (Fig. 2.9). Positive Ba and K anomalies are the result of the very low abundance of Th in the NVF mafic xenolith population. The positive Sr anomalies on the PM-n spider diagrams appear to be coupled with a slightly postive Eu anomaly and Al_2O_3 values of 14-22 wt%, which may indicate the presence of cummulus plagioclase in these samples.

Significant Ta-Nb depletions can be observed in Groups I, II, IV, V, & VIII. In Groups II, VI, & VII Ta-Nb is variable. In Group II and VI one of the two samples show Ta-Nb depletion. Group VII has three of five samples with slight Ta-Nb depletions and the remainder with no depletion in Ta or Nb.

The HFSE for the NVF mafic xenoliths are less variable than LILE with abundances ranging from <3x PM values for Groups III, VIII, 1 to 10x PM values for Groups I, II, V and VI, and 5-20x PM values for Groups IV and VII. Group I shows Hf & Zr enriched over Ti, Yb, & Y and a slight positive Eu anomaly. In Group II and Group III

Hf & Zr are slightly depleted relative to Eu, Ti, Yb, & Y, with small positive Eu anamolies (Fig. 2.9). Group IV shows enrichement in Hf, Zr, & Eu relative to Ti, Yb, & Y and they have no Eu anamoly (Fig. 2.9). Groups V and VII have flat HFSE distributions, although MT14 (Group VI) shows a small negative Ti anomaly. Group VII is variable in HFSE, three of the five samples (GR13, MR46, & RM60) have flat HFSE with slightly positive Eu, the two remaining samples (TH44 & MR52) are slightly enriched in Hf & Zr relative to Yb & Y. Group VIII shows depletions in Hf, Zr, & Ti relative to Eu, Yb, & Y, and have distinctly positive Eu anomlaies on the PM-n Spidergraph (Fig. 2.9).

Since Ta and Nb are highly immobile during hydrous alteration due to their very low ionic potential, the occurrence of such a strong Ta-Nb depletion coupled with positive Ba and K anomalies and enrichments in LILE relative to HFSE in many of the NVF mafic xenoliths suggests that these samples have been altered in a metasomatic environment.

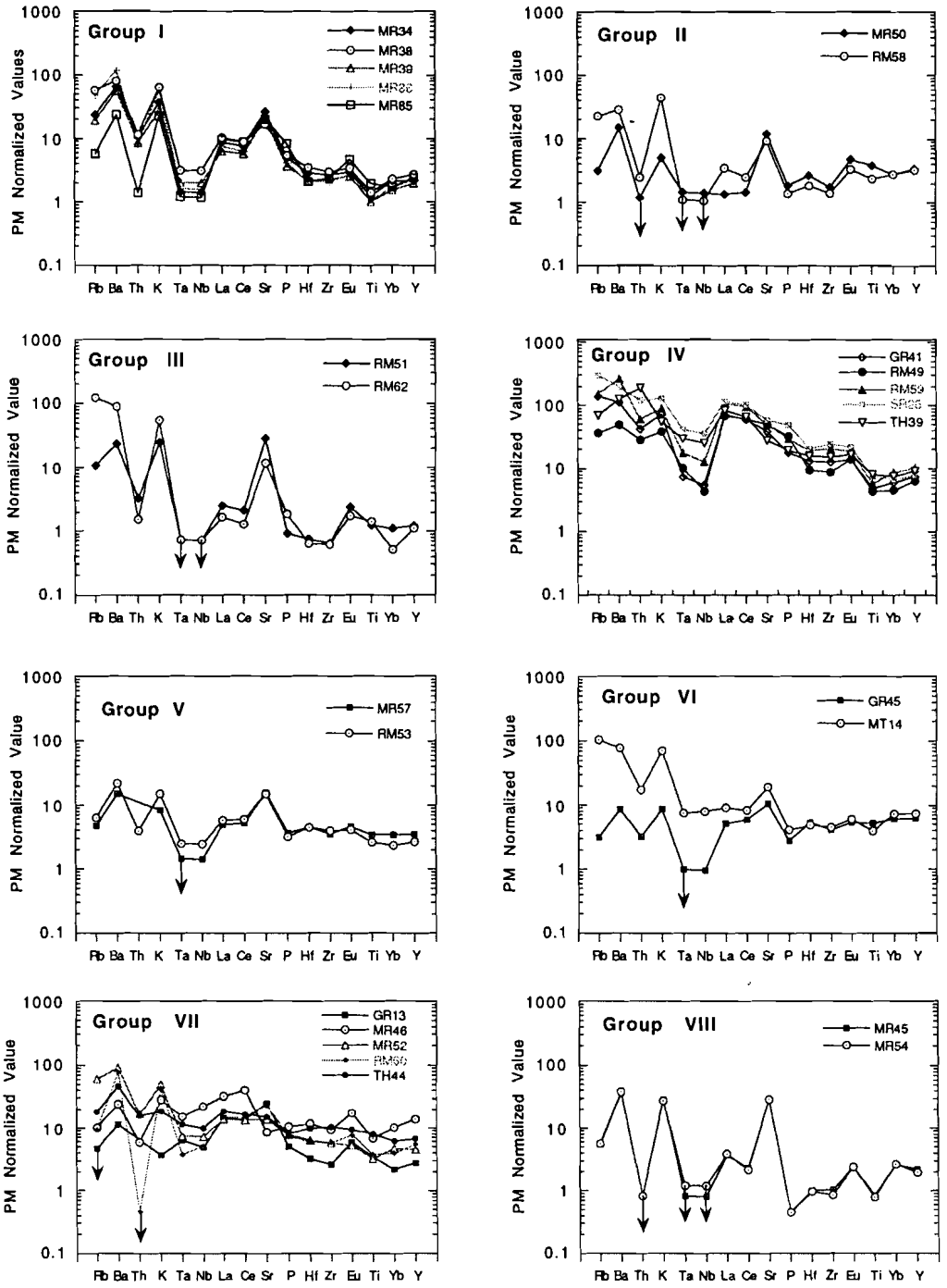

Fig. 2.9. Primitive-mantle normalized (PM-n)incompatible element distribution diagrams for NVF mafic xenoliths. The majority of xenoliths show Ta-Nb depletion, variable LILE and positive Sr,Ba,Eu, K anomalies. Arrows indicate values that were below the lower limits of detection. (Nb was below detection in all of the samples in Groups I, II, and III indicating Nb levels below the detection limit of 2 ppm for XRF analysis, Nb was estimated from Ta data from INAA using the following relationship for mafic rocks: (Nb = Ta * 17); Ta was below the lower limits of detection (LLD) for many of the samples in Groups II, III, V, VI, & VIII the LLD was used for Ta to produce the PM-n spidergrams.) Primitive mantle values from McDonough et al. (1992).

Compatible Elements

All the mafic xenoliths appear to have been affected by fractional crystallization (FXL) as observed on log-plots of incompatibale vs compatible elements such as Cr or Ni vs. Zr (Figure 2.10 a & b). The steep slope observed for each of the geochemical groups on Figure 2.10 indicates FXL in contrast to a shallow slope which would be more typical of a partial melting trend (Cochrie, 1986). Group I has the most distinct FXL trend which overlies the FXL trend for Group II on Ni-Zr plot (Fig. 2.10a). Group III and Group IV have FXL trends that cannot be related to Group I or II by simple differences in FXL and suggest that the Groups represent distinctly different magmas. The wide distribution of the Group VII samples shows a relatively steep trend that suggests FXL processes. Groups V, VI, and VIII are limited to only two samples and therefore make it difficult to infer FXL, but when they are evaluated together with the entire NVF xenolith population it appears that they may also be related by FXL processes .

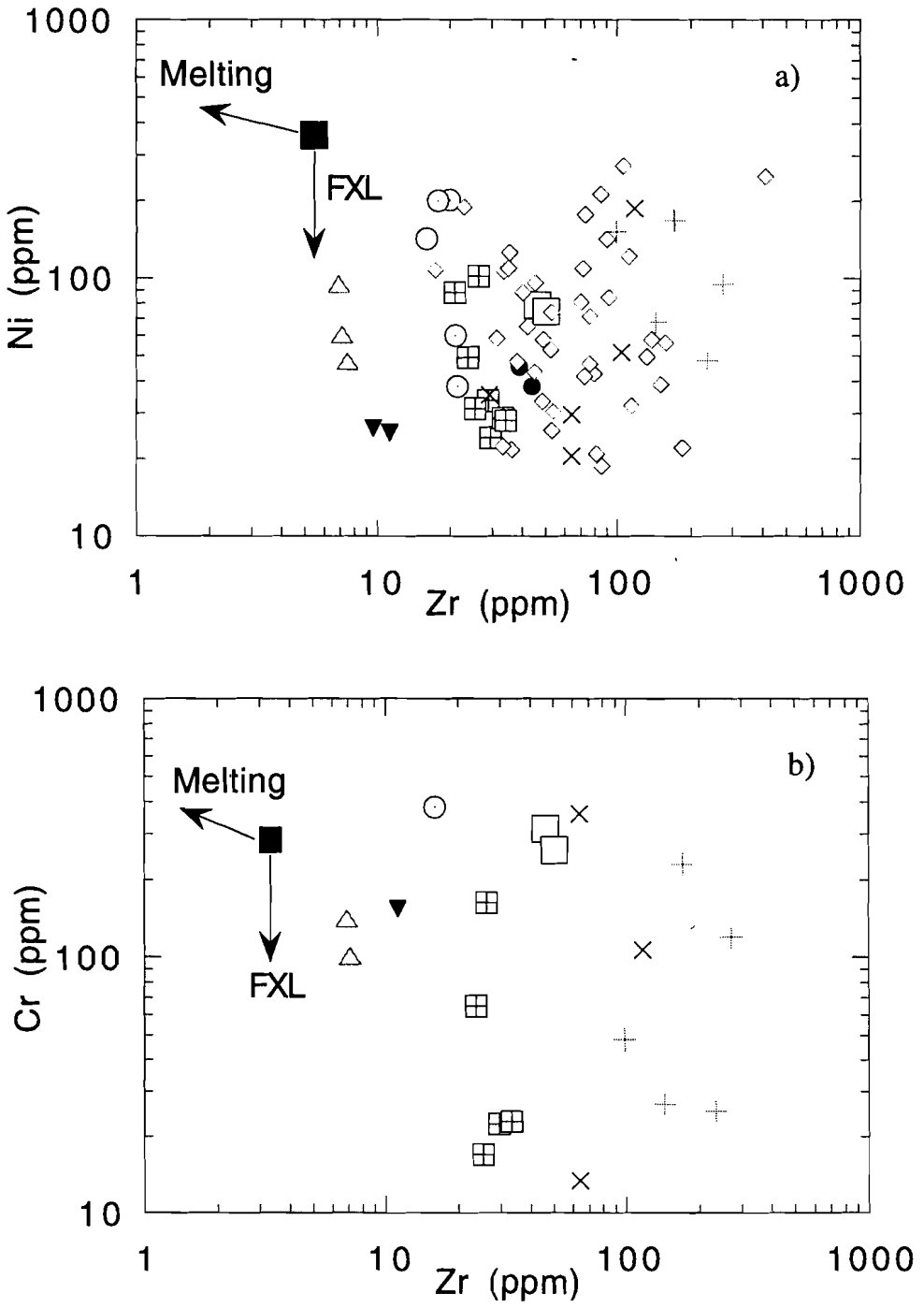

Fig. 2.10 a & b. Log plots of Cr and Ni vs Zr. (FXL and Partial Melting trends as defined by Cocherie(1989) indicated by arrows) Note the steep slopes of each geochemical group. Symbols the same as in figure 2.5.

Incompatible Element Ratios

Incompatible element ratios for the NVF mafic xenoliths also characterizes the eight geochemical populations. Incompatible element ratios can often see through metamorphic alteration and hence are useful in characterizing mantle sources (Condie, 1996). The eight NVF xenolith groups can be observed on plots of Th/Yb vs. Ta/Yb, La/Yb vs. Sr/Y, and V/Ti vs. Ti/Zr (Fig. 2.11, 2.12, & 2.13). Ranges for these incompatible element ratios are listed in Table 2.5.

Table 2.5. Range in incompatible element ratios for the Navajo Volcanic Field mafic xenoliths.

Group	*Th/Yb*	*Ta/Yb*	*Th/Ta*	*La/Yb*	*Sr/Y*	*V/Ti*	*Ti/Zr*
Group I	0.1-1	0.05-0.1	2-11	5.0-8.0	20-57	0.04-0.12	30-100
	(5)	(5)	(5)	(5)	(9)	(9)	(9)
Group II	0.15	0.035	4.5	1.9	13-95	0.04-0.095	185-275
	(1)	(1)	(1)	(2)	(5)	(5)	(5)
Group III	--	--	--	3.0-6.0	49-110	0.09-0.15 (3)	200-275 (2)
				(2)	(3)		
Group IV	1.0-5.0	0.1-0.6	5-15	15-25	14-36	0.01-0.03 (5)	30-60
	(5)	(5)	(5)	(5)	(5)		(5)
Group V	0.28	0.03-0.09	3.24	2.0-3.5	20-60	0.05	78-114
	(1)	(2)	(1)	(2)	(2)	(2)	(2)
Group VI	0.09-0.4	0.087	4.74	1.2-1.8	8.0-12	0.045-0.05	100-144
	(2)	(1)	(1)	(2)	(2)	(2)	(2)
Group VII	0.09-0.6	0.08-0.25	0.8-4.7	4.0-9.5	2.0-43	0.02-0.05	64-152
	(3)	(5)	(3)	(5)	(5)	(5)	(5)
Group VIII	--	--	--	1.9-2.0	62-69	0.1	96-106
				(2)	(2)	(2)	(2)

(#) idicates the number of samples that define the range.

Group I has lowest Ti/Zr and intermediate values for Th/Yb, Ta/Yb, Th/Ta, La/Yb, & V/Ti ratios of the NVF xenoliths (Figs. 2.11- 2.13). Groups II, V, & VI are poorly defined on Figure 2.11 having only one data point available for each group. But, these

three groups show distinctly on plots using La/Yb, Sr/Y and Ti/Zr ratios (Figs. 2.12 &2.13). Groups II and III have the highest Ti/Zr ratios of the xenolith population. Group III has the highest Ti/Zr and V/Ti ratios of all the groups. Group IV has the highest Th/Yb, Ta/Yb, & La/Yb and lowest Ti/Zr & V/Ti ratios relative to the NVF mafic xenolith population (Fig. 2.11-2.13). Group VII is defined by intermediate Th/Yb, La/Yb, and Ta/Yb ratios (Fig. 2.11 &2.12). Group VIII only has two samples but has very unique trace element ratios that can be observed on Figs. 2.11 & 2.13. Groups I, IV, and VII define distinct regions on each of the Figs. 2.11-2.13, which suggests that each group represents a different mantle source.

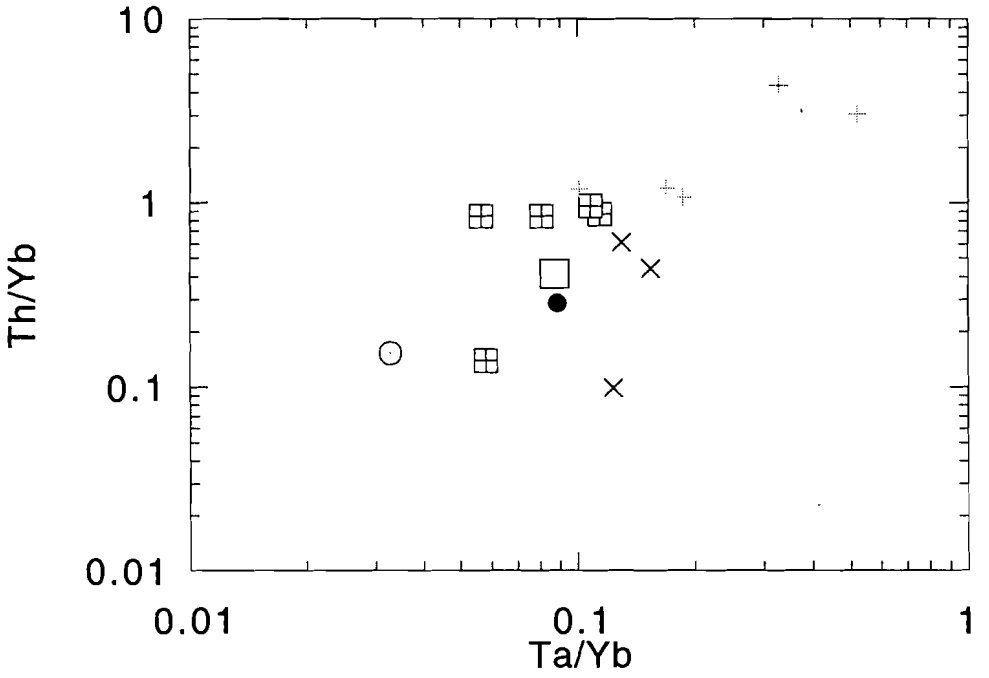

Fig. 2.11. Th/Yb vs. Ta/Yb graph showing the distribution of the NVF mafic xenoliths. Symbols are the same as in fig. 2.1. Note that Group IV has the highest Th/Yb & Ta/Yb ratios of the NVF mafic xenoliths. Group III was not included in this plot since both Th & Ta were below the lower limits of detection by INAA.

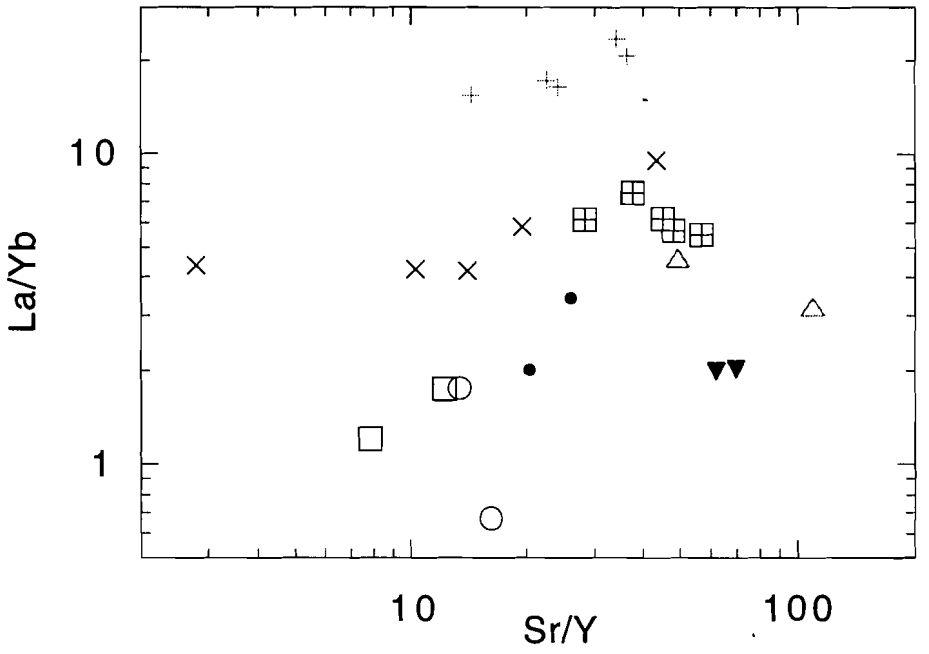

Fig. 2.12. La/Yb vs. Sr/Y graph showing the distribution of the NVF mafic xenoliths. Symbols are the same as in fig. 2.1. Groups I, IV, and VII define distinct regions.

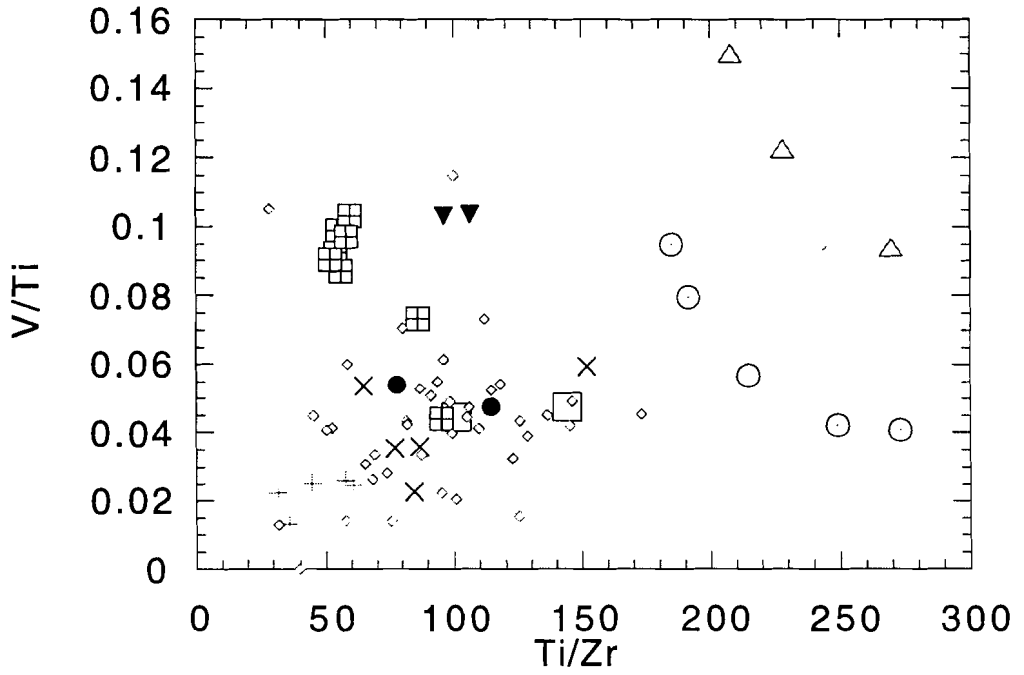

Fig. 2.13. V/Ti vs. Ti/Zr graph showing the distribution of the NVF mafic xenoliths. Plotting symbols are defined in fig. 2.1. Note that Group III has the highest Ti/Zr and V/Ti relative to the NVF mafic xenoliths. five groups plot in distinct regions on this graph.

Rare Earth Element Distributions

Figure 2.14 show typical chondrite normalized rare earth element distributions for the minette and kimberlite host rocks. Figure 2.15 shows the chondrite normalized rare earth element (REE) distributions for the NVF mafic xenoliths. Group I xenoliths show REE patterns that are slightly enriched in light rare earth elements (LREE) (10-20x chondrite) relative to the heavy rare earth elements (HREE). Group II xenoliths show REE distributions that 3 to 9x chondrite values and are slightly depleted in both LREE & HREE relative to Sm, Eu, & Tb creating a "humped shaped" pattern. Group III xenoliths show REE patterns that are depleted in HREE relative to LREE with abundances near 5x chondrite values for LREEs. Group IV xenolith REE patterns are enriched in LREE relative to HREE with LREE abundances averaging ~200x chondrite values. Group IV mafic xenoliths are the most enriched in REE. Group V mafic xenoliths have flat to slightly HREE depleted REE patterns with abundances between 4 and 10x chondrite. In contrast, Group VI shows flat to slightly LREE depleted REE patterns with abundances between 10 and 20x chondrite. Group VII has a strong LREE enrichment relative to HREE with abuncances of LREE ranging from 30-70x chondrite values. All the samples in Group VII exhibit variable depletions in Eu relative to other REE, excluding GR13. Sample MR46 in Group VII, has a negative Eu anomaly and is the most enriched in REE of group VII, suggestive of a REE pattern from continental flood basalts. Group VIII garnet granulites have a unique pattern that is enriched in both LREE and HREE relative to the middle REE creating a "concave up" pattern and positive Eu anomalies. Rudnick (1987) obtained a similar pattern on a garnet granulite from Hill 32 Queensland volcanic provence Australia, which she suggested was the result of positive enrichment of HREE in garnets that were in equilibrium with an igneous melt. However, Wendlandt (1993) found this behaviour in eclogites from the NVF and suggested it is the result of LREE enrichment.

Groups I, IV and VII all have REE patterns that are enriched in LREE relative to HREE. Group IV shows the most enriched REE distributions with abundances as high as 200x chondrite for LREEs. These are similar in enrichment to alkali basalts and host kimberlite and minette (Fig. 2.14.). Groups II and III show REE patterns that are concave down in strong contrast to the majority of the NVF mafic xenoliths. Groups V and VI have flat REE distributions that are similar to NMORB REE distributions. The distinct patterns displayed by each of the five groups is suggestive of multiple sources represented in the NVF mafic xenolith suite.

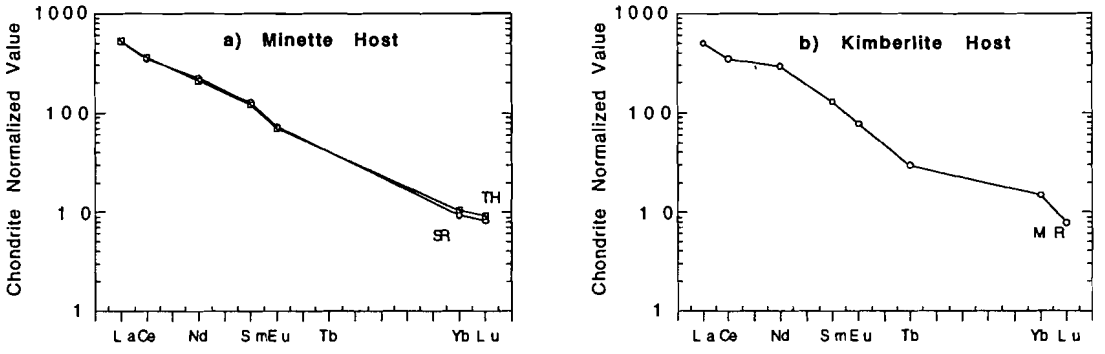

Fig. 2.14 a-b. Chondrite normalized rare earth element distributions for the NVF minette and kimberlite hosts. SR=Shiprock Diatreme; TH=The Thumb Diatreme; MR=Moses Rock Dike. Chondrite values from Haskin et al. (1968). Minette values from Alibert et al., (1986); kimberlite value from Laughlin, et al., (1986).

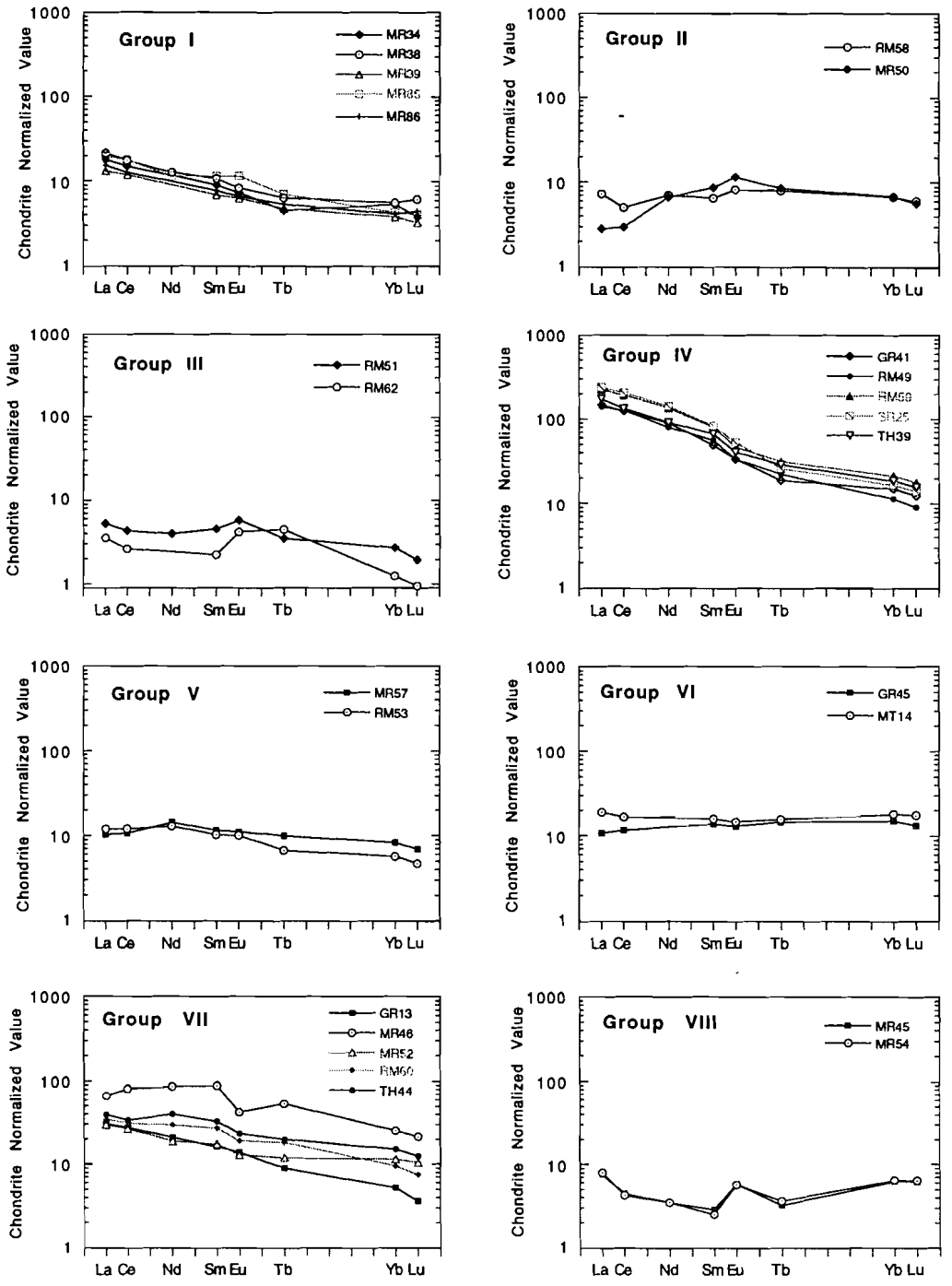

Fig. 2.15. Chondrite normalized rare earth element distributions for the NVF mafic xenoliths. Chondrite values from Haskin et al. (1968).

2.4 Summary

Eight geochemical groups can be identified from the 73 mafic xenoliths collected from the NFV. Each group has distinct trace element abundances that are most easily identified on incompatible element ratio plots, incompatible element distribution graphs, and chondrite normalized REE distribution graphs. Groups I, IV, and VII (except MR46) are the most homogeneous groups. Most of the xenoliths contain Ta-Nb depletions coupled with positive Ba and K anomalies and enrichments in LILE relative to HFSE.

CHAPTER 3: DISCUSSION

3.1. Introduction

Numerous xenoliths studies have been conducted in the southwestern United States (Ehrenberg, 1982; Broadhurst, 1986; O'Brien, 1983; Wendlandt et al., 1993 & 1996; Ehrenberg and Griffin, 1979; Wilshire, et al. 1988; Kempton et al., 1994; Chen and Arculus 1994; and others). In the following section previously published data from mafic xenoliths collected in the NVF are compared with the results from this study in an attempt to constrain the origin of the mafic xenolith suite as well as to provide constraints on the distribution and abundance of the various lithologies and geochemical groups within the lower crust of the Colorado Plateau.

3.2. NVF Mafic Xenoliths

Pervious works have separated xenoliths from NVF into six lithologic groups: 1) garnet granulites; 2) pyroxene granulites; 3) garnet amphibolites; 4) amphibolites; and 5) meta-igneous; 6) Volcanogic (Wendlandt, 1993; O'Brien, 1983; Ehrenberg and Griffin, 1979; Broadhurst, 1986; McGetchin and Silver, 1972). These lithologies are found in varying abundances at dikes and diatremes in the NVF (see appendix E)(Fig. 3.1.).

The mafic xenoliths were collected from six localities covering an area over 10,000 km^2 (see Fig. 1.1 in Geology Section). It is interesting to compare samples collected at each location to see if any lithologic or chemical groups can be correlated with geographical area. The fact that the kimberlite diatremes produce more and a greater variety of crustal xenoliths may introduce a bias when considering the abundance of these rock types and of each geochemical group within the crust of the Colorado Plateau (Fig.3.1.). However, even with the limited distribution of xenoliths from the minette diatremes 3 out of the 8 geochemical groups are represented in the minette as well as the kimberlite diatremes in the samples collected in the current study. If Group I is ignored since it occurs as a distinct geochemical and lithological

(gabbro) group found only at the Moses Rock diatreme, and quite possibly represents a sill or dike that has been intruded into the crust, then the xenoliths from the minette locations are found in 3 out of the 7 geochemical groups. Thus, nearly 45% of the groups are represented in the minette xenolith population which represents only 4 of the 24 total xenolith samples that define these geochemical groups. With these observations taken into consideration and that the minette and kimberlite sampling localities are nearly 100 km apart, it is likely that the 8 geochemical groups make up significant portions of the crust in the Colorado plateau.

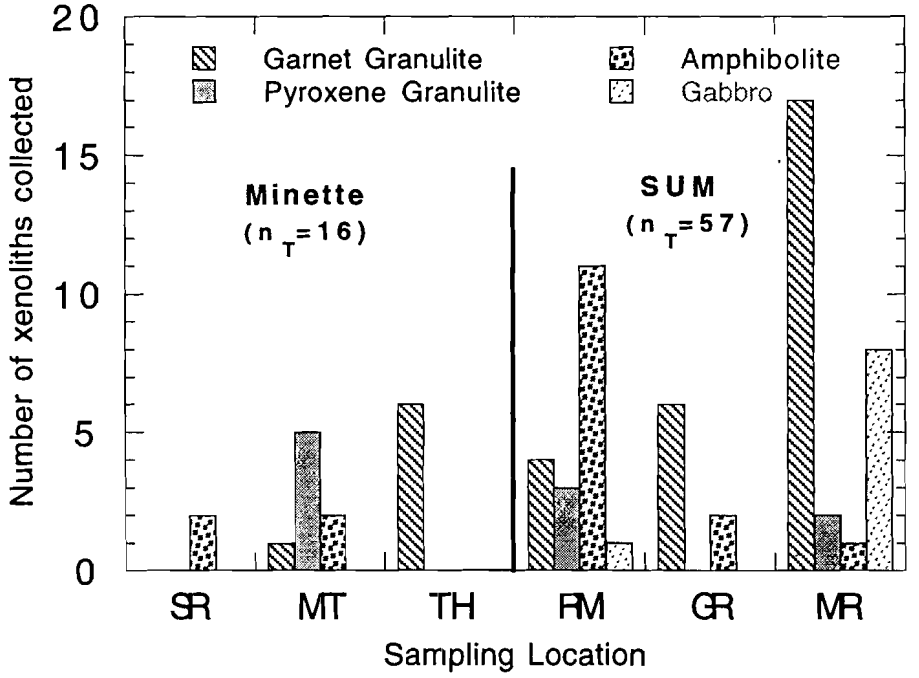

Fig. 3.1. Histrogram of lithologic types and sampling locality. Xenolith count based on samples collected in this study.(n_T = total number of xenoliths for host type) SUM=kimberlite diatremes.

The majority of mafic xenoliths from the NVF have basaltic calc-alkaline compositions (Figure 3.2). Apart from this general compositional homogeneity, the NVF xenoliths are quite heterogeneous when considering trace element abundances. As pointed out in the preceding chapter, eight geochemical populations can be defined by trace element ratios and REE on xenoliths collected from the 6 diatremes and dikes

reported in this study. Prior to this study, REE data on NVF mafic xenoliths were limited to the work of Wendlandt et al. (1993) on xenoliths collected at Moses Rock diatreme, Mules Ear Diatreme, Garnet Ridge Diatreme, and The Thumb and of O'Brien (1983) on xenoliths collected at the Buell Park-Green Knobs Diatremes. Chondrite normalized REE distribution patterns for all published data from NVF mafic xenoliths are summarized in Figures 3.3 a-d & 3.4 a-e. Published mafic xenolith analyses are sorted and plotted with one of the 8 geochemical groups that is most similar. Nineteen of the 25 mafic xenoliths from the previous two studies are similar to 6 of the 8 geochemical groups defined in this study. Seven of 13 samples from Buell Park are similar to 3 geochemical groups defined in this study. The remaining six samples (Fig. 3.3a) are homogeneous and have distinct REE element distributions that are not grouped with any of the groups defined in this study although the six samples somewhat resemble Group II xenoliths. These samples may represent a metamorphosed gabbroic sill or dike that is locally dominant. The strong positive Eu anomaly is characteristic of plagioclase accumulation exhibited by gabbroic rocks. All of the Four Corners mafic xenolith samples from Wendlandt et al. (1993) can be grouped into five of the eight groups. The strong correlation of geochemistry of the mafic xenoliths from the northern to the southernmost portions of NVF is remarkable considering the lateral distances between the various host dikes and diatremes. The similarity of REE distributions in the xenoliths over such a large area may attest to the lateral continuity of the various geochemical sources within the crust of the Colorado plateau.

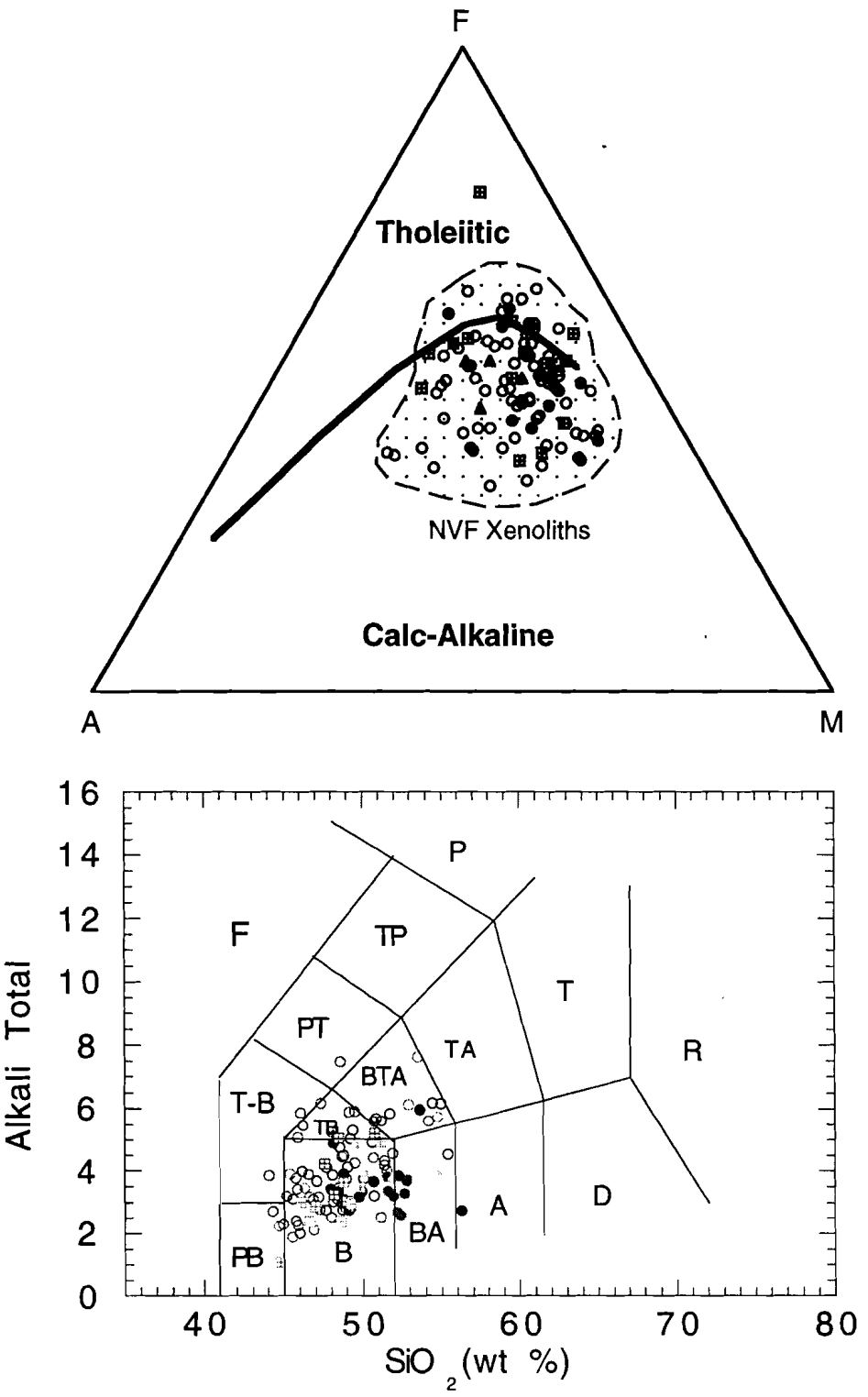

Fig. 3.2. AFM & TAS Diagrams for NVF Xenoliths. AFM: A=K $_2$O + Na$_2$O ; F= total Fe ; M= MgO; TAS: Alkali Total= Na $_2$O + K$_2$O ; Crossed boxes=mafic xenoliths (Wendlandt et al.,1993); Solid Circles=Buell Park Mafic Xenoliths (O'Brien, 1983); Solid triangles=mafic xenoliths from Four Corners (Broadhurst, 1986); Open circles=four corners xenoliths (this study); solid line calc-alkaline-tholeiitic boundary (after Kuno, 1968). Total Fe calculated from (Fe2O3* 0.8998). B=Basalt; BA=Basaltic Andesite; A=Andesite; D=Dacite; R=Rhyolite; T=Trachyte; TA=Trachyandesite; BTA=Basaltic Trachyandesite; TB=Trachybasalt; PB=Picrobasalt; T-B= Tephrite-Basanite; PT=Phonotephrite; TP=Tephriphonolite; P=Phonolite; F=Fiodite (after Le Maitre et al., 1989).

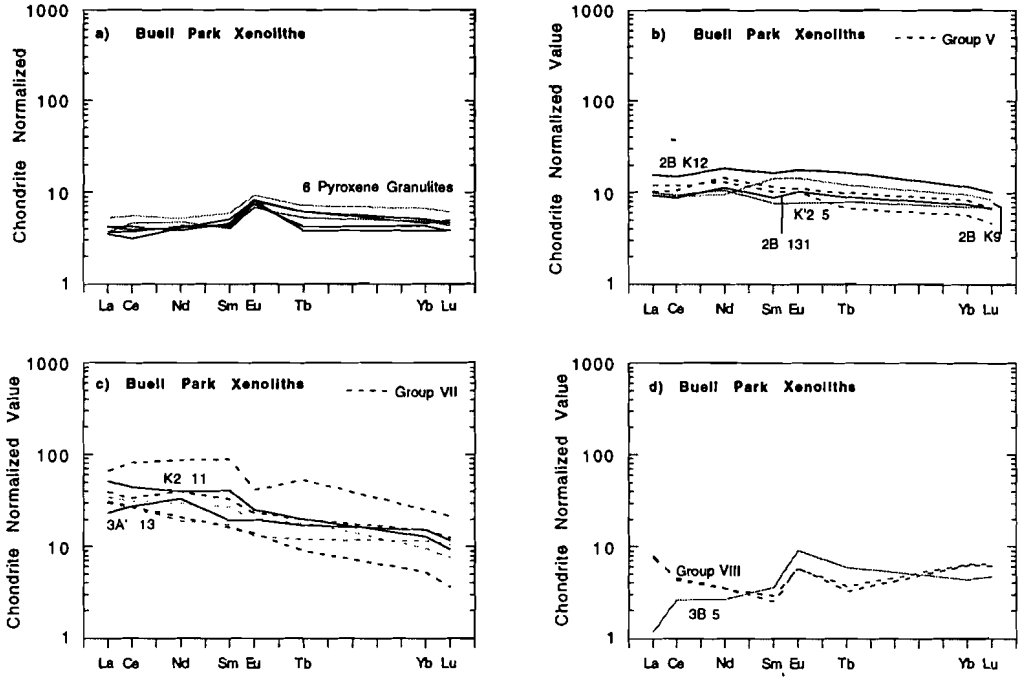

Fig. 3.3 a-d. Chondrite normalized REE distributions for NVF mafic xenoliths. Dashed lines indicate results from this study; solid lines represent previous results. Buell Park mafic xenolith data from O'Brien (1983). Chondrite values from Haskin et al., 1968.

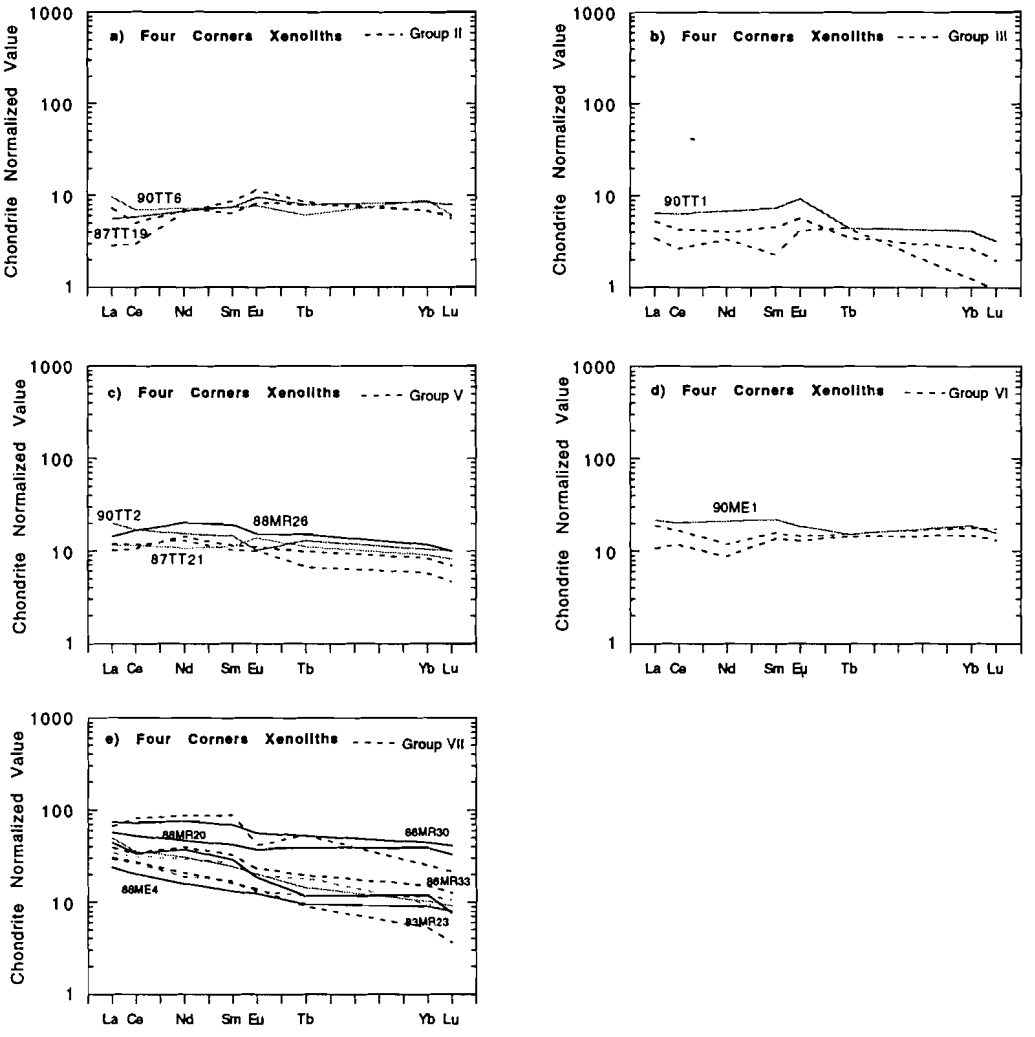

Fig. 3.4 a-e. Chondrite Normalized REE distributions for NVF mafic xenoliths. Dashed lines indicate results from this study; solid lines represent previous results. Four Corners mafic xenolith data from Wendlandt et al. (1993). (Chondrite values after Haskin et al., 1968).

3.3 Age of NVF Mafic Xenoliths

When considering the origin of the NVF xenoliths it is necessary to have constraints on the age of the xenolith suite. Wendlandt et al. (1993) reported Sm/Nd model ages for a suite of granulite and garnet amphibolite xenoliths from diatremes in the NVF. Since both Moses Rock and the Thumb diatremes were sampled by Wendlandt et al. (1993) as well as in this study, Nd isotopic data on similar samples can be evaluated with the current xenolith results. Wendlandt et al. (1993) found that Nd model ages of thirteen of the fifteen xenoliths fell between 1.63 and 1.98 Ga and that these ages are consistent with Proterozoic crustal accretion. Wendlandt et al. (1993 & 1996) concluded that

these results do not support the occurance of any young underplating of mafic material to the lower crust. Two of the samples from the Thumb diatreme have young Nd Model ages of 0.48 and 1.15 Ga and it could be argued that they represent additions to the crust since 1.63 Ga. However, several observations may refute this interpretation. First, four of the five youngest model ages are from xenoliths from the Thumb diatreme. Second, all of the Thumb samples observed in this study, as well as by previous authors (Wendlandt et al., 1993; O'Brien, 1983; Ehrenberg and Griffin, 1979), have significant quantities of dark material occurring along grain boundaries and intergranular cracks. This material may result from partial melting or intrusion of host material. The systematically younger ages for four out of five Thumb xenoliths and the occurrence of intergranular material only in the Thumb samples may indicate a preferential sampling of a large quantity of this host material which could explain the apparent younger ages for the Thumb xenoliths.

Based on the similarities between lithology and geochemistry of mafic xenoliths collected by Wendlandt et al. (1993 & 1996) and xenolith samples collected in this study, it is likely that the Nd model ages presented by Wendlandt et al (1993 & 1996) are representative of the age distribution of the current xenolith suite. Thus, it appears that the crust within the NVF is Proterozoic in age and that there is no isotopic evidence for any significant later additions to the crust.

3.4 Mafic Xenolith Petrogenesis

Granulite and amphibolite grade mafic xenoliths may have been formed from several different processes including: basaltic melts or cumulates that crystallized at deep crustal levels and underwent metamorphism in situ, or they could represent restite after extraction of a partial melt (Rudnick, 1992). Given these possible origins, each of the eight groups defined for the NVF mafic xenolith population is evaluated using criteria established by previous authors (Rudnick, 1992; Rudnick and Taylor, 1987; Rudnick et al., 1986)

Xenolith Groups I, II, III, V, and VI are interpreted as mafic cumulates. These samples have positive Sr anomalies coupled with small positive Eu anomalies and high Al_2O_3 (14-22 wt%) which is consistent with plagioclase accumulation (Figs. 2.9 & 2.15). Groups III and V are HREE depleted relative to LREE, and all show REE patterns that may reflect the influence of pyroxene accumulation (Ehrenberg, 1981)(Fig. 2.15). The lack of an strong positive Eu anomaly in many of these samples suggests that the plagioclase may have crystallized from an interstitial melt or exsolved from high pressure pyroxene (Rudnick and Taylor, 1987; Rudnick et al., 1986). Cumulates show a decreasing abundance of compatible elements with a relatively constant low incompatible element abundance (Nielson, 1987; Cocherie, 1986), which is characteristic of the mafic xenoliths in these groups (Fig. 2.10 a &b).

Xenolith Groups IV and VII show REE abundances of 3-300x chondrite, LREE enrichment and no Eu anomalies (excluding MR46 which has a strong negative Eu anomaly), all of which are consistent with a non-cumulate melt origin for these xenoliths (Rudnick, 1992; Rudnick and Taylor, 1987; Rudnick et al., 1986; Loock et al., 1990; O'Brien 1983)(Fig. 2.15). However, these mafic xenoliths also have low Mg numbers between 26 and 42, a negative correlation of SiO2 with MgO, and a negative correlation of incompatible to compatible trace elements (Fig. 2.10 a & b), all of which are consistent with FXL processes as the main control of chemical variations (Nielsen, 1987; Cocherie, 1986). Several of the mafic xenoliths in those 2 groups also have high Al2O3 (16-20%), which may indicate the effects of crystal accumulation (Rudnick,1992)(Fig. 2.5). These groups have low Cr and Ni abundances, <500 ppm and <200 ppm respectively. Melts traditionally have a much higher abundance of these elements. A cumulate origin for these groups is therefore favored, however it is difficult to give any solid evidence due to the possible mobility of some of the incompatible elements during alteration.

Group VIII xenoliths are interpreted to be either restite or cumulate in origin. Group VIII xenoliths have positive Eu anomalies, high Sr content (>600 ppm) and high Al2O3 concentrations (>20%), which is consistent with plagioclase enrichment by crystal accumulation or melt extraction leaving plagioclase in the residua (Rudnick and Taylor, 1987)(Figs. 2.5, 2.9, & 2.15). Group VIII xenoliths have HREE enrichment which is interpreted to be the result of fractionation of HREE into garnet, which is abundant within the samples. Distinguishing between cumulates and restite in granulite and amphibolite grade xenoliths historically has been a difficult task, but Rudnick and Taylor (1987) suggest that the variation in incompatible and compatible trace elements (i.e. Cr, Ni, vs. Zr) can be used. However, for Group VIII xenoliths there are only two samples, which makes that method inconclusive. Group VIII xenoliths show some of the highest abundances of SiO_2 and lowest MgO and Fe_2O_3, which one would not expect to be the case for a sample of restite (Fig 2.5). Given these factors, a cumulate origin for the Group VIII mafic xenoliths is preferred, although due to the limited number of samples it is difficult to resolve.

3.5 Tectonic Setting of Protolith

Given the chemical heterogeneity of the NVF mafic xenoliths resulting from mobilization of some LILE and recrystallization during high-pressure conditions, it is difficult to use traditional bi-variant trace or major element tectonic discrimination diagrams with confidence. However, when trace element ratio diagrams are employed they can minimize the effects of magmatic and metamorphic processes (Condie, 1996). Primitive mantle normalized trace element diagrams can also be a useful indicator of distinguishing basaltic sources.

With few exceptions, on PM-n spidergrams, the NVF mafic xenoliths show depletions in Th, Ta, Nb, Hf, & Zr and enrichment in Sr, K, Rb, and Ba characteristic of subduction related signatures (Pearce, 1982) (Fig. 2.9). Enrichment of LILE and high variability in LILE abundances on PM-n spidergrams is characteristic of mantle

metasomatic processes in a subduction-related environment (Pearce, 1982; Pearce, 1983). On a Th-Hf-Ta diagram (Wood, 1980), 25 of the 32 NVF mafic xenoliths define a region that plots over the island arc basalt field (IAB) defined by Wood (1980) (Fig. 3.5). On a plot of Th/Yb-Ta/Yb (Pearce, 1982) the NVF xenoliths have high Th/Yb (>0.07) characteristic of subduction-related material (Fig. 3.6). Thirty-one of 34 samples define a region that falls within the island arc region defined by Pearce (1983). Of the seven samples that plot away from the majority of NVF mafic samples on Figure 3.5, five are from Moses Rock Dike. Three of these samples (88MR26, 86MR23, 86MR33) also plot outside the NVF region in Figure 3.6. These anomalies may indicate alteration during metamorphism or metasomatism resulting in the loss of Th which is singular to Moses Rock.

The origin of the NVF mafic xenoliths within a subduction zone environment is consistent with results from mafic xenoliths from the neighboring San Francisco Volcanic Field and exposed Proterozoic crust outside the Colorado Plateau (Arizona and Colorado) (Nealy and Unruh, 1991; Copeland and Condie, 1986; Boardman and Condie; 1986). It has been determined by previous authors that the mafic xenoliths from the NVF yield Nd Model ages between 1.8-2.0 Ga (Wendlandt et al., 1993). Thus, the crust in the Colorado Plateau is not likely to have been significantly altered since it was formed in the Mid-Proterozoic. In light of this, any modification of the mafic xenoliths must have occurred during the Proterozoic crust-forming event. As previously mentioned, the eight NVF groups show chemical variations consistent with an origin in an arc environment. The chemical variations within the eight geochemical groups may be the result of: 1) metasomatism and subsequent melting of a *depleted* mantle wedge by infiltration of subduction-related fluids; 2) metasomatism and melting of an *enriched* mantle wedge by infiltration of subduction-related fluids; 3) interaction of melts from the previous two sources with sediment-derived melts; 4) crustal contamination

during emplacement of melts (Weaver and Tarney, 1982; Pearce, 1982; Pearce, 1983; Saunders et al., 1990). Distinguishing between these sources is problematic.

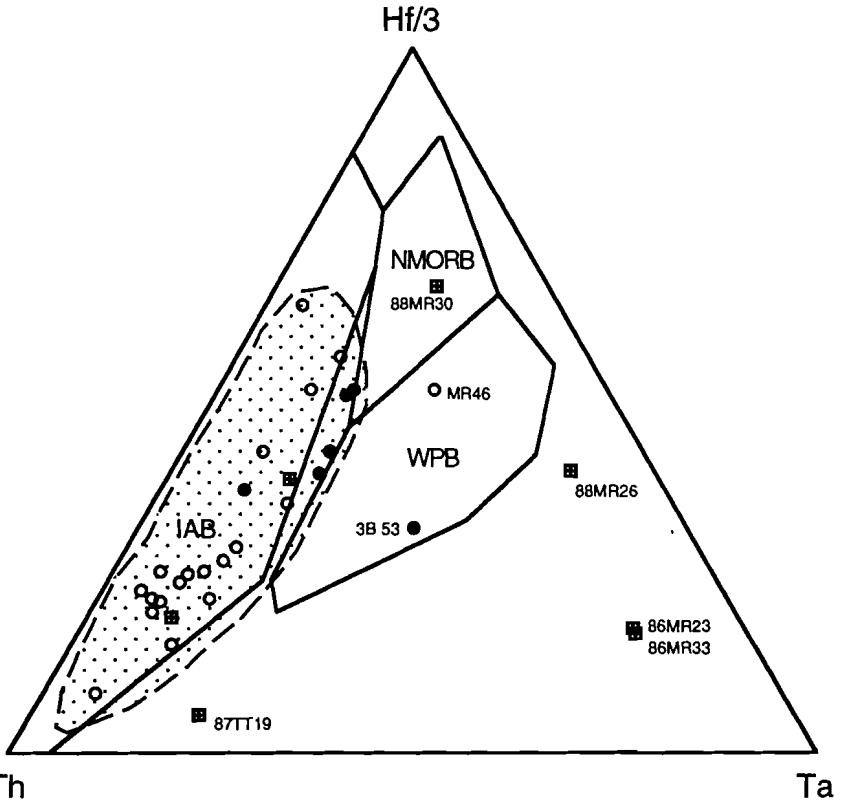

Fig. 3.5. Hf/3-Th-Ta Diagram for NVF mafic Xenoliths. IAB= Island Arc Basalt; WPB= Within Plate Basalt; fields defined by Wood (1980). Open circles=mafic xenoliths from this study; filled circles=mafic xenoliths from O'Brien (1983); crossed boxes=mafic xenoliths from Wendlandt et al. (1993).

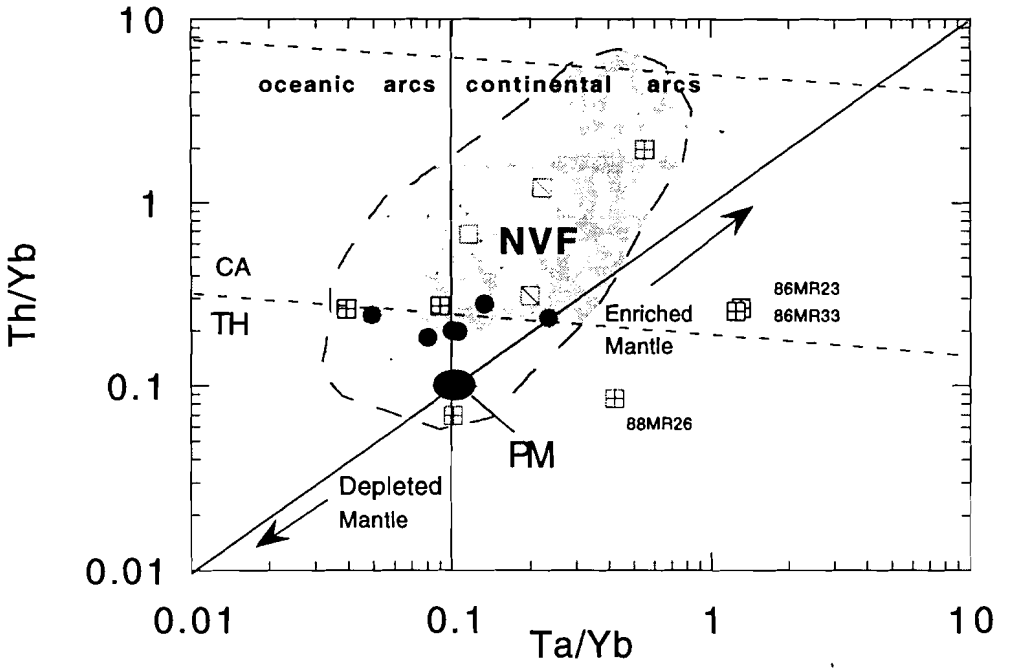

Fig. 3.6. Th/Yb-Ta/Yb after Pearce (1982). Crossed boxes=mafic xenoliths from NVF (Wendlandt et al. 1993); slashed boxes= eclogites from NVF (Wendlandt et al. 1993); solid circles=mafic xenoliths from Buell Park (O'Brien, 1982); shaded region NVF mafic xenolith population from this study; arrows indicate direction of enrichment or depletion from a primitive mantle source (after Pearce, 1983).

Groups II, V, VI and VIII show REE patterns similar to gabbroic to tonalitic rocks from the Talkteena Arc and gabbroic to dioritic rocks from the Canyon Mt. ocean arc (Pearcy et al., 1989) (Fig. 3.7). These samples may represent unmodified ocean arc material (i.e. source = metasomotized *depleted* mantle wedge). However, the chemical affinities of the NVF mafic xenoliths Groups I, IV & VII are similar to calc-alkaline melts from active continental margins (e.g. Andes)(Fig. 3.7). This would suggest that these groups have been significantly altered by contamination with upper crustal material (sediments or contamination during emplacement) or originate within a metasomatized enriched mantle wedge (Pearce, 1983) .

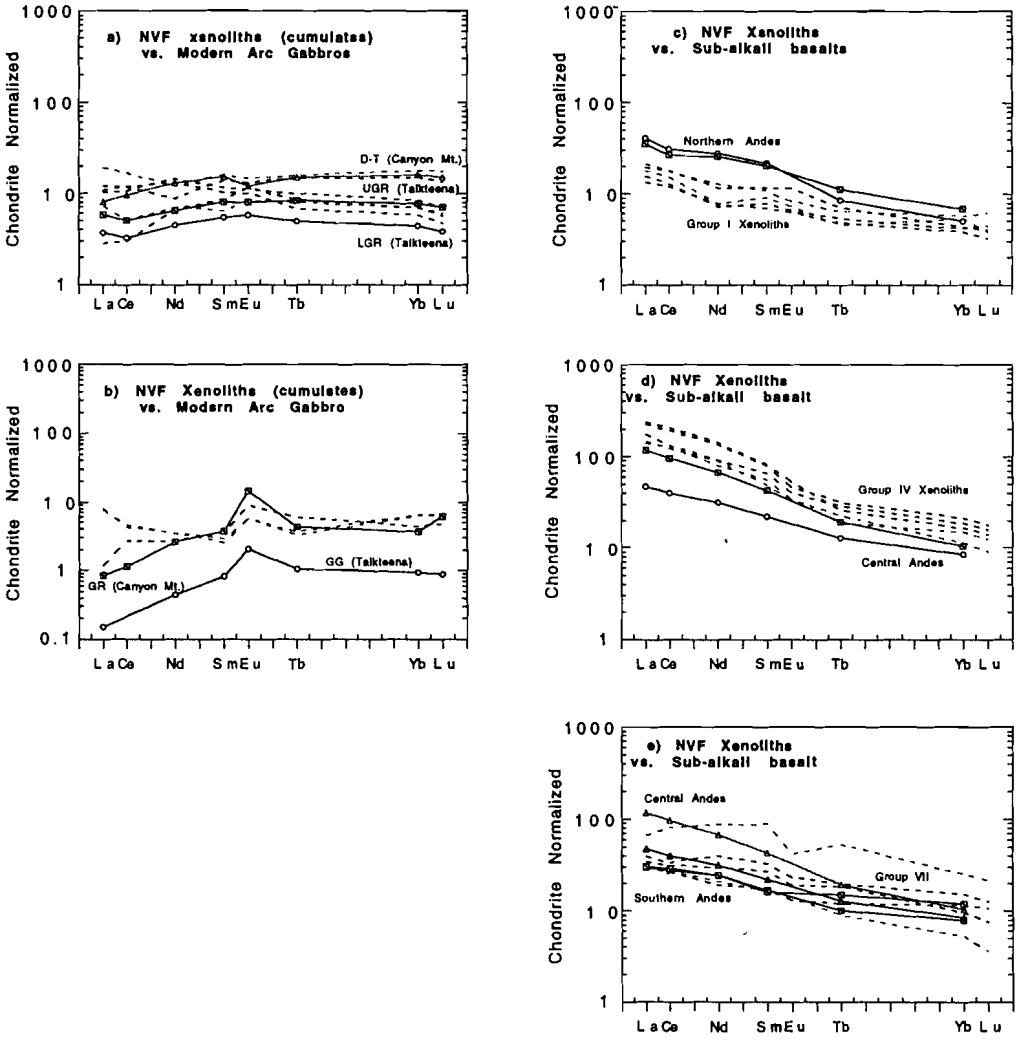

Fig. 3.7 a-e. Chondrite normalized REE distributions for the NVF xenoiths and arc related volcanic rocks. a) NVF xenolith groups II, V, & VI vs. Modern arc gabbro from Canyon Mt. and Talkteena Arcs; D-T=Dioritic-Trondhjemitic, UGR=upper gabbroic rocks, LGR=lower gabbro rocks; b) NVF xenolith group V vs. Modern arc gabbro from Canyon Mt. and Talkteena Arcs; GG=garnet gabbro, GR=gabbroic rocks; c) NVF xenolith group I vs. Sub-alkali basalt from Andes; Northern Anedes=averages of Northern Andes basalt. d) NVF xenolith group IV vs. Sub-alkali basalt from Andes; Central Andes= averages of central Andes basalts; e) NVF group VII vs. Sub-alkali basalt from central and southern Andes. (Talkteena and Canyon Mt. Data from Pearcy et al., 1989; Andesite data from Thorpe et al., 1984; Marriner and Milward, 1984; Hickey et al., 1986).

Chapter 4: Conclusions

Thirty-three of the 73 xenoliths in this study are grouped into eight distinct geochemical populations. These groups can be traced laterally throughout the NVF. Of these eight groups, six are similar to NVF xenoliths analyzed in previous studies. The ability to recognize distinct geochemical groups from the northernmost to the southernmost regions of the NVF suggests that the crust beneath the this volcanic province is laterally continuous. Two groups, Group I (this study) and 6 pyroxene granulites (O'Brien, 1983), have been identified as local gabbroic sills or dikes. By combining these resluts with pressure-temperature studies, a vertical distribution of these geochemcial regions beneath the NVF may be obtained.

The occurrence of paragneiss xenoliths with 1.84-2.0 Ga Nd model ages with the NVF mafic xenoliths indicates that upper continental crustal sediments were tectonically emplaced during the Proterozoic accretionary event (Wendlandt, 1992). The existence of tectonically emplaced sedimentary material may indicate sediments as a potential source of the enriched xenoliths rather than an enriched continental lithosphere. There is sufficient evidence for occurrence of unmodified arc material (depleted wedge source), continental margin melts (enriched wedge source), and upper crustal meta-sedimentary material at mid to lower crustal levels, which suggests a complex interaction between multiple sources. There is no geochemical or isotopic evidence for later additions to the lower crust after the primary crustal forming event during the Early Proterozoic (1.75-1.70 Ga)(Wendlandt et al., 1993 & 1996). These observations suggest that continental lower crust formed by a complex process within a heterogeneously enriched mantle wedge in a subduction environment resulting in vertical accretion of melts from a metasomatized mantle wedge during horizontal accretion of oceanic island arc terranes (e.g. Weaver and Tarney, 1982; Condie, 1992).

References

Alibert, C., Michard, A., and Albarede, F., (1986). Isotope and trace element geochemistry of Colorado Plateau volcanics. Geochimica Cosmochimica Acta, 50, 2735-2750.

Blakey, R. C., and Baars, D.L. (1987). Moument Valley, Arizona and Utah. In S. S. Beaus (Ed.), Rocky Mountain Section of the Geological Society of America, 2. Geological Society of America.

Boardman, S. J., and Condie, K.C. (1986). Early Proterozoic bimodal volcanic rocks in central Colorado, U.S.A., Part II: geochemistry, petrogenesis, and tectonic setting. Precambrian Research, 34, 37-68.

Broadhurst, J. R. (1986). Mineral reactions in xenoliths from the Colorado Plateau; implications for lower crustal conditions and fluid composition. Geological Society Special Publication, 24, 331-349.

Chen, W., Arculus, R.J. (1995). Geochemical and isotopic characteristics of lower crustal xenoliths, San Francisco Volcanic Field, Arizona, U.S.A. Lithos, 36, 203-225.

Cocherie, A. (1986). Systematic use of trace element distribution patterns in log-log diagrams for plutonic suites. Geochemica et Cosmochimica Acta, 50, 2217-2522.

Condie, K. C. (1992). Proterozoic terranes and continental accretion in Southwestern North America. In K.C. Condie (Ed), Proterozoic Crustal Evolution, 447-478.

Condie, K. C. (1996). Sources of mafic dyke swarms; constraints from Th/Ta-La/Yb Ratios. Precambrian Research, in press.

Copeland, P., and Condie, K.C. (1986). Geochemistry and tectonic setting of lower Proterozoic supracrustal rocks of the Pinal Schist, southeastern Arizona. Geological Society of America Bulletin, 97, 1512-1520.

Delaney, P. T., and Pollard, D.D. (1981). Deformation of host rocks and flow of magma during growth of minette dikes and breccia-bearing intrusions near Ship Rock, New Mexico. Geological Survey Professional Paper 1202.

Delaney, P. T. (1987). Ship Rock, New Mexico: the vent of a violent volcanic eruption. In S. S. Beus (Ed.), Rocky Mountain Section of the Geologic Society of America, 2 (pp. 411-416).

Ehrenberg, S. N., and Griffin, W.L. (1979). Garnet granulite and associated xenoliths in minette and serpentinite diatremes of the Colorado Plateau. Geology, 7, 483-487.

Ehrenberg, S. N. (1981). Rare earth element geochemistry of garnet lherzolite and megacrystalline nodules from minette of the Colorado Plateau province. Earth and Planetary Science Letters, 57, 191-210.

Ehrenberg, S. N. (1982). Petrogenesis of garnet lherzolite and megacrystalline nodules from the Thumb, Navajo Volcanic field. Journal of Petrology _, 23 (4), 507-547.

Fitzsimmons, J. P. (1973). Tertiary igneous rocks of the Navajo Country, Arizona, New Mexico, and Utah. In H. L. James (Ed.), New Mexico Geological Society Field Conference, 24 (pp. 106-109).

Gregory, H. (1917). Geology of the Navajo Country. USGS Professional Paper, 93 , 161.

Govindaraju, K. (1994). 1994 Compilation of working values and sample description for 383 geostandards. Geostandards Newsletter, Special Issue, 18 , 1-158.

Hallett, B. R., and Kyle, P.R. (1993). XRF and INAA Determinations of Major and Trace Elements in Geological Survey of Japan Igneous and Sedimentary Rock Standards. Geostandards Newsletter, 17 (1), 127-133.

Haskin L.A., H. M. A., Frey F.A., Wildman T.R. (1968). Relative and absolute terrestrial abundances of the rare earths. In A. L.H. (Ed.), Origin and distribution of the elements (pp. 889-911). Oxford: Pergamon.

Haynes, D. D., Vogel, J.D., and Wyant, D.G. (1972). Geology, structure, and uranium deposits of the Cortez Quadrangle, Colorado and Utah. InUSGS Map I-629.

Hickey, R. L., Frey, F.A., and Gerlach, D.C. (1986). Multiple sources for basaltic arc rocks from the southern volcanic zone of the Andes (34-31°S):trace element and isotopic evidence for contributions from subducted oceanic crust, mantle and continental crust. Journal of Geophysical Research , 91 , 5963-83.

Karlstrom, K.E., and Bowring, S.A. (1988). Early Proterozoic assembly of tectonostratigraphic terranes in southwestern North America. Journal of Geology, 96 , 561-576.

Kay, R. W., Kay,S.M, and Arculus, R.J. (1992). Magma genesis and crustal processing. In A. R. J. Fountian D.M. Kay R.W. (Ed.), Developments in Geotectonics: Continental Lower Crust (pp. 434-445). Elsevier.

Kempton, P. D., and Dungan, M.A. (1989). Geology and petrology of basalt and included mafic, ultramafic, and granulitic xenoliths of the Geronimo volcanic field, southeastern Arizona. In Silicic Calderas to Mantle Nodules: Creatceous to Quaternary volcanism southeastern basin and range provence, Arizona and New Mexico _, 46 (pp. 161-173). NM Bureau of Mines and Min. Res. Mem.

Kuno, H. (1968). Differentiation of basalt magmas. In H. H. Hess Poldervaart, A. (Ed.), Basalts: The Poldervaart treatise on rocks of basaltic composition _ (pp. 623-688). New York: Interscience.

Laughlin, A. W., Aldrich, M.J., Jr, Shafiqullah, M., and Husler, J. (1986). Tectonic implications of the age, composition, and orientation of lamprophyre dikes, Najvo Volcanic Field, AZ. EPSL, 76 , 361-374.

Laughlin, A. W., and Charles, R.W. (1992). Lamprophyric Dikes of the Navajo volcanic field. In S. C. Semken (Ed.), Western Slope Conference Field Guide, (pp. 41-55). Four Corners: Navajo Community College.

Le Maitre, R. W., Bateman, P., Dudek, A., Keller, J., Lameyre Le Bas, M.J., Sabine, P.A., Sorensen, H., Streckeisen A., Woodley, A.R., Zanettin, B. (1989). A classification of igneous rocks and glossary of terms . Oxford: Backwell.

Loock, G., Stosch, H.G., and Seck, H.A. (1990). Granulite facies lower crustal xenoliths from the Eifel, West Germany: petrological and geochemical aspects. Contrib. Mineral. Petrology , 105 , 25-41.

Marriner, G. F., and Millward, D. (1984). The petrology and geochemistry of Cretaceous to Recent volcanism in Columbia: the magmatic history of an accretionary plate margin. Journal Geological Society of London , 141 , 473-86.

McGetchin, T., and Silver, LT (1972). A crustal-upper-mantle model for the Colorado Plateau based on observations of crystalline rock fragments in the Moses Rock dike. Journal of Geophysical Research , 77 , 7022-7037.

McGetchin, T. R., Nikhanj, Y.S., and Chodos, A.A. (1973). Carbonatite-Kimberlite relations in the Cane Valley diatreme, San Juan County, Utah. Journal of Geophysical Research, 78 (11), 1854-1869.

McGetchin, T. R., Smith, D., Ehrenberg, S.N., Roden, M., and Wilshire, H.G. (1977). Navajo kimberlites and minettes. In Second International Kimberlite Conference , (pp. 37).

Naeser, C. W. (1971). Geochronology of the Najvo-Hopi diatremes, Four Corners Area. Journal of Geophysical Research , 76 , 4978-4985.

Nealey, D. L., and Unruh, D.M. (1991). Geochemistry and isotopic characteristics of deep crustal xenoliths from Tule Tank, San Francisco Volcanic Field, Northern Arizona. Arizona Geological Society Digest , 19 , 153-163.

Neilsen, R. L. (1988). A model for the simulation of combined major and trace element liquid lines of descent. Geochimica et Cosmochimica Acta, 52 , 27-38.

Northrop, S. A. (1973). Lexicon of stratigraphic names of the Monument Valley-Four Corners Region. In H. L. James (Ed.), New Mexico Geological Society Field Conference , 24 (pp. 157-176).

O'Brien, T. F. (1983). Evidience for the nature of the lower crust beneath the central Colorado Plateau as derived from xenoliths in the Buell Park-Green Knobs Diatremes . Ph.D., Cornell University.

O'Sullivan, R. B., and Beikman, H.M. (1963). Geology, structure, and uranium deposits of the Shiprock Quadrangle New Mexico and Arizona. InUSGS Map I-345.

O'Sullivan, R. B., and Craig, L.C. (1973). Jurassic rocks of northeast Arizona and adjacent areas. In H. L. James (Ed.), New Mexcio Geological Society Field Conference , 24th (pp. 79-85).

O'Sullivan, R. B., and Green, M.W. (1973). Triassic rocks of northeast Arizona and adjacent areas. In H. L. James (Ed.), New Mexico Geologic Society Field Conference, 24th (pp. 72-78).

Pearce, J. A. (1982). Trace element characteristics of lavas from destructive plate boundaries. In R. S. Thorpe (Ed.), Andesites New York: John Wiley & Sons.

Pearce, J. A. (1983). Role of sub-continental lithosphere in magma genesis at active continental margins. In N. M. J. Hawkesworth C.J. (Ed.), Continental Basalts and Mantle Xenoliths (pp. 230-249). Cambridge: Shiva Publishing Ltd.

Pearcy, L. G., DeBari, S.M., and Sleep, N.H. (1989). Mass Balance calculations for two sections of island arc crust and implications for the formation of continents. Earth and Planetary Science Letters, 96, 427-442.

Percival, J. A., Fountian, D.M., and Salisbury, M.H. (1992). Exposed crustal sections as windows on the lower crust. In A. R. J. Fountian D.M. Kay R.W. (Ed.), Developments in Geotectonics: Continental Lower Crust (pp. 317-362). Elsevier.

Roden, M. F. (1981). Origin of coexisting minette and ultramafic breccia; Navajo volcanic field. Contrib. Mineral. Petrol., 77, 195-206.

Rudnick, R. L., McDonough, W.F., McCulloch, M.T., and Taylor, S.R. (1986). Lower crustal xenoliths from Queensland, Australia: Evidience for deep crustal assimilation and fractionation of continental basalts. Geochimica et Cosmochimica Acta, 50, 1099-1115.

Rudnick, R. L., and Taylor, S.R. (1987). The composition and petrogenesis of the lower crust: A xenolith study. Journal of Geophysical Resarch, 92, 13,981-14,005.

Rudnick, R. L. (1992). Xenoliths; samples of the lower continental crust. In D. M. Fountian Arculus, R., and Kay, R.W. (Ed.), Continental Lower Crust (pp. 269-316). New York: Elsevier.

Saunders, A. D., Norry, M.J., and Tarney, J. (1990). Fluid influence on the trace element compositions of subduction zone magmas. In P. K. T. Tarney J. Knipe R.J., Dewey J.F. (Ed.), The behaviour and influence of fluids in subduction zones: Proceedings of a Royal Society discussion metting held on 8 and 9 November 1990 Cambridge: University Press.

Semken, S. C. (1992). Field guide to a geologic excursion in the northeastern Navajo Nation. In S. C. Semken (Ed.), Western Slope Geologic Field Conference, . Navajo Community College.

Sun, S. S., McDonough, W.F. (1989). Chemical and Isotopic systematics of ocean basalts: implications for mantle composition and processes. In A. D. Saunders Norry, M.J. (Ed.), Magmatism in ocean basins (pp. 313-345). London: Geological Society of London.

Thompson, R. N. (1984). Dispatches from the basalt front. In Proc. Geol. Ass., 95 (pp. 249-262).

Thorpe, R. S., Francis, P.W., and O'Callaghan, L.O. (1984). Relative roles of source composition, fractional crystallization and crustal contamination in the petrogenesis of Andean volcanic rocks. Phil Trans R. Soc. Lond., A310 (675-92).

Weaver, B. L., and Tarney, J. (1982). Andesitic magmatism and continental growth. In R. S. Thorpe (Ed.), Andesites (pp. 639-661). New York.

Wendlandt, E., Depaolo, D.J., Baldridge, W.S. (1993). Nd and Sr isotope chronostratigraphy of Colorado Plateau lithosphere: implications for magmatic and tectonic underplating of the continental crust. Earth and Planetary Science Letters, 116, 23-43.

Wendlandt, E., Depaolo, D.J., and Baldridge, W.S. (1996). Thermal history of Colorado Plateau lithosphere from Sm-Nd mineral geochronology of xenoliths. GSA Bulletin, 108 (7), 757-767.

Williams, H. (1936). Pliocene volcanoes of the Najvo-Hopi country. Geol. Soc. Am. Bull., 47, 111-172.

Wood, D. A. (1980). The application of a Th-Hf-Ta diagram to problems of tectonomagmatic classification and to establishing the nature of crustal contamination of basaltic lavas of the British Tertiary volcanic province. Earth and Planetary Science Letters, 50, 11-30.

Woodward, L. A. (1973). Structural framework and tectonic evolution of the Four Corners region of the Colorado Plateau. In H. L. James (Ed.), New Mexico Geological Society Field Conference, 24 (pp. 94-98).

Young, R. G. (1973). Cretaceous stratigraphy of the Four Corners area. In H. L. James (Ed.), New Mexico Geological Society Field Conference, 24 (pp. 86-93).

Appendix A
Sampling and Sample Preparation

A.1 Sampling

Over 250 xenolith samples were collected from the four corners area of Colorado, New Mexico, Arizona, and Utah, during a one week field excursion conducted in October of 1994 (sampling localities discussed in Chapter 1). Many xenolith types were collected including: granitoid, metasediment, felsic granulite, mafic granulite, and amphibolite. Ultramafic and eclogitic xenoliths were avoided since they have been addressed by several previous studies and the current project required a selection of crustal xenoliths. Field descriptions were recorded and the xenoliths were divided broadly into the five rock types mentioned above. Care was taken to select samples that were larger than 6 cm in diameter and samples without a highly weathered appearance in efforts to obtain the least altered samples. The xenolith samples were divided in the following manner: 1) each granitoid xenolith sample collected in the field was split at the time of collection, one piece was taken for chemical analysis at New Mexico Tech, and the remainder was collected by W.R. Van Schmus for U/Pb zircon studies at University of Kansas; 2) metasediment and mafic xenoliths were taken to New Mexico Tech and divided in the following manner: each xenolith was cut in half with a diamond blade rock saw, one half was kept for a reference hand sample and the other was divided into two pieces, one for chemical analysis and one for a thin section billet. Thin section billets from the mafic and metasedimentary xenoliths were sent to J. Selverstone at the University of New Mexico for microprobe analysis and P-T determinations. Of the xenolith samples, 88 were determined to be mafic to intermediate and selected for chemical analysis; 40 of these samples were selected for thin section study.

A.2 Sample Preparation

The geochemical sample was trimmed to remove weathered rind or host material. The trimmed chip was first crushed in an electrical steel jaw crusher to 1-2 cm chips. These chips were then ground to less than 1-2 mm sized chips by a Bico pulverizer, using porcelain plates. At this time the sample was split; one split for INAA analysis was hand ground with ceramic mortar and pastel, and the second split was ground to a fine powder in a steel swing mill(TEMA). Pure quartz sand was run through the TEMA bowl between each sample run to avoid contamination.

Appendix B

Thin Section Descriptions

GR13: primary mineralogy includes garnet (10-15%), plagioclase (40-50%), clinopyroxene (20-25%) and hornblende (<5%). Secondary alteration minerals are ilmenite, green amphibole, clinozoisite-epidote, and white mica. The texture is medium-grained granoblastic, with large garnets. Garnet fractures are filled with white mica and the garnet crystals have numerous inclusions of cpx. Plagioclase crystals are obscured by alteration to clinozoisite and epidote. Clinopyroxene is altered to green amphibole pseudomorphs. Several cpx-pseudomorphs occur as large optically continuous grains 2-5 mm in diameter.

GR21: primary mineralogy includes garnet (30%), plagioclase (30%), clinopyroxene (20%), and hornblende (10%). Secondary alteration minerals are white mica (muscovite), ilmenite, and green amphibole. Texturally medium grained with layering formed by garnet-rich layers alternating with plagioclase-rich layers. Some high-pressure grain boundaries visible. Garnet fractures filled with white mica. Garnets contain numerous inclusions of cpx and are rimmed by cpx and green amphibole. Plagioclase grains are altered to very fine-grained clinozoisite. Clinopyroxene is pseudomorphed by green amphibole, although relic cpx is preserved in center of many pseudomorphs. Hornblende occurs as small fragments altered to green amphibole. Ilmenite common throughout section.

GR45: primary mineralogy includes garnet (10%), plagioclase (30-40%), hornblende (30%), clinopyroxene (20%), and oxides (<5%). Secondary, alteration minerals are clinozoisite-epidote and green amphibole. Hornblende defines the

foliation. Plagioclase highly altered to epidote and clinozoisite and clinopyroxene is pseudomorphed by green amphibole.

MR34: primary mineralogy includes plagioclase(40-50%), clinopyroxene (25-30%), and oxides (<1%). Secondary alteration minerals of biotite (15-20%), amphibole, clinozoisite, chlorite(?). Displays medium-grained relic gabbroic texture of interlocking plagioclase grains. Plagioclase is highly altered to clinozoisite; clinopyroxene forms centers of amphibole and chlorite pseudomorphs. Biotite is fine grained and occurs in the intergranular spaces.

MR37: primary mineralogy includes plagioclase (40-50%), orthopyroxene (10%), clinopyroxene (20-25%). Secondary alteration minerals of biotite (10%), clinozoisite, green amphibole, oxides (<5%). Displays a medium-grained relic gabbroic texture defined by interlocking grains of plagioclase with large porphyroblasts of pseudomorphic orthopyroxene rimmed by clinopyroxene and green amphibole. Orthopyroxene grains are large, 1-4 mm in diameter in some cases and altered to various degrees to clinopyroxene and amphibole. Plagioclase altered to clinozoisite, but relic texture well preserved.

MR38: primary mineralogy includes plagioclase (45-55%), clinopyroxene (25-35%) and orthopyroxene (<2%). Secondary alteration minerals of green amphibole, clinozoisite, and chlorite(?). Displays a medium-grained relic gabbroic texture defined by interlocking grains of plagioclase with pseudomorphic opx rimmed by cpx. Green amphibole commonly occurs as porphyroblasts. Plagioclase altered to clinozoisite. Orthopyroxene preserved as fragments within the center of poryphyroblasts. Clinopyroxene is pseudomorphed by green amphibole and chlorite rimmed?

MR39: primary mineralogy includes plagioclase (40-50%), clinopyroxene (30-40%), orthopyroxene (2-5%) and oxides (<2%). Secondary alteration minerals of biotite, clinozoisite and green amphibole. Displays a medium-grained relic gabbroic texture of interlocking plagioclase grains. Plagioclase is altered to clinozoisite. Clinopyroxene pseudomorphed by green amphibole. Orthopyroxene occurs as fragments within center of cpx-green amphibole pseudomorphs. Biotite occurs as fine-grained intergranular growths.

MR40: primary mineralogy includes plagioclase (40-50%), clinopyroxene (20-25%), orthopyroxene (10-25%), and oxides (<2%). Secondary minerals of hornblende, clinozoisite, and ilmenite. Displays a medium- to fine-grained relic gabbroic texture of interlocking plagioclase grains. Plagioclase grains are altered to clinozoisite, opx occurs as fragments in center of pseudomorphic grains. Cpx is rimmed by green amphibole. Oxides are common and may be secondary.

MR50: Primary mineralogy includes garnet (30%), clinopyroxene (25-30%), and plagioclase (20-25%). Secondary alteration mineralogy of clinozoisite, rutile, and oxides. Displays a coarse texture with garnets up to 2 cm in diameter. Plagioclase is altered to clinozoisite, cpx occurs as large crystals relatively unaltered. No hornblende in section.

MR57: primary mineralogy includes plagioclase (30%), hornblende (30%), garnet (20%), clinopyroxene (10-15%), and oxides (5%). Secondary alteration mineralogy of clinozoisite-epidote, green amphibole, and chlorite(?). Medium-grained texture with no foliation observed. Plagioclase altered to epidote. Hornblende occurs as subhedral grains that are unaltered. Garnet altered along fractures to chlorite? Clinopyroxene occurs as fragments altered to green amphibole.

MR58: Primary mineralogy of clinopyroxene (40%), plagioclase (20-30%), and hornblende (10-15%). Secondary alteration mineralogy of hornblende, green amphibole, clinozoisite, white mica, and oxides. Medium-grained rock with no distinct foliation. Plagioclase is altered to clinozoisite and white mica. Clinopyroxene is altered to green amphibole and rimmed by hornblende. Amphibole occurs as two types, green amphibole and brown hornblende. Several of the hornblende crystals are unaltered and euhedral. Most, however are altered to green amphibole and white mica.

MR60: Primary mineralogy includes plagioclase (40-45%), garnet (15-20%), hornblende (10-15%), clinopyroxene (10%) and oxides. Secondary alteration mineralogy of ilmenite, clinozoisite, green amphibole, and white mica. Plagioclase is altered to clinozoisite. Garnets have numerous inclusions of cpx with fractures filled with white mica. Clinopyroxene has relic intergrowths of orthopyroxene, defined by secondary oxides occurring along lamellae. Clinopyroxene commonly is rimmed by green amphibole. Hornblende associated with clinopyroxene and may be secondary.

MR66: Primary mineralogy includes clinopyroxene (45-50%), plagioclase (20-25%), and garnet (20-25%). Secondary alteration minerals of epidote-clinozoisite and rutile. Displays coarse-grained texture of large grains of clinopyroxene and garnet. Clinopyroxene abundant and unaltered. Clinopyroxene with orthopyroxene intergrowths is common. Plagioclase is altered to clinozoisite and epidote.

MR86: Primary mineralogy includes plagioclase (40-50%), clinopyroxene (20-25%), and orthopyroxene (5-10%). Secondary alteration mineralogy of green amphibole, clinozoisite, and chlorite(?). Displays a medium-grained relic gabbroic texture defined by interlocking plagioclase grains. Plagioclase altered to clinozoisite.

Clinopyroxene pseudomorphed by green amphibole. Orthopyroxene occurs as fragments in the center of altered grains. One large opx grain 3-5mm in diameter was observed.

MT14: Primary mineralogy includes hornblende (35-40%), plagioclase (20-25%), and clinopyroxene (5-10%). Secondary alteration mineralogy of biotite and oxides. Displays a medium-grained granoblastic texture with fine-grained alteration minerals and abundant oxides. Oxides are widespread and give the section a "peppered" texture. Plagioclase is unaltered and subhedral. Clinopyroxene occurs as anhedral grains pseudomorphed by biotite and hornblende. Hornblende crystals are covered with oxides and altered to biotite along the edges.

MT20: Primary mineralogy includes clinopyroxene (30-35%); plagioclase (20-25%); and garnet (10-15%). Secondary mineralogy of hornblende (10%); and clinozoisite. Displays a medium to coarse grained texture with subhedral to anhedral plagioclase and clinopyroxene and triple junction grain boundaries. Clinopyroxene and plagioclase altered to hornblende and clinozoisite. Garnets are completely disseminated and altered to dark black fine-grained material, only tiny garnet fragments remain in the center of the pseudomorph. Hornblende occurs as subhedral secondary alteration crystals which are in some cases being altered to clinozoisite and other fine grained alteration minerals.

MT22: Primary mineralogy includes hornblende (45-50%), plagioclase (20-25%), and clinopyroxene (<2%). Secondary alteration minerals of biotite and oxides. Displays a medium-grained foliated texture, defined by layers of plagioclase and biotite with the long axis parallel to the foliation direction. Abundant oxides create a "peppered" texture only occurring in samples from the Mitten Rock Diatreme. Plagioclase is unaltered and subhedral. Hornblende is almost completely rimmed by

oxides and commonly altered to biotite along the grain boundaries. Clinopyroxene is rare and occurs as fragments in the center of highly altered grains.

MT24: Primary mineralogy includes plagioclase (?) and hornblende (?). Secondary minerals include biotite and oxides. Primary mineralogy completely pseudomorphed by alteration products, some triple junctions preserved. Hornblende is altered to a "peppered" appearance by oxides, crystals are pseudomorphed and some crystal shapes are preserved. Hornblende is dark in crossed-polars no interference colors are observed, only grain boundaries can be distinguished. Biotite occurs as thin laths.

MT28: Primary mineralogy includes plagioclase (40%), and clinopyroxene (40%). Secondary alteration minerals of biotite and oxides are abundant. Displays a medium-grained relic gabbroic texture quite a bit less distinct than other samples with a relic gabbroic texture. Abundant oxides cover the entire section and create a "peppered" texture common to the sections from the Mitten Rock Diatreme. Plagioclase altered to clinozoisite. Clinopyroxene occurs as fine-grained and well-rounded fragments surrounded by biotite laths. Difficult to estimate modal proportions of minerals due to severe alteration.

RM41: Primary mineralogy includes plagioclase (40-45%); clinopyroxene (30-35%); and hornblende (10-15%). Secondary mineralogy of biotite (2%) and oxides (2%). Medium to coarse grained, which plagioclase and clinopyroxene occurring as subhedral grains. Plagioclase appears to display a relic cumulate texture. No triple junctions observed. Clinopyroxene and plagioclase are in various degrees of alteration to hornblende and biotite. Hornblende occurs as large crystals surrounding clinopyroxene and plagioclase grains.

RM42: Primary texture hornblende (50-60%), plagioclase (40%), and cpx (?). Secondary alteration minerals of clinozoisite. Displays a medium-grained texture with well-developed foliation defined by elongate hornblende and plagioclase crystals aligned parallel to the foliation direction. Plagioclase grains altered to clinozoisite, but well preserved and unaltered in portions of the section. Amphibole occurs as two types, a green amphibole and a brown hornblende. Hornblende crystals are slightly altered along their rims to green amphibole. Clinopyroxene grains are completely altered to green amphibole and only a relic crystal structure is preserved. Most of the alteration occurs in close proximity to a clinozoisite vein that runs through the section.

RM43: Primary mineralogy includes clinopyroxene (40-50%), plagioclase (25-30%), oxides (5-10%), and orthopyroxene (<5%). Secondary alteration mineralogy of clinozoisite and green amphibole. Displays a medium- grained relic gabbroic texture defined by interlocking grains of plagioclase. Oxides are abundant and occur as euhedral to subhedral octahedrons (magnetite?) and appear to be primary. Some of the oxides have inclusions. Plagioclase altered to clinozoisite. Clinopyroxene slightly altered to green amphibole. Orthopyroxene occurs as fragments in the center of altered crystals.

RM46: Primary mineralogy includes hornblende (30-40%), clinopyroxene (10%) and plagioclase(?). Secondary alteration minerals of white mica, clinozoisite, and epidote. Displays a medium-grained and highly altered texture. Hard to discern primary mineralogy due to complete alteration of most minerals. If primary plagioclase was present, relic crystal shapes and twinning are not preserved in the alteration mineralogy. Hornblende crystals are altered to white mica and clinozoisite. Clinopyroxene occurs as anhedral grains highly altered to green amphibole. The secondary mineralogy obscures the primary minerals and texture almost completely.

RM47: Primary mineralogy includes plagioclase (40%), clinopyroxene (30%), and garnet (20%). Alteration mineralogy includes ilmenite, epidote, clinozoisite, hornblende, biotite, and green amphibole. Displays a medium-grained granoblastic texture with some triple junctions preserved. Plagioclase is altered to clinozoisite and epidote. Clinopyroxene is rimmed by hornblende and green amphibole, and commonly occurs with intergrowths of orthopyroxene preserved. Ilmenite is common throughout the section and biotite occurs as small laths.

RM49: Primary mineralogy includes plagioclase (?), clinopyroxene (?), and hornblende (?). Alteration mineralogy includes biotite, clinozoisite and oxides. Displays a medium-grained texture defined by the relic crystal shapes of the primary mineralogy; a few triple junctions along the grain boundaries are preserved. Alteration mineralogy very fine grained and pervasive. Plagioclase completely altered to clinozoisite. Clinopyroxene and hornblende completely altered to green amphibole. Biotite flakes very large and unaltered. Oxides are common and are slightly altered along boundaries. One large hornblende crystal is unaltered in the section.

RM53: Primary mineralogy includes plagioclase (40-50%), garnet (20-25%), hornblende (15-20%), and clinopyroxene. Alteration mineralogy includes clinozoisite, epidote, ilmenite, and biotite. Displays a medium-grained texture with no foliation. Plagioclase is altered to clinozoisite and epidote. Garnet is altered along fractures and grain boundaries to white mica. Garnets commonly have cpx inclusions. Clinopyroxene is partially pseudomorphed by green amphibole.

RM60: Primary mineralogy includes plagioclase (30-40%), garnet (25-30%), clinopyroxene (5-10%), and hornblende (5-10%). Alteration mineralogy includes ilmenite, white mica, and green amphibole. Displays a medium-grained granoblastic

texture. Garnets are fractured parallel to layering defined by garnet-rich layers alternating with plagioclase-rich layers. Plagioclase is altered to clinozoisite. Garnets are large and inclusion rich. Garnet crystals are altered along fractures and rimmed with white mica. Clinopyroxene is partially pseudomorphed by green amphibole. Brown hornblende occurs as small anhedral grains and is altered to a green amphibole along the rims. Ilmenite is common throughout the thin section.

RM62: Primary mineralogy includes hornblende (90%) and plagioclase (?). Alteration mineralogy includes clinozoisite, muscovite, and white mica. Displays a medium-grained texture with no foliation. Hornblende dominates and appears to occurs in two types: an early well-developed brown amphibole that is highly altered to a secondary green amphibole. If there was plagioclase it is completely altered to clinozoisite and neither the relic crystal shape nor twining are preserved.

TH34: Primary mineralogy includes hornblende (35-40%), clinopyroxene (25-30%), plagioclase (20%), and biotite (10%). Alteration minerals include biotite. Displays a medium-grained texture with triple junction grain boundaries and a slight foliation defined by biotite grains. Hornblende occurs in subhedral to euhedral crystals with biotite alteration along the grain boundaries. Hornblende is common around clinopyroxene grains. Plagioclase occurs as unaltered subhedral fragments. Clinopyroxene occurs in the center of hornblende grains and is generally unaltered. A fine-grained alteration produces dark rims along all of the grain boundaries which is a common alteration that occurs in all of the samples collected from the Thumb minette. Aside from grain boundaries, most crystals are unaltered.

TH38: Primary mineralogy includes plagioclase (25-30%); clinopyroxene (25-30%); garnet (20-25%); and hornblende (10-15%). Displays a medium to coarse grained texture with triple junctions along the majority of grain boundaries. Garnets are fractured and fragments are surrounded by fine-grained dark black alteration material. The garnets are not visible in hand sample and appear as dark black areas. Clinopyroxene and plagioclase are altered primary along their grain boundaries. Hornblende relatively fresh and appears in areas where the clinopyroxene and plagioclase alteration is the greatest.

TH39: Primary mineralogy includes plagioclase (30-40%), clinopyroxene (20-30%) and garnet (10-20%). Displays a medium-grained texture with intergranular cracks filled with very fine-grained alteration product common to all Thumb sections investigated. Clinopyroxene occurs as large grains well preserved and rimmed by fine-grained alteration. Plagioclase occurs as subhedral grains that are unaltered. Secondary alteration is minimal, but fine-grained alteration occur along all crystal boundaries.

TH41: Primary mineralogy includes plagioclase (35-40%); clinopyroxene (30-35%); and garnet (?). Medium grained texture made up of subhedral plagioclase, clinopyroxene, and garnets, with some triple junctions preserved. Garnets are completely altered to dark black fine grained material, with very few tiny fragments remaining to in the center of dark material. Clinopyroxene and plagioclase are fractured with dark fine grained material within the voids. Clinopyroxene and plagioclase show dissolution along grain boundaries.

TH46: Primary mineralogy includes plagioclase (25-30%), hornblende (15-20%), garnet (20%), and clinopyroxene (10-15%). Alteration minerals include white mica and ilmenite. Displays a medium-grained texture with foliation defined by hornblende

crystals. Plagioclase is unaltered and occurs as subhedral grains. Clinopyroxene is unaltered and in contact with hornblende. Hornblende is unaltered and appears to be primary. Garnet is altered along fractures and rimmed by white mica. Interstitial oxides are abundant. Dark alteration product occurs along all grain boundaries and is similar to alteration found in all of the sections from the Thumb minette.

Appendix C

Analytical Methods

C.1 X-Ray Flourescence

Major elements and trace elements including As, Ba, Cr, Cu, Ga, Mo, Nb, Ni, Pb, Rb, Sr, Th, U, V, Y, Zn, and Zr were determined by X-ray flourescence (XRF) at New Mexico Institute of Mining and Technology. The samples were analyzed by an automated Philips PW2400 XRF spectrometer and associated software. The fused disks were prepared following methods described by Hallett and Kyle (1993) and analyzed for major elements (SiO_2, TiO_2, Al_2O_3, Fe_2O_3-T, MgO, MnO, CaO, Na_2O, K_2O, and P_2O_5) in oxide weight percent. Pressed powder pellets were prepared using 7 grams of sample, mixed with seven drops of polyvinyl achohol and pressed with a boric acid backing to 10 tons of pressure under a hydraulic press.

A discussion of the precision and detection limits for both the INAA and XRF analysis is contained within Hallett and Kyle (1993). Calculated lower limits of detection (LLD) at a 2 sigma confidience interval are listed in Table C.1 for XRF analysis.

Table C.1: Lower Limits of Dection (LLD) for XRF analysis; Lower Detection Limit determined using BIR-1 as the standard.

Trace Element	LLD (ppm)
As	4
Ba	10
Cr	3
Cu	4
Ga	1
Mo	2
Nb	2
Ni	2
Pb	2
Rb	1
Sr	1
Th	3
U	2
V	6
Y	2
Zn	4
Zr	2

C.2 Instrumental Neutron Activation Analysis

Trace elements including Sc, Cr, Co, Zn, As, Br, Rb, Sb, Cs, Ba, La, Ce, Nd, Sm, Eu, Tb, Yb, Lu, Hf, Ta, W, Th and U were analyzed by Instrumental Neutron Activation Analysis (INAA) at New Mexico Institute of Mining and Technology's INAA Lab. Approximately 80 mg of each sample powder was sealed in ultrapure suprasil glass vials and irradiated at the research reactor facility University of Missouri for 30 hours at a flux of 2.4×10^{13} n $\cdot$ $cm^{-2} \cdot sec^{-1}$.

Analysis procedures followed Hallett and Kyle (1993). Two counts were conducted one 6 to 12 days after irradiation and a second 35-45 days after irradiation. Samples were counted using two high-purity Ge detectors (resolution 1.85 keV @ 1332 keV, efficiency 25%) and associated Nuclear Data 9900 system which included a VAXstation computer. Data were reduced using TEABAGS (Trace Element Analysis By Automated Gamma-ray Spectrometry) software.

Table C.2.a: BCR Standard run for Neutron Activation Analysis for this run and mean for previous runs compared to accepted values for BCR from the literature.

Element	This Run (ppm)	Mean (n=26) (ppm)	Standard Deviation	Accepted Values* (ppm)
Na2O	3.27	3.30	0.02	3.27
FeO	12.03	12.08	0.11	12.08
Sc	32.05	32.03	0.2	32.60
Cr	10.9	11.0	0.46	16.00
Co	36.95	37.23	0.21	37.00
Zn	134	132	4.83	130.0
As	ND	0.32	0.42	0.7
Br	ND	0.05	0.08	0.072
Rb	48.8	48.5	0.8	47.0
Sb	0.56	0.58	0.03	0.62
Cs	0.95	0.96	0.02	0.96
Ba	656	674	18	681.0
La	24.69	25.35	0.32	24.90
Ce	52.85	53.27	0.45	53.70
Nd	28.7	26.64	0.94	28.8
Sm	6.675	6.77	0.08	6.59
Eu	1.94	1.94	0.02	1.95
Tb	1.03	1.05	0.02	1.05
Yb	3.3	3.33	0.03	3.38
Lu	0.487	0.48	0.01	0.510
Hf	5.29	5.16	0.07	4.95
Ta	0.747	0.748	0.01	0.81
W	ND	0.31	0.5	0.40
Th	5.68	5.69	0.05	5.98
U	1.6	1.66	0.08	1.75

* accepted values from Govindaraju, (1994).

Table C.2.b: G-2 Standard results for this run with mean from previous runs by Neutron Activation Analysis comapred with accepted values for G-2 from the literature

Element	This Run (ppm)	Mean (n=26) (ppm)	Standard Deviation	Accepted Values* (ppm)
FeO	2.35	2.37	0.03	2.4
Sc	3.33	3.32	0.03	3.5
Cr	7.79	7.67	0.39	8.7
Co	4.36	4.40	0.06	4.6
Zn	81.0	80.56	4.85	86
As	ND	ND	--	ND
Rb	168.5	168.11	2.19	170
Sb	0.05	0.05	0.01	0.07
Cs	1.32	1.34	0.02	1.34
Ba	1832.5	1861.58	34.75	1882
La	88.56	88.56	1.21	89.0
Ce	163.3	163.77	1.82	160.0
Nd	55.35	54.2	2.0	55.0
Sm	7.29	7.33	0.09	7.20
Eu	1.308	1.33	0.02	1.4
Tb	0.466	0.46	0.01	0.48
Yb	0.711	0.74	0.02	0.8
Lu	0.101	0.1	0.00	0.110
Hf	8.795	8.5	0.22	7.90
Ta	0.788	0.78	0.01	0.88
Th	23.680	23.73	0.29	24.70
U	1.925	2.09	0.19	2.07

* accepted values from Govindaraju, (1994).

Appendix D:

Chemical Analyses

Table D.1: Major Element Analyses in Wt % (XRF)

Sample	Type	Group	SiO2	TiO2	Al2O3	Fe2O3	MgO	CaO	Na2O	K2O	MnO	P2O5	LOI	Total	Mg#
MR34	G	I	50.70	0.27	20.33	7.88	4.89	10.45	2.11	1.10	0.12	0.11	1.60	99.56	38.29
MR37	G	I	51.19	0.26	19.44	7.87	6.00	7.33	3.84	1.78	0.14	0.10	2.08	100.03	43.26
MR38	G	I	50.60	0.31	19.09	8.53	6.27	8.43	3.04	1.89	0.13	0.12	2.41	100.82	42.36
MR39	G	I	49.24	0.22	22.25	6.74	4.85	12.11	2.02	0.81	0.11	0.08	1.33	99.76	41.85
MR40	G	I	48.55	0.30	17.21	8.48	9.42	8.52	3.47	1.28	0.18	0.08	1.85	99.34	52.63
MR71	G	I	51.71	0.34	16.02	9.68	6.70	7.39	3.55	2.31	0.17	0.13	1.54	99.54	40.90
MR85	G	I	48.08	0.42	17.86	8.29	8.27	11.05	3.19	0.68	0.13	0.18	2.11	100.26	49.94
MR86	G	I	47.68	0.23	20.62	7.57	6.52	9.78	2.35	1.75	0.13	0.09	2.87	99.59	46.27
GR21	AM	II	45.75	0.77	18.22	12.03	6.06	11.96	2.12	0.29	0.20	0.15	1.36	98.91	33.50
MR50	GG	II	48.79	0.83	13.97	13.39	9.45	9.87	2.93	0.15	0.22	0.04	0.45	100.09	41.37
MR66	GG	II	48.69	0.81	14.09	13.15	9.09	9.71	2.87	0.12	0.21	0.04	0.48	99.26	40.87
RM56	GG	II	48.70	0.65	18.25	11.32	7.14	11.52	2.26	0.50	0.13	0.02	1.15	101.64	38.68
RM58	AM	II	46.16	0.51	15.80	10.56	8.66	11.38	2.67	1.32	0.18	0.03	1.91	99.18	45.06
RM46	AM	III	44.65	0.26	20.86	7.94	6.67	13.69	1.40	0.84	0.14	0.01	2.89	99.35	45.65
RM51	AM	III	45.50	0.27	21.15	6.80	7.48	15.44	1.17	0.73	0.11	0.02	1.01	99.68	52.38
RM62	AM	III	44.94	0.31	17.52	9.24	9.87	12.86	0.66	1.65	0.16	0.04	2.33	99.58	51.65
GR41	AM	IV	52.89	1.07	16.25	9.20	5.13	6.79	3.94	2.18	0.17	0.39	0.83	98.84	35.80
RM49	PG	IV	45.35	0.95	19.32	10.66	7.67	6.84	2.76	1.16	0.23	0.71	3.61	99.26	41.84
RM59	AM	IV	54.76	1.24	15.22	9.56	4.35	5.37	3.03	2.70	0.16	0.64	0.85	97.88	31.27
SR25	AM	IV	53.48	1.62	14.52	8.67	5.29	5.81	3.76	3.86	0.15	1.08	0.93	99.17	37.89
TH39	GG	IV	46.30	1.74	12.42	12.73	9.08	9.78	1.79	1.68	0.20	0.43	2.32	98.47	41.63
MR57	GG	V	50.04	0.74	18.33	10.03	5.91	9.41	3.51	0.25	0.16	0.08	1.87	100.33	37.08
RM53	GG	V	49.03	0.57	19.06	8.93	5.11	10.56	3.67	0.45	0.14	0.07	1.12	98.71	36.40
GR45	GG	VI	45.99	1.11	14.75	13.60	7.60	12.68	1.75	0.26	0.21	0.06	1.62	99.63	35.85
MT14	PG	VI	49.37	0.85	13.88	12.65	8.63	9.41	3.18	2.13	0.23	0.09	0.90	101.32	40.55
GR13	GG	VII	47.65	0.74	18.16	10.19	6.23	9.14	2.65	0.11	0.15	0.11	2.52	97.65	37.94
MR46	GG	VII	47.09	1.46	15.61	15.69	6.18	8.49	2.81	0.87	0.24	0.23	0.48	99.15	28.26
MR52	GG	VII	55.42	0.69	15.41	11.11	4.05	6.52	3.05	1.50	0.15	0.17	1.27	99.34	26.72
RM60	GG	VII	49.23	0.82	19.25	10.95	4.02	8.29	3.72	1.30	0.21	0.16	1.23	99.18	26.85
TH44	GG	VII	45.54	1.70	13.37	13.67	7.41	10.28	2.54	0.56	0.13	0.18	4.34	99.72	35.15
MR45	GG	VIII	54.42	0.18	20.29	6.13	3.16	7.54	5.29	0.89	0.12	0.01	1.15	99.18	34.02
MR54	GG	VIII	54.97	0.17	20.30	6.12	3.36	7.57	5.32	0.85	0.11	0.01	1.14	99.92	35.44

* Lithologic Rock Type; GG=garnet granulite; AM=amphibolite; G=Gabbro; PG=Pyroxene granulite; GROUP = Geochemical groups defined in text ;
Mg# = 100[MgO/(MgO+Fe total)]

Table D.1 Cont'd. Major Element Analyses in Wt % (XRF)

Sample	Type	Group	SiO2	TiO2	Al2O3	Fe2O3	MgO	CaO	Na2O	K2O	MnO	P2O5	LOI	Total	Mg#
GR11	GG	UG	45.17	2.37	13.04	18.72	7.70	9.16	2.73	0.47	0.33	0.83	0.63	101.15	29.14
GR23	GG	UG	51.37	0.71	20.11	7.77	3.43	10.81	3.87	0.45	0.07	0.08	1.45	100.12	30.63
GR26	GG	UG	48.79	1.74	14.79	13.94	6.46	6.10	3.17	1.32	0.17	0.26	1.99	98.73	31.67
GR46	AM	UG	48.45	0.72	12.97	14.18	9.81	9.75	3.20	0.25	0.24	0.13	0.58	100.28	40.89
MR44	GG	UG	50.68	0.76	19.00	10.84	8.97	7.59	3.39	1.02	0.16	0.08	1.68	104.17	45.28
MR49	AM	UG	45.74	0.52	18.80	8.83	9.35	9.69	2.87	0.91	0.10	0.06	2.51	99.38	51.43
MR51	GG	UG	44.40	0.22	23.50	7.32	5.17	9.48	2.97	0.84	0.14	0.05	1.78	95.87	41.39
MR53	GG	UG	51.91	0.71	17.22	10.71	4.89	7.23	3.65	0.91	0.17	0.17	1.38	98.95	31.35
MR55	GG	UG	46.88	1.64	12.92	16.26	6.76	11.16	1.97	0.15	0.24	0.15	0.90	99.03	29.37
MR58	GG	UG	49.75	0.35	19.84	7.33	6.66	9.96	3.71	0.58	0.11	0.03	1.78	100.10	47.61
MR59	GG	UG	50.71	0.88	17.50	10.54	4.62	8.37	4.68	0.91	0.17	0.22	0.90	99.50	30.47
MR60	GG	UG	48.95	0.74	17.89	11.95	6.67	8.30	2.89	0.86	0.20	0.12	1.39	99.96	35.82
MR61	GG	UG	49.12	1.55	14.23	14.73	7.25	10.95	2.58	0.16	0.20	0.16	0.84	101.77	32.98
MR63	GG	UG	51.36	0.98	16.69	12.21	4.81	8.61	3.26	0.93	0.23	0.21	0.93	100.22	28.26
MR64	GG	UG	44.27	1.27	22.22	11.14	4.77	11.08	1.60	1.11	0.56	0.18	0.57	98.77	29.98
MR78	PG	UG	46.58	1.21	15.40	13.80	6.68	8.74	2.70	1.20	0.16	0.10	1.93	98.50	32.62
MR81	AM	UG	50.85	0.69	18.59	8.49	5.68	8.33	4.36	1.34	0.12	0.15	0.78	99.38	40.08
MR83	PG	UG	48.15	2.51	14.35	14.84	5.59	8.71	2.68	0.34	0.18	0.21	1.81	99.37	27.36
MT13	PG	UG	47.36	1.71	13.01	15.15	5.83	8.05	3.36	2.80	0.23	0.19	0.88	98.57	27.79
MT15	PG	UG	49.50	1.04	12.79	13.30	6.75	9.09	3.54	2.37	0.21	0.11	0.55	99.25	33.67
MT20	GG	UG	44.03	1.77	13.55	13.41	9.23	9.92	2.19	1.67	0.16	0.43	1.37	97.73	40.77
MT22	PG	UG	49.13	0.55	16.09	9.48	8.22	8.59	3.72	2.16	0.22	0.05	0.60	98.81	46.44
MT24	AM	UG	45.87	1.72	14.07	15.69	6.86	8.43	3.11	1.96	0.21	0.06	1.35	99.33	30.42
MT27	PG	UG	48.60	2.16	10.46	8.69	9.27	8.73	2.27	5.20	0.13	0.85	1.89	98.25	51.61
MT28	AM	UG	46.06	0.43	8.87	15.26	10.81	9.76	1.50	4.37	0.18	0.06	1.68	98.98	41.47
RM36	AM	UG	47.27	0.29	17.31	8.79	9.24	10.90	1.68	1.10	0.15	0.09	2.15	98.97	51.25
RM41	AM	UG	48.91	0.65	16.09	8.57	8.73	11.91	2.09	0.73	0.14	0.13	2.05	100.00	50.46
RM42	AM	UG	45.86	0.77	14.13	12.64	10.72	11.57	2.05	0.22	0.21	0.15	1.66	99.98	45.89
RM43	AM	UG	51.55	2.33	13.01	15.23	4.34	5.20	3.13	0.88	0.25	0.45	2.71	99.08	22.18
RM44	PG	UG	54.17	0.32	18.80	5.94	4.44	7.55	4.81	0.81	0.08	0.08	1.93	98.93	42.77
RM47	GG	UG	48.39	1.11	15.96	11.27	7.51	11.95	2.88	0.23	0.16	0.14	1.00	100.60	39.99
RM48	AM	UG	48.01	0.98	14.14	12.18	8.12	9.67	2.32	0.19	0.19	0.18	3.28	99.26	40.00
RM54	AM	UG	51.15	0.71	15.51	9.79	5.61	12.33	2.04	0.47	0.16	0.20	1.26	99.23	36.43
RM57	AM	UG	49.15	0.93	13.59	12.86	7.93	10.07	1.64	1.14	0.19	0.07	1.76	99.33	38.14
RM64	PG	UG	49.49	0.95	14.86	11.56	8.37	6.70	3.98	0.28	0.18	0.14	2.98	99.49	42.00
SR22	AM	UG	48.69	0.86	14.18	11.49	7.22	10.43	3.37	1.09	0.20	0.09	0.83	98.45	38.59
TH34	AM	UG	46.20	0.83	15.65	8.08	9.39	10.03	2.90	2.56	0.10	0.35	2.49	98.58	53.75
TH37	GG	UG	47.21	0.63	14.69	9.78	9.16	11.52	2.37	0.79	0.15	0.13	3.16	99.59	48.36
TH38	GG	UG	46.84	1.22	14.81	11.65	8.77	10.75	2.12	0.96	0.17	0.19	1.75	99.23	42.95
TH41	GG	UG	46.62	0.72	16.70	11.89	6.78	10.03	2.63	0.54	0.13	0.14	2.55	98.73	36.31
TH46	GG	UG	45.82	1.29	13.92	13.84	7.25	10.32	2.40	1.01	0.14	0.12	4.84	100.95	34.38

* Lithologic Rock Type; GG=garnet granulite; AM=amphibolite; G=Gabbro; PG=Pyroxene granulite; GROUP = Geochemical groups defined in text ;
Mg# = 100[MgO/(MgO+Fe total)]

Table D.2. Trace Element Analyses in ppm (XRF)

Sample	TYPE*	GROUP	V(6)**	Ni (2)	Cu (4)	Zn (4)	Ga (1)	As (4)	Rb (1)	Sr (1)	Y (2)	Zr (2)
MR34	G	I	170	24	125	62	13	ND	15	559	10	30
MR37	G	I	150	33	31	66	11	ND	45	347	10	29
MR38	G	I	169	29	102	67	12	ND	36	354	13	33
MR39	G	I	122	31	35	49	13	ND	12	434	9	25
MR40	G	I	137	88	59	61	11	ND	28	207	10	21
MR71	G	I	201	26	147	76	12	ND	50	331	15	34
MR85	G	I	112	99	7	86	15	ND	4	422	11	26
MR86	G	I	128	46	60	58	12	ND	30	464	10	24
GR21	AM	II	310	42	ND	79	17	ND	1	563	14	22
MR50	GG	II	243	218	97	116	16	ND	2	253	16	20
MR66	GG	II	238	222	119	113	17	ND	ND	280	18	18
RM56	GG	II	463	69	ND	73	18	ND	2	624	7	21
RM58	AM	II	263	146	ND	135	13	ND	14	197	15	16
RM46	AM	III	240	47	8	74	14	ND	18	449	5	8
RM51	AM	III	212	61	48	51	12	ND	7	601	6	7
RM62	AM	III	174	92	ND	87	10	ND	78	247	5	7
GR41	AM	IV	166	67	12	111	18	ND	87	813	34	144
RM49	PG	IV	144	144	ND	183	21	ND	23	1045	29	99
RM59	AM	IV	192	52	ND	131	20	ND	97	1058	47	234
SR25	AM	IV	145	101	31	134	21	8	190	1213	36	272
TH39	GG	IV	305	184	104	128	17	6	44	588	41	172
MR57	GG	V	224	46	ND	90	17	ND	ND	329	16	39
RM53	GG	V	210	40	8	76	18	ND	4	317	12	44
GR45	GG	VI	337	80	76	103	17	7	ND	221	28	46
MT14	PG	VI	260	80	43	135	16	7	66	407	33	51
GR13	GG	VII	285	36	ND	98	21	ND	ND	534	12	29
MR46	GG	VII	207	52	ND	332	29	ND	6	178	64	103
MR52	GG	VII	256	22	13	98	16	ND	37	288	21	64
RM60	GG	VII	215	34	32	87	20	ND	6	493	25	64
TH44	GG	VII	375	184	91	125	21	6	12	316	31	118
MR45	GG	VIII	127	27	ND	41	20	ND	3	614	10	11
MR54	GG	VIII	123	29	ND	41	21	ND	4	619	9	10

**(#) Lower Dection Limit(ppm); * Lithologic Rock Type; GG=garnet granulite; PG=pyroxene-granulite; AM= amphibolite; G=Gabbro; NA (Not Analyzed) ; ND (Not Detected)

Table D.2. Cont'd Trace element analyses in ppm (XRF)

Sample	TYPE*	GROUP	Nb (2)	Mo (2)	Ba (7)	Pb (2)	Th (2)	U (2)	Sr/Y	V/Ti	Ti/Zr
MR34	G	I	ND	6	455	5	ND	ND	57	0.10	55
MR37	G	I	ND	5	355	4	ND	ND	34	0.10	54
MR38	G	I	ND	5	570	4	ND	ND	28	0.09	56
MR39	G	I	ND	4	387	4	ND	ND	48	0.09	52
MR40	G	I	ND	5	1094	4	ND	ND	21	0.08	86
MR71	G	I	ND	0	891	5	ND	ND	22	0.10	60
MR85	G	I	ND	3	162	5	ND	ND	38	0.04	95
MR86	G	I	ND	ND	839	5	ND	ND	45	0.09	58
GR21	AM	II	ND	13	228	4	ND	ND	39	0.07	215
MR50	GG	II	ND	12	105	5	ND	ND	16	0.05	249
MR66	GG	II	ND	14	91	4	ND	ND	15	0.05	273
RM56	GG	II	ND	17	196	5	ND	ND	96	0.12	185
RM58	AM	II	ND	7	202	7	ND	ND	13	0.09	191
RM46	AM	III	ND	4	267	7	ND	ND	93	0.15	208
RM51	AM	III	ND	6	165	7	ND	ND	109	0.13	228
RM62	AM	III	ND	2	617	15	ND	ND	49	0.09	270
GR41	AM	IV	4	4	795	21	3	ND	24	0.03	44
RM49	PG	IV	3	1	344	12	3	ND	36	0.03	58
RM59	AM	IV	9	11	1835	16	7	ND	23	0.03	32
SR25	AM	IV	26	10	1352	21	14	6	34	0.01	36
TH39	GG	IV	18	13	872	16	20	3	14	0.03	61
MR57	GG	V	ND	6	105	3	ND	ND	20	0.05	114
RM53	GG	V	ND	10	156	5	ND	ND	26	0.06	78
GR45	GG	VI	ND	6	61	5	ND	ND	8	0.05	144
MT14	PG	VI	6	11	545	23	4	2	12	0.05	101
GR13	GG	VII	4	7	79	6	ND	ND	43	0.06	152
MR46	GG	VII	16	5	173	6	ND	ND	3	0.02	85
MR52	GG	VII	ND	11	637	12	ND	ND	14	0.06	65
RM60	GG	VII	4	16	547	7	ND	ND	19	0.04	77
TH44	GG	VII	7	4	327	10	5	ND	10	0.04	87
MR45	GG	VIII	ND	11	262	5	ND	ND	62	0.12	96
MR54	GG	VIII	ND	12	269	4	ND	ND	70	0.12	106

(#) Lower Dection Limit(ppm); * Lithologic Rock Type; GG=garnet granulite; PG=pyroxene-granulite; AM= amphibolite; G=Gabbro; NA (Not Analyzed) ; ND (Not Detected)

Table D.2. Trace element analyses in ppm (XRF) Cont'd

Sample	TYPE*	GROUP	V (6)	Ni (2)	Cu (4)	Zn (4)	Ga (1)	As (4)	Rb (1)	Sr (1)	Y (2)	Zr (2)
GR11	GG	UG	243	33	78	248	25	ND	4	278	69	114
GR23	GG	UG	251	22	ND	22	17	ND	1	337	14	36
GR26	GG	UG	336	36	80	155	22	ND	15	279	38	151
GR46	AM	UG	254	41	ND	130	11	ND	3	228	23	45
MR44	GG	UG	245	69	ND	113	15	ND	9	274	11	31
MR49	AM	UG	135	176	ND	90	15	ND	10	356	10	23
MR51	GG	UG	92	24	ND	49	17	ND	12	729	8	33
MR53	GG	UG	211	23	19	124	19	ND	3	408	37	81
MR55	GG	UG	375	47	35	155	19	ND	ND	169	38	80
MR58	GG	UG	116	42	ND	70	18	ND	8	656	8	112
MR59	GG	UG	210	25	20	129	22	ND	2	708	19	53
MR60	GG	UG	271	37	21	127	19	ND	4	227	16	49
MR61	GG	UG	385	42	73	152	20	ND	ND	190	30	72
MR63	GG	UG	169	19	21	141	19	ND	3	274	23	86
MR64	GG	UG	137	57	ND	181	29	ND	69	224	29	132
MR78	PG	UG	334	63	65	99	19	ND	26	907	17	42
MR81	AM	UG	190	83	ND	84	20	ND	11	888	20	92
MR83	PG	UG	343	56	109	122	22	ND	2	348	36	158
MT13	PG	UG	303	58	87	143	19	17	99	583	43	139
MT15	PG	UG	294	48	30	139	17	10	73	471	33	76
MT20	GG	UG	232	277	92	134	16	5	56	758	30	105
MT22	PG	UG	187	108	22	157	14	8	127	368	23	35
MT24	AM	UG	530	81	266	151	20	23	77	681	51	71
MT27	PG	UG	174	247	42	105	19	4	137	1275	27	410
MT28	AM	UG	288	144	35	227	15	5	133	433	30	90
RM36	AM	UG	203	105	123	58	13	ND	23	285	9	17
RM41	AM	UG	167	126	121	72	14	5	12	1614	17	36
RM42	AM	UG	256	88	96	95	14	ND	4	519	16	40
RM43	AM	UG	211	22	3	164	21	11	16	307	54	184
RM44	PG	UG	80	47	25	60	18	ND	ND	946	7	38
RM47	GG	UG	284	83	18	100	17	ND	ND	262	21	76
RM48	AM	UG	251	106	105	102	16	18	4	363	24	72
RM54	AM	UG	250	61	273	79	14	ND	9	296	25	49
RM57	AM	UG	283	75	213	101	15	ND	47	509	24	53
RM64	PG	UG	237	90	145	107	13	ND	5	454	21	46
SR22	AM	UG	266	53	105	116	17	ND	18	175	23	52
TH34	AM	UG	306	207	32	146	15	ND	73	487	18	85
TH37	GG	UG	293	108	10	172	14	ND	11	255	13	34
TH38	GG	UG	237	122	77	104	17	9	17	369	33	112
TH41	GG	UG	314	30	95	108	16	ND	6	364	25	54
TH46	GG	UG	349	172	103	213	22	27	20	232	37	74

(#) Lower Dection Limit(ppm); * Lithologic Rock Type; GG=garnet granulite; PG=pyroxene-granulite; AM= amphibolite; G=Gabbro; NA (Not Analyzed) ; ND (Not Detected)

Table D.2. Trace element analyses in ppm (XRF) Cont'd

Sample	TYPE*	GROUP	Nb (2)	Mo (2)	Ba (7)	Pb (2)	Th (2)	U (2)	Sr/Y	V/Ti	Ti/Zr
GR11	GG	UG	13	8	97	7	ND	ND	4	0.02	125
GR23	GG	UG	ND	7	94	5	ND	ND	25	0.06	118
GR26	GG	UG	5	ND	483	7	ND	ND	7	0.03	69
GR46	AM	UG	ND	ND	173	6	ND	ND	10	0.06	96
MR44	GG	UG	ND	19	320	8	ND	ND	26	0.05	145
MR49	AM	UG	ND	ND	267	5	ND	ND	36	0.04	136
MR51	GG	UG	ND	12	485	4	ND	ND	97	0.07	40
MR53	GG	UG	5	14	419	8	ND	ND	11	0.05	52
MR55	GG	UG	ND	13	77	3	ND	ND	5	0.04	123
MR58	GG	UG	ND	7	360	5	ND	ND	78	0.06	19
MR59	GG	UG	3	3	360	9	ND	ND	37	0.04	99
MR60	GG	UG	3	14	410	6	ND	ND	14	0.06	91
MR61	GG	UG	3	6	132	3	ND	ND	6	0.04	128
MR63	GG	UG	3	8	466	7	ND	ND	12	0.03	68
MR64	GG	UG	3	18	914	10	ND	ND	8	0.02	58
MR78	PG	UG	ND	3	468	6	ND	ND	54	0.05	173
MR81	AM	UG	ND	4	348	11	ND	ND	46	0.05	45
MR83	PG	UG	5	4	193	4	ND	ND	10	0.02	95
MT13	PG	UG	5	6	845	23	4	8	14	0.03	74
MT15	PG	UG	5	8	1059	16	2	3	14	0.05	82
MT20	GG	UG	10	7	1003	31	4	ND	25	0.02	101
MT22	PG	UG	4	4	352	35	ND	5	16	0.06	94
MT24	AM	UG	8	5	589	36	2	3	13	0.05	146
MT27	PG	UG	58	5	2191	25	41	5	47	0.01	32
MT28	AM	UG	ND	6	1628	33	5	2	14	0.11	29
RM36	AM	UG	ND	3	476	7	ND	ND	31	0.12	100
RM41	AM	UG	ND	5	454	8	ND	ND	97	0.04	110
RM42	AM	UG	ND	6	102	8	ND	ND	32	0.06	114
RM43	AM	UG	9	6	221	8	3	2	6	0.02	76
RM44	PG	UG	ND	4	611	6	2	ND	130	0.04	50
RM47	GG	UG	ND	19	131	8	ND	ND	13	0.04	88
RM48	AM	UG	2	3	184	7	ND	ND	15	0.04	82
RM54	AM	UG	ND	9	368	6	3	2	12	0.06	87
RM57	AM	UG	ND	6	305	8	ND	ND	21	0.05	106
RM64	PG	UG	ND	0	165	2	ND	ND	22	0.04	125
SR22	AM	UG	ND	5	282	7	ND	ND	8	0.05	98
TH34	AM	UG	8	4	1143	15	9	2	27	0.06	59
TH37	GG	UG	ND	6	418	6	ND	ND	20	0.08	112
TH38	GG	UG	8	5	1019	6	6	ND	11	0.03	65
TH41	GG	UG	3	4	350	7	4	ND	15	0.07	80
TH46	GG	UG	7	3	373	22	2	2	6	0.05	105

(#) Lower Dection Limit(ppm); * Lithologic Rock Type; GG=garnet granulite; PG=pyroxene-granulite; AM= amphibolite; G =Gabbro; NA (Not Analyzed) ; ND (Not Detected)

Table D.3. Trace element analysis in ppm (INAA)

	Group I					*Group II*	
Element	**MR34**	**MR38**	**MR39**	**MR85**	**MR86**	**MR50**	**RM58**
Na2O (wt%)	2.135	2.739	1.865	2.783	2.32	2.886	2.323
Sc	29.31	33.1	25.2	25.33	29.84	25.13	45.8
Cr	22.3	22.9	16.9	162.8	64.5	NA	382
FeO(T)(wt%)	7.14	7.95	6.15	7.28	6.83	12.44	9.73
Co	28.39	32	28.41	35.4	35	48.6	47.4
Zn	80	75	67	71	54.3	97	134
As	0.78	1.23	0.46	0.78	0.75	1.99	ND
Br	ND	ND	ND	ND	ND	0.58	ND
Rb	15	37	8	4	29.8	7	12.3
Sb	0.16	0.211	ND	0.023	0.129	0.144	ND
Cs	0.47	0.54	0.28	ND	0.75	0.13	0.14
Ba	382	606	368	136	799	102	228
La	5.91	6.99	4.36	6.45	5.11	0.93	2.41
Ce	13.3	15.6	10.6	15.7	11.2	2.6	4.39
Nd	ND	7.7	ND	6.9	ND	4	4.2
Sm	1.64	1.934	1.251	2.094	1.401	1.562	1.162
Eu	0.5	0.581	0.43	0.794	0.453	0.801	0.567
Tb	0.215	0.299	0.224	0.329	0.251	0.402	0.375
Yb	1.08	1.14	0.77	0.86	0.83	1.39	1.37
Lu	0.129	0.209	0.111	0.137	0.151	0.193	0.206
Hf	0.88	1.07	0.68	0.65	0.64	0.83	0.57
Ta	0.081	0.13	0.083	0.05	0.067	0.02	0.045
W	ND	ND	ND	ND	ND	1.4	0.2
Th	0.91	0.99	0.74	0.12	0.7	ND	0.21
U	0.54	0.63	0.49	ND	0.52	ND	0.35
[Sm]N	9.06	10.69	6.91	11.57	7.74	8.63	6.42
[Eu]N	7.25	8.42	6.23	11.51	6.57	11.61	8.22
***[Gd]N**	5.73	7.55	5.39	8.26	6.03	8.56	7.41
Eu/Eu*	1.01	0.94	1.02	1.18	0.96	1.35	1.19
Th/Yb	0.84	0.87	0.96	0.14	0.84		0.15
Ta/Th	0.09	0.13	0.11	0.42	0.10		0.21
Ta/Yb	0.08	0.11	0.11	0.06	0.08	0.01	0.03
La/Yb	5.47	6.13	5.66	7.50	6.16	0.67	1.76

Normalization values after Haskin et al. (1968) for composite chondrite

[Gd]N estimated by the following relation: Gd={[(Sm/0.181)((Tb/0.047)^2)]^0.333}

Wt% (weight percent); NA (Not Analyzed); ND (Not dectected)

Table D.3. Trace element analyses in ppm (INAA) Cont'd

	Group III		*Group IV*				
Element	**RM51**	**RM62**	**GR41**	**RM49**	**RM59**	**SR25**	**TH39**
Na2O (wt%)	1.269	0.721	3.61	2.82	3.15	3.66	1.869
Sc	37.1	34.2	20.5	22.31	20.86	13.45	41.7
Cr	100.9	141.2	26.7	48.2	25.1	119.2	229.9
FeO(T)(wt%)	3.22	8.47	8.4	9.93	8.98	7.71	12.08
Co	36.2	45.4	34.9	42.5	28.43	26.08	48
Zn	47	83	95	150	110	116	132
As	0.35	0.52	ND	1.1	1.6	7.4	5.2
Br	ND	0.13	0.29	ND	0.11	ND	ND
Rb	9	68	85	23	93	188	43
Sb	0.023	0.12	0.016	ND	0.038	0.36	0.06
Cs	ND	1.07	2.83	0.5	2.13	5.16	1.35
Ba	121	509	767	386	1780	1450	1037
La	1.729	1.15	49	46.6	73.6	78.3	57.9
Ce	3.8	2.3	108.6	110.4	169.7	180.9	117.4
Nd	2.4	ND	54	48	81	85	55.2
Sm	0.819	0.409	8.88	10.07	14.45	15.07	12.07
Eu	0.398	0.29	2.33	2.33	3.2	3.7	2.81
Tb	0.164	0.21	0.88	1.05	1.47	1.22	1.35
Yb	0.54	0.25	2.98	2.25	4.27	3.32	3.73
Lu	0.067	0.032	0.423	0.311	0.597	0.476	0.529
Hf	0.23	0.2	4.03	2.96	5.93	6.42	4.86
Ta	ND	ND	0.3	0.42	0.72	1.73	1.22
W	ND	0.69	1.1	ND	1	1.1	1.3
Th	0.28	0.13	3.54	2.41	5.11	10.14	16.14
U	0.14	0.13	2.25	0.81	3.41	9.9	3.87
[Sm]N	4.52	2.26	49.06	55.64	79.83	83.26	66.69
[Eu]N	5.77	4.20	33.77	33.77	46.38	53.62	40.72
***[Gd]N**	3.80	3.56	25.73	30.18	42.58	38.14	37.90
Eu/Eu*	1.39	1.48	0.95	0.82	0.80	0.95	0.81
Th/Yb	0.52	0.52	1.19	1.07	1.20	3.05	4.33
Ta/Th			0.08	0.17	0.14	0.17	0.08
Ta/Yb			0.10	0.19	0.17	0.52	0.33
La/Yb	3.20	4.60	16.44	20.71	17.24	23.58	15.52

Normalization values after Haskin et al. (1968) for composite chondrite

[Gd]N estimated by the following relation: Gd={[(Sm/0.181)((Tb/0.047)^2)]^0.333}

Wt% (weight percent); NA (Not Analyzed); ND (Not dectected)

Table D.3. Trace element analyses in ppm (INAA) cont'd

	Group V		*Group VI*		*Group VII*		
Element	**MR57**	**RM53**	**GR45**	**MT14**	**GR13**	**MR46**	**MR52**
Na2O (wt%)	3.56	3.77	1.754	3.18	2.77	2.871	2.967
Sc	32.7	28.44	55.8	46.6	27.3	44.3	28.78
Cr	NA	NA	314	259.8	NA	NA	13.4
FeO(T)(wt%)	9.23	8.28	12.77	11.48	9.6	14.51	10.27
Co	39.3	34.2	53.2	45.3	36.2	45.1	29.89
Zn	82	73	90	144	109	335	94
As	1.4	1.2	11.2	7.8	ND	ND	ND
Br	ND	ND	0.43	0.13	ND	ND	ND
Rb	ND	4	ND	71	ND	ND	37
Sb	ND	0.026	0.12	0.7	ND	ND	ND
Cs	ND	ND	0.1	9.75	0.1	ND	0.94
Ba	102	137	68	644	138	254	652
La	3.36	3.94	3.57	6.23	10.1	21.95	9.68
Ce	9.3	10.6	10.4	14.7	24.3	71.8	23.4
Nd	8.6	7.8	ND	ND	12.5	52.1	11.4
Sm	2.091	1.851	2.495	2.9	2.94	16.06	3.12
Eu	0.773	0.694	0.898	1.015	0.966	2.92	0.89
Tb	0.467	0.313	0.686	0.74	0.421	2.5	0.559
Yb	1.67	1.15	2.96	3.56	1.06	5.03	2.32
Lu	0.235	0.159	0.452	0.594	0.124	0.727	0.363
Hf	1.38	1.38	1.61	1.5	0.99	3.6	1.94
Ta	0.06	0.102	ND	0.31	0.26	0.62	0.3
W	2.2	1.4	0.24	ND	0.8	1.8	0.3
Th	ND	0.33	0.27	1.47	ND	0.5	1.42
U	ND	0.15	0.31	1.84	0.28	0.22	0.93
[Sm]N	11.55	10.23	13.78	16.02	16.24	88.73	17.24
[Eu]N	11.20	10.06	13.01	14.71	14.00	42.32	12.90
***[Gd]N**	10.42	7.67	14.28	15.79	10.90	62.82	13.42
Eu/Eu*	1.02	1.14	0.93	0.92	1.05	0.57	0.85
Th/Yb		0.29	0.09	0.41		0.10	0.61
Ta/Th		0.31		0.21		1.24	0.21
Ta/Yb	0.04	0.09		0.09	0.25	0.12	0.13
La/Yb	2.01	3.43	1.21	1.75	9.53	4.36	4.17

Normalization values after Haskin et al. (1968) for composite chondrite

[Gd]N estimated by the following relation: Gd={[(Sm/0.181)((Tb/0.047)^2)]^0.333}

Wt% (weight percent); NA (Not Analyzed); ND (Not detected)

Table D.3. Trace element analyses in ppm (INAA) cont'd

			Group VIII	
Element	**RM60**	**TH44**	**MR45**	**MR54**
Na2O (wt%)	3.72	2.73	5.4	5.29
Sc	27.5	55.2	20.94	19.99
Cr	NA	106.6	NA	NA
FeO(T)(wt%)	10.21	12.6	5.62	5.66
Co	27.69	48	16.95	16.98
Zn	81	128	37	44
As	2.5	7.4	ND	ND
Br	0.02	ND	0.16	ND
Rb	7.4	11	4	3
Sb	0.041	0.36	0.106	0.028
Cs	0.36	0.57	0.34	0.11
Ba	533	286	232	255
La	11.24	12.89	2.51	2.62
Ce	27	29.8	4	3.8
Nd	17.6	23.8	2.1	2.1
Sm	4.85	5.84	0.529	0.457
Eu	1.308	1.61	0.401	0.4
Tb	0.861	0.94	0.154	0.173
Yb	1.93	3.05	1.26	1.3
Lu	0.255	0.429	0.208	0.215
Hf	1.82	2.97	0.31	0.3
Ta	0.154	0.47	ND	ND
W	1.2	ND	ND	ND
Th	ND	1.34	ND	ND
U	ND	1.53	ND	ND
[Sm]N	26.80	32.27	2.92	2.52
[Eu]N	18.96	23.33	5.81	5.80
***[Gd]N**	20.73	23.38	3.15	3.24
Eu/Eu*	0.80	0.85	1.92	2.03
Th/Yb		0.44		
Ta/Th		0.35		
Ta/Yb	0.08	0.15		
La/Yb	5.82	4.23	1.99	2.02

Normalization values after Haskin et al. (1968) for composite chondrite
[Gd]N estimated by the following relation: Gd={[(Sm/0.181)((Tb/0.047)^2)]^0.333}
Wt% (weight percent); NA (Not Analyzed); ND (Not dectected)

Table D.4. CIPW Norm

	MR34	MR37	MR38	MR39	MR40	MR71	MR85	MR86	GR21	MR50	MR66
GP	I	I	I	I	I	I	I	I	II	II	II
%AN	70.54	48.46	56.09	74.24	52.91	41.09	59.01	67.10	68.68	49.73	50.93
Q	2.90	0.00	0.00	0.62	0.00	0.00	0.00	0.00	0.00	0.00	0.00
or	6.68	10.81	11.43	4.89	7.81	14.04	4.12	10.76	1.77	0.90	0.73
ab	18.34	33.38	26.32	17.45	25.38	30.90	23.09	20.68	18.58	25.16	24.86
an	43.92	31.39	33.62	50.30	28.51	21.56	33.23	42.18	40.74	24.89	25.81
lc	0.00	0.00	0.00	0.00	0.00	0.00	0.00	0.00	0.00	0.00	0.00
ne	0.00	0.00	0.00	0.00	2.68	0.00	2.49	0.00	0.00	0.00	0.00
kal	0.00	0.00	0.00	0.00	0.00	0.00	0.00	0.00	0.00	0.00	0.00
C	0.00	0.00	0.00	0.00	0.00	0.00	0.00	0.00	0.00	0.00	0.00
di	7.03	4.31	6.81	8.54	11.76	12.48	17.54	6.22	16.22	20.03	18.97
hy	17.71	2.90	7.66	15.04	0.00	3.09	0.00	2.67	6.23	8.24	11.69
ol	0.00	13.85	10.59	0.00	20.39	14.21	15.43	14.22	11.18	15.66	12.85
mt	2.64	2.62	2.69	2.55	2.70	2.74	2.85	2.61	3.41	3.43	3.43
il	0.53	0.51	0.60	0.43	0.59	0.66	0.82	0.45	1.51	1.60	1.57
hem	0.00	0.00	0.00	0.00	0.00	0.00	0.00	0.00	0.00	0.00	0.00
ap	0.26	0.24	0.28	0.19	0.19	0.31	0.43	0.22	0.36	0.09	0.09
ru	0.00	0.00	0.00	0.00	0.00	0.00	0.00	0.00	0.00	0.00	0.00
Total	100.00	100.00	100.00	100.00	100.00	100.00	100.00	100.00	100.00	100.00	100.00

* values expressed in wt% ** CIPW Norms calculated using IGPET computer program

Table D.4. CIPW Norm Cont'd

	RM56	RM58	RM46	RM51	RM62	GR41	RM49	RM59	SR25	TH39	MR57
GP	II	II	III	III	III	IV	IV	IV	IV	IV	V
%AN	66.63	69.08	82.71	87.97	87.74	37.75	55.64	43.77	26.28	57.97	53.02
Q	0.00	0.00	0.00	0.00	0.00	0.00	0.00	8.15	0.00	0.00	0.00
or	2.97	8.09	5.18	4.39	10.10	13.23	7.23	16.56	23.35	10.43	1.51
ab	19.21	12.64	10.50	7.01	5.79	34.25	24.63	26.61	32.57	15.91	30.41
an	38.34	28.24	50.25	51.24	41.42	20.77	30.89	20.71	11.61	21.95	34.32
lc	0.00	0.00	0.00	0.00	0.00	0.00	0.00	0.00	0.00	0.00	0.00
ne	0.00	5.84	1.01	1.67	0.00	0.00	0.00	0.00	0.00	0.00	0.00
kal	0.00	0.00	0.00	0.00	0.00	0.00	0.00	0.00	0.00	0.00	0.00
C	0.00	0.00	0.00	0.00	0.00	0.00	2.94	0.00	0.00	0.00	0.00
di	15.48	24.45	16.66	21.39	19.69	9.12	0.00	2.12	8.54	21.06	10.57
hy	10.68	0.00	0.00	0.00	0.46	14.50	15.85	17.74	13.29	12.29	12.84
ol	8.91	16.63	13.21	11.11	19.11	1.29	11.08	0.00	0.29	8.91	5.40
mt	3.13	3.02	2.66	2.61	2.72	3.83	3.75	4.12	4.63	4.93	3.32
il	1.24	1.00	0.52	0.52	0.61	2.09	1.90	2.44	3.15	3.47	1.44
hem	0.00	0.00	0.00	0.00	0.00	0.00	0.00	0.00	0.00	0.00	0.00
ap	0.05	0.07	0.02	0.05	0.10	0.93	1.73	1.54	2.56	1.05	0.19
ru	0.00	0.00	0.00	0.00	0.00	0.00	0.00	0.00	0.00	0.00	0.00
Total	100.00	100.00	100.00	100.00	100.00	100.00	100.00	100.00	100.00	100.00	100.00

* values expressed in wt% ** CIPW Norms calculated using IGPET computer program

Table D.4. CIPW Norm cont'd

	RM53	GR45	MT14	GR13	MR46	MR52	RM60	TH44	MR45	MR54	GR11
GP	V	VI	VI	VII	VII	VII	VII	VII	VIII	VIII	UG
%AN	53.13	68.11	47.96	62.48	53.55	48.11	50.40	52.15	39.31	39.18	48.71
Q	0.00	0.00	0.00	0.12	0.00	8.74	0.00	0.00	0.00	0.00	0.00
or	2.74	1.59	12.67	0.69	5.28	9.12	7.91	3.51	5.39	5.11	2.80
ab	31.14	15.28	18.90	23.77	24.41	26.56	32.42	22.78	45.87	45.78	23.33
an	35.30	32.63	17.42	39.58	28.15	24.62	32.95	24.84	29.71	29.49	22.15
lc	0.00	0.00	0.00	0.00	0.00	0.00	0.00	0.00	0.00	0.00	0.00
ne	0.49	0.00	4.43	0.00	0.00	0.00	0.00	0.00	0.00	0.00	0.00
kal	0.00	0.00	0.00	0.00	0.00	0.00	0.00	0.00	0.00	0.00	0.00
C	0.00	0.00	0.00	0.00	0.00	0.00	0.00	0.00	0.00	0.00	0.00
di	14.96	26.15	23.64	6.31	11.25	6.26	6.93	22.84	7.01	7.06	15.08
hy	0.00	8.34	0.00	24.33	11.38	19.68	2.32	6.56	5.03	6.21	8.82
ol	10.98	9.79	17.69	0.00	11.74	0.00	12.02	10.70	4.12	3.53	15.67
mt	3.10	3.90	3.43	3.44	4.41	3.27	3.46	4.92	2.50	2.46	5.67
il	1.12	2.18	1.62	1.49	2.85	1.35	1.60	3.42	0.35	0.33	4.55
hem	0.00	0.00	0.00	0.00	0.00	0.00	0.00	0.00	0.00	0.00	0.00
ap	0.17	0.14	0.21	0.27	0.55	0.41	0.38	0.44	0.02	0.02	1.94
ru	0.00	0.00	0.00	0.00	0.00	0.00	0.00	0.00	0.00	0.00	0.00
Total	100.00	100.00	100.00	100.00	100.00	100.00	100.00	100.00	100.00	100.00	100.00

* values expressed in wt% ** CIPW Norms calculated using IGPET computer program

Table D.4. CIPW Norm Cont'd

	GR23	GR26	GR46	MR44	MR49	MR51	MR53	MR55	MR58	MR59	MR60
GP	UG	UG	UG	UG	UG	UG	UG	UG	UG	UG	UG
%AN	52.49	45.32	42.83	53.96	66.12	68.95	47.48	60.90	54.05	39.68	57.66
Q	0.00	0.00	0.00	0.00	0.00	0.00	1.24	0.00	0.00	0.00	0.00
or	2.71	8.15	1.50	5.93	5.59	5.31	5.56	0.92	3.51	5.50	5.21
ab	33.38	28.04	27.49	28.23	19.03	22.49	31.93	17.22	31.11	37.40	25.06
an	36.87	23.24	20.60	33.08	37.15	49.94	28.86	26.82	36.59	24.60	34.12
lc	0.00	0.00	0.00	0.00	0.00	0.00	0.00	0.00	0.00	0.00	0.00
ne	0.00	0.00	0.00	0.00	3.37	2.37	0.00	0.00	0.54	1.68	0.00
kal	0.00	0.00	0.00	0.00	0.00	0.00	0.00	0.00	0.00	0.00	0.00
C	0.00	0.00	0.00	0.00	0.00	0.63	0.00	0.00	0.00	0.00	0.00
di	14.14	5.43	22.61	2.80	9.99	0.00	5.84	24.29	11.09	13.52	5.97
hy	7.70	23.38	0.26	7.61	0.00	0.00	21.45	21.78	0.00	0.00	15.93
ol	0.38	2.76	22.58	17.53	20.66	16.03	0.00	0.71	13.67	11.54	8.67
mt	3.27	4.91	3.27	3.22	3.04	2.67	3.31	4.70	2.74	3.53	3.33
il	1.37	3.45	1.39	1.42	1.03	0.45	1.39	3.22	0.68	1.71	1.44
hem	0.00	0.00	0.00	0.00	0.00	0.00	0.00	0.00	0.00	0.00	0.00
ap	0.19	0.63	0.31	0.18	0.14	0.12	0.41	0.36	0.07	0.52	0.28
ru	0.00	0.00	0.00	0.00	0.00	0.00	0.00	0.00	0.00	0.00	0.00
Total	100.00	100.00	100.00	100.00	100.00	100.00	100.00	100.00	100.00	100.00	100.00

* values expressed in wt% ** CIPW Norms calculated using IGPET computer program

Table D.4. CIPW Norm Cont'd

	MR61	MR63	MR64	MR78	MR81	MR83	MT13	MT15	MT20	MT22	MT24
GP	UG	UG	UG	UG	UG	UG	UG	UG	UG	UG	UG
%AN	55.09	50.52	78.75	53.57	44.93	53.53	39.32	36.46	61.10	50.71	50.84
Q	0.00	0.82	0.00	0.00	0.00	3.47	0.00	0.00	0.00	0.00	0.00
or	0.95	5.59	6.74	7.43	8.08	2.08	17.15	14.35	10.35	13.10	11.97
ab	21.88	28.06	13.91	23.93	34.03	23.51	19.43	21.44	14.83	20.77	18.64
an	26.84	28.65	51.53	27.61	27.76	27.08	12.59	12.30	23.30	21.37	19.27
lc	0.00	0.00	0.00	0.00	0.00	0.00	0.00	0.00	0.00	0.00	0.00
ne	0.00	0.00	0.00	0.00	1.97	0.00	5.44	5.01	2.50	6.24	4.64
kal	0.00	0.00	0.00	0.00	0.00	0.00	0.00	0.00	0.00	0.00	0.00
C	0.00	0.00	0.00	0.00	0.00	0.00	0.00	0.00	0.00	0.00	0.00
di	21.83	11.12	3.06	14.10	10.89	13.37	22.77	27.29	20.54	17.82	19.43
hy	17.34	19.72	7.45	5.30	0.00	19.03	0.00	0.00	0.00	0.00	0.00
ol	3.41	0.00	10.29	14.86	12.34	0.00	13.98	13.56	18.94	16.46	17.70
mt	4.43	3.66	4.13	4.12	3.24	6.03	4.82	3.77	4.97	3.05	4.83
il	2.95	1.89	2.48	2.41	1.34	4.94	3.37	2.02	3.53	1.07	3.38
hem	0.00	0.00	0.00	0.00	0.00	0.00	0.00	0.00	0.00	0.00	0.00
ap	0.37	0.49	0.43	0.24	0.35	0.50	0.46	0.26	1.04	0.12	0.14
ru	0.00	0.00	0.00	0.00	0.00	0.00	0.00	0.00	0.00	0.00	0.00
Total	100.00	100.00	100.01	100.00	100.00	100.00	100.00	100.00	100.00	100.00	100.00

* values expressed in wt% ** CIPW Norms calculated using IGPET computer program

Table D.4. CIPW Norm cont'd

	MT27	MT28	RM36	RM41	RM42	RM43	RM44	RM47	RM48	RM54	RM57
GP	UG	UG	UG	UG	UG	UG	UG	UG	UG	UG	UG
%AN	23.83	100.00	71.94	64.67	62.33	41.58	40.16	55.13	58.44	64.80	65.51
Q	0.00	0.00	0.00	0.00	0.00	9.35	0.37	0.00	0.00	5.00	0.67
or	32.06	16.06	6.76	4.43	1.34	5.46	4.96	1.38	1.18	2.86	6.98
ab	9.98	0.00	14.79	18.17	17.83	27.81	42.14	24.68	20.66	17.76	14.38
an	3.12	4.76	37.92	33.26	29.51	19.80	28.28	30.33	29.06	32.69	27.30
lc	0.00	8.51	0.00	0.00	0.00	0.00	0.00	0.00	0.00	0.00	0.00
ne	5.45	7.17	0.00	0.00	0.00	0.00	0.00	0.00	0.00	0.00	0.00
kal	0.00	0.00	0.00	0.00	0.00	0.00	0.00	0.00	0.00	0.00	0.00
C	0.00	0.00	0.00	0.00	0.00	0.00	0.00	0.00	0.00	0.00	0.00
di	28.48	37.12	14.30	21.36	23.12	3.50	8.04	23.40	16.46	23.63	19.62
hy	0.00	0.00	10.81	11.98	1.70	22.52	12.67	2.22	25.96	12.91	25.40
ol	9.04	22.49	11.93	6.01	21.27	0.00	0.00	11.70	0.49	0.00	0.00
mt	5.54	2.92	2.70	3.20	3.38	5.83	2.73	3.83	3.78	3.30	3.65
il	4.28	0.85	0.57	1.27	1.50	4.65	0.63	2.14	1.96	1.39	1.83
hem	0.00	0.00	0.00	0.00	0.00	0.00	0.00	0.00	0.00	0.00	0.00
ap	2.05	0.14	0.22	0.31	0.36	1.09	0.19	0.33	0.44	0.48	0.17
ru	0.00	0.00	0.00	0.00	0.00	0.00	0.00	0.00	0.00	0.00	0.00
Total	100.00	100.00	100.00	100.00	100.00	100.00	100.00	100.00	100.00	100.00	100.00

* values expressed in wt% ** CIPW Norms calculated using IGPET computer program

Table D.4. CIPW Norm cont'd

	RM64	SR22	TH34	TH37	TH38	TH41	TH46
GP	UG	UG	UG	UG	UG	UG	UG
%AN	39.36	45.70	68.99	57.48	61.00	59.11	54.40
Q	0.00	0.00	0.00	0.00	0.00	0.00	0.00
or	1.73	6.66	15.84	4.88	5.87	3.35	6.28
ab	35.23	25.00	10.41	20.96	18.57	23.37	21.38
an	22.86	21.04	23.17	28.34	29.05	33.79	25.50
lc	0.00	0.00	0.00	0.00	0.00	0.00	0.00
ne	0.00	2.43	8.28	0.00	0.00	0.00	0.00
kal	0.00	0.00	0.00	0.00	0.00	0.00	0.00
C	0.00	0.00	0.00	0.00	0.00	0.00	0.00
di	8.90	26.02	21.18	24.63	20.14	14.37	22.62
hy	13.44	0.00	0.00	0.38	7.26	7.45	1.71
ol	11.90	13.40	15.09	16.01	12.17	12.51	15.38
mt	3.72	3.54	3.54	3.23	4.08	3.38	4.26
il	1.89	1.69	1.65	1.25	2.40	1.44	2.58
hem	0.00	0.00	0.00	0.00	0.00	0.00	0.00
ap	0.34	0.22	0.85	0.31	0.46	0.34	0.29
ru	0.00	0.00	0.00	0.00	0.00	0.00	0.00
Total	100.00	100.00	100.00	100.00	100.00	100.00	100.00

* values expressed in wt%

** CIPW Norms calculated using IGPET computer program

Appendix E

Field Observations

The following section details the field observations on 33 volcanic necks and dikes located in the Navajo Volcanic Field (NVF) complied from field notes taken on three separate excursions to the NVF: 1) K.C. Condie, March 1990; 2) K.C. Condie, P.D. Mattie, & J. Selverstone, October 1994; 3) K.C. Condie, P.D. Mattie, & N. Latysh, June 1996. Figure E.1 shows the location of 42 known dikes and volcanic necks that occur in the NVF. The majority of the intrusions are of minette composition (35 of 42), which may in part be due to the fact that the serpentinized ultramafic breccia pipes are easily eroded and usually form topographic lows while the minette pipes are more resistant and generally form topographic highs.

Chino Valley:

Access roads are east and west of Chino Valley. Xenoliths are chiefly eclogite, pyroxenite, amphibolite with eclogite dominating. At three localities examined no felsic granulites or positive mafic granulites identified. Xenoliths are variably altered and most appear to have white deposits around grain boundaries. Xenoliths range in size from xenocryst of clinopyroxene and garnet to xenoliths up to one foot across. Large xenoliths are well rounded and suggestive of attrition in gas-fluid mixture. Good location for eclogite collection by not very good for other xenolith lithologies.

Church Rock

Located approximately 8 miles east of Kayenta, AZ on Highway 160. Church Rock has very few xenoliths. Mostly local sediments. Granitoid xenoliths are uncommon and extremely altered. No mafic or ultramafic xenolith lithologies were observed.

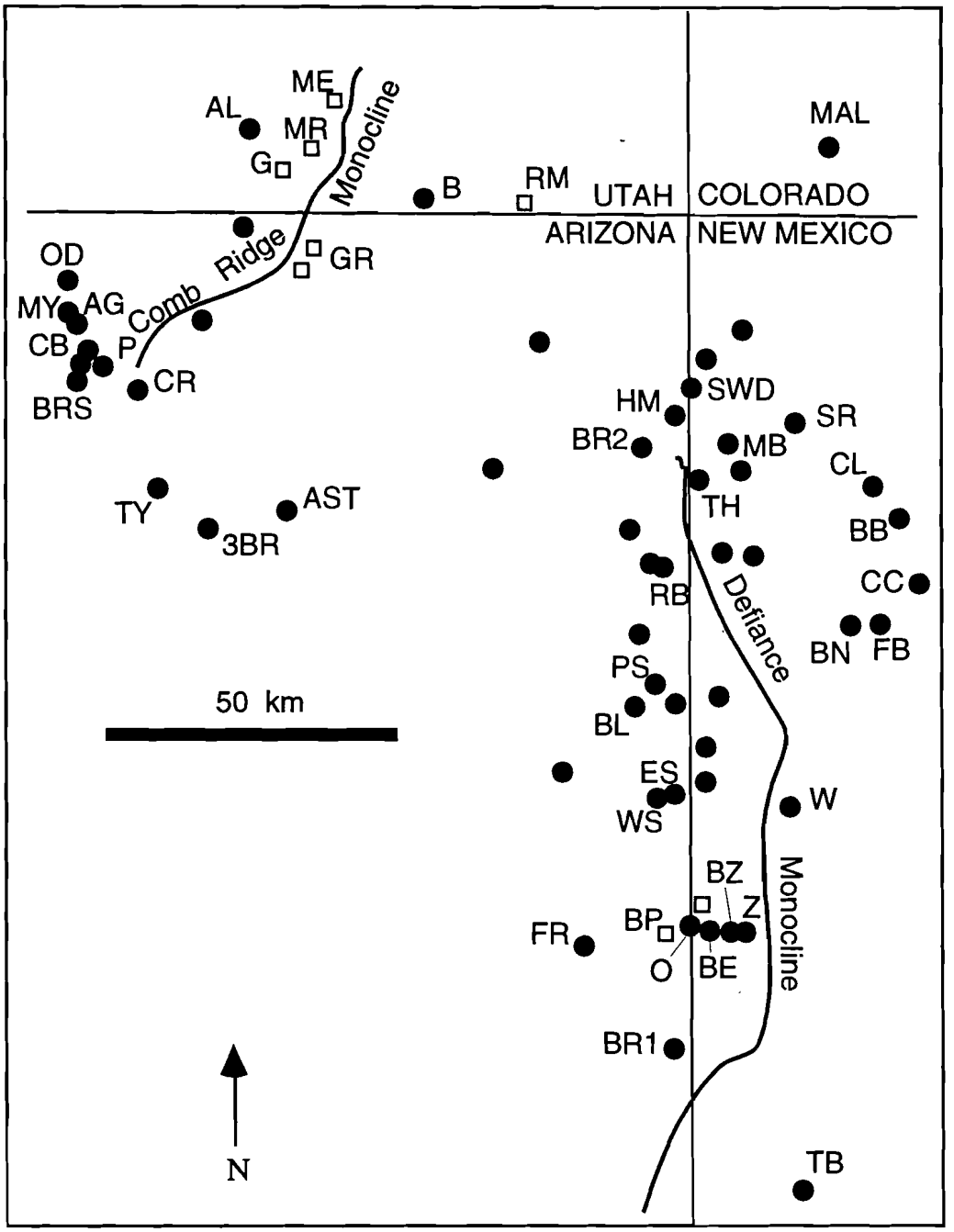

Figure E.1. Location Map for 42 Navajo Volcanic Field dikes and volcanic necks. Solid circles indicate minette and open boxes indicate serpentinized ultramafic breccia. ME=Mules Ear; AL= Alhambra Rock; MR=Moses Rock; G=Gypsum Wash; B=Boundary Butte; RM=Red Mesa; AG=Agathla Peak; P=Porras Dikes; CR=Church Rock; GR=Garnet Ridge; S=Shiprock; MB=Mitten Butte; TH=The Thumb; BN=Bennett Peak; PS=Psaile Butte (Tubby); BL=Black Pinnacle; ES=East Sonsella Butte; WS=West Sonsella Butte; BP=Buell Park; O=Outlet Peak; FR=Fluted Rock; BE=The Beast; BZ=Beczelbub; Z=Zilditloi Mtn.; B1=Black Rock I; TB=Twin Buttes; FB=Ford Butte; BB=Barber Peak; MAL=Malpais Butte; CC=Coal Creek Butte; B2=Black Rock II; HM=Horse Mesa Wash Butte; RB=Roof Butte; SWD=Salt Wash Complex; CL=Cathedral Cliff; CB=Chaistla Butte; BRS=Black Rock Standing; TY=Tyende Butte; 3BR=Three Black Rocks; AST=Ah Tse Toh; MY=Mystery Butte; OD=Ojeta Dike.

Agathla Peak

Minette diatreme located approx. 10 miles north of Kayenta, AZ along Highway 163. South side of neck yields abundant xenoliths. Local sedimentary xenoliths predominate, but may other lithologies can be found. Xenolith types recognized include granitoids, mafic garnet granulites, gneisses, greenschist, and lherzolites. Mafic garnet granulites are rare compared with other rock lithologies and are usually small in size ranging from 2 to 6 cm in diameter. Granitoid types are numerous ranging in size from 2 cm to 30 cm in diameter. Granitoid types include gneissic granitoids (some with disseminated garnets), fine grained pink granite, pegmatitic granitoids, and porphyroblastic granitoids with garnet porphyroblasts. Many of the xenoliths are partially altered. Notable observations include: 1) amphibolites and metasediments are missing from the xenolith population; 2) one sample resembled meta gabbro from Moses Rock; 3) garnet granitoids seem to be particularly abundant here and at Chiastla.

Moses Rock

Moses Rock is a serpentinized ultramafic breccia dike located along the Comb Ridge Monocline, just east of Cane Valley approx. 10 miles NW of Mexican Water, AZ. A wide variety of xenolith lithologies are represented here. Xenolith lithologies include metagabbro, amphibolites, mafic garnet granulites, metasediments (of various types including bio-gar-qtz schist, sill-qtz-feldspar schist and gneiss), granitoids of several types, garnet amphibolite, eclogite and various mantle xenoliths. Xenolith abundances vary along strike of the dike with mantle xenoliths apparently more abundant at the south end. Notable observations include: 1) mafic rocks greatly dominate the abundance of lower crustal lithologies, 2) metasediments being the next abundant lithologic type.

Garnet Ridge

Garnet Ridge is a series of serpentinized ultramafic breccia dikes cropping out along Garnet Ridge located along the Comb Ridge Monocline approx. 15 miles SW of Mexican Water, AZ. Xenoliths are abundant along garnet ridge with dominant lithologies varying along strike of Garnet Ridge. Xenolith types similar to those are Moses Rock and include granitoids, amphibolites, garnet amphibolites, mafic granulites, mafic garnet granulites, metasediments, and few ultramafics. Granitoids are huge, up to 3 meters across, and include biotite granodiorite, pegmatitic granted, gneissic granitoids with leucosomes, fine to medium grained pink granites and some leucogranites. Amphibolites are very common, and occur in several textural variants. Garnet Amphibolites appear to be more common here than at Moses Rock.

Boundary Butte

Besides local sedimentary xenoliths only one type of granitoid xenolith has bee found here. It appears to be granodiorite and fresh samples of this granitoid can be found here.

Black Pinnacle

Located near Navajo Community College. Xenoliths are few in number and all that have been found show some alteration. Only Granitoid xenoliths have been found in various states of alteration.

West Sonsella Butte

Xenoliths here are few in number and are very small in size. Only local sediments and granitoids have been found. The granitoids appear to be altered.

Outlet Peak and the Beast

Xenoliths are uncommon and chiefly local sediments. Granitoid xenoliths are small and highly altered.

Black Rock I

Xenoliths are more abundant here than at Outlet Peak and the Beast, but they are very small and highly altered.

Mitten Rock

Mitten rock is a minette diatreme located 10 miles SW of the Shiprock diatreme just east of Red Rock, AZ. Xenoliths are abundant and mafic xenoliths of a variety of types are particularly abundant. Xenolith types found here include mafic granulites, amphibolites, granitoid, and ultramafics. No metasedimentary xenoliths have been found here.

Shiprock

Shiprock is a minette diatreme located south west of Shiprock, NM. Lots of granitoid xenoliths have been found here of several textural types. Granitoid xenoliths can be very large, up to 1 meter across. Few mafic xenoliths were found. No metasedimentary xenoliths were found here.

Twin Buttes

Twin Buttes is located just west of Gallup, NM. Not xenoliths other that small fragments of local sediments were found.

Malpais Butte

Located about 14 km NNW of Shiprock, NM, just west of highway 666. Xenoliths are few and almost all very small fragments of Mesozoic red beds. Some very small xenoliths (<1cm across) could be crustal.

Barber Peak

Located along highway 666, about 22 km south of Shiprock, NM. Bedded tuff and breccia dominates fragments. Numerous small sandstone fragments. Few xenoliths most <3cm across and mostly comprised of Mesozoic sediments. A few granitoids have been found up to 10 cm across mostly undeformed. No mafic or deep seated crustal xenoliths have been found here.

Coal Creek Diatreme

Located 5.5 km SE of Barber Peak in the center of the Hogback monocline. Mixed dike and breccia material with only small sedimentary xenoliths. No granitoid or other crustal or mantle xenoliths have been found here.

Black Rock II

Located 8 km NW of Red Rock, AZ. Xenoliths are sparse. Granitoid xenoliths can be found especially on the SE side. Granitoids can be found as deformed or undeformed, some occur with garnets and reaction rims. Few ultramafic xenoliths were found occurring as small fragments <1cm across. No mafic granulites or metasediments were found.

Horse Mesa Wash Pinnacle

Located about 10 km north of Red Rock, AZ and 2 km west of Horse Mesa. Matrix is hard and black, looks magmatic and full of olivine and clinopyroxene xenocrysts. Only one granitoid xenolith was found. No other lithologies were found here.

Red Mesa Kimberlite

Located about 4 km north-northwest of Red Mesa on UT-AZ border. The serpentinized ultramafic breccia is eroded forming a crater about 75 meters in diameter. A large array of xenolith types can be found here including metasedimentary, mafic granulites, mafic amphibolites, local sedimentary fragments, fragments of underlying paradox limestones, granitoids of several types, cherts. Good location of a variety of crustal xenolith types, but no mantle xenoliths were observed here.

Roof Butte

Located about 15 km southwest of Red Rock, AZ. Roof Butte (with microwave tower on top) is capped with basalt flows resting on tuffaceous sediments. No xenoliths of any type were found here or neighboring unnamed butte 2 km NW of roof butte.

Salt Wash Diatreme

Located approximately 6 km northwest of Mitten Rock Diatreme. Consists of several diatremes connected by dikes. A few small <1 cm in diameter xenoliths of local country rock and granitoid. No other xenolith types were observed.

Cathedral Cliff

Located 19 km south of Shiprock along highway 666. Large diatreme easily accessible. Mostly small (< 3cm in diameter) xenoliths of sedimentary origin. A few granitoid xenoliths were found. No other lithologies were seen.

Ford Butte

Located along highway 666 south of Shiprock east of Bennett Peak. Large rafts of sandstone in diatreme, as well as small sandstone fragments and autoliths of minette are common. Granitoid xenoliths are rare and usually small (<3cm in diameter). Granitoid xenoliths are commonly altered and undeformed. No other xenolith types were found.

Three Black Rocks

Located along state highway 59 south of Kayenta, AZ. Xenoliths were few and small and most were altered. Granitoids are the dominant lithologic type and diorite xenoliths can be found. No other lithologic types were noted here.

Ah Tse Toh

Located north of highway 59 near county line. Very few xenoliths were found here and most were very small. Some interesting felsic garnet gneisses and granitoids were found and some mantle xenoliths. Most are altered to some degree. No other lithologic types were noted.

Chaistla Butte

Located north of Kayenta, AZ, along highway 163, just south of Agathala. Xenoliths are rare but can be found in an irregular distribution around the pipe. Deep crustal xenoliths are uncommon. Types found include granitoid, serpentine, greenschists, and possible blueschists. Granitoid ranged in size from 2 to 12 cm and types found include

disseminated garnet granite, gneissic garnet granitoid, and porphyroblastic garnet granitoids. Greenschist facies rocks most abundant around the north side and range from 2 to 8 cm in diameter. One possible metagabbro was found. No metasedimentary xenoliths were found here.

Black Rock Standing

Located on northeast side of Kayenta, AZ. Very few xenoliths were found here. All were very small and very altered. No metasedimentary fragments were found.

Tyende Butte *(Previously unnamed)

Located southeast of Kayenta along highway 59, approximately 6 miles north of Chilchinbito, AZ. Tyende Butte is a minette diatreme with a few associated xenoliths. Xenolith types found include granitoids, amphibolite, felsic volcanic and local sedimentary fragments. Granitoids are most common by still relatively rare and occur as fine leucogranite, diorite, coarse pegmatite, gneissic granite with disseminated garnets, and pink medium grained granite. Metasedimentary and mafic granulites were conspicuously absent.

Porras Dikes

Located northeast of Kayenta, AZ, just north of the Comb Ridge Monocline. Xenoliths here were uncommon and when found generally very small (<4 cm in diameter). Xenolith lithologies found include leucogranite, garnetiferous granitoids (disseminated garnet), garnet granites with large garnet porphyroblasts, some amphibolites and hornblendites, and a few mafic granulites. No metasedimentary xenoliths were found.

Mystery Butte* (previously unnamed)

Located north of Agathla along highway 163, just south of Monument Valley Navajo Tribal Park. Mystery Butte consists of mostly intersection dikes of what appear to be minette. Xenoliths are common but not abundant. Xenolith types encountered include garnet granitoids, diorite, and amphibolites. Granitoids are most abundant rock type. No metasedimentary xenoliths were observed.

Oljeta Dyke* (previously unnamed)

Located south of Oljeta, AZ, along Indian Route 6420, just NW of Horse Trail Canyon. Small minette? dike with mostly granitoid xenoliths. Xenolith population similar to Agathala and Chiastla. One possible mafic amphibolite was found. No metasedimentary xenoliths were found.

Alhambra Rock

Located southwest of Mexican Hat, AZ, along state highway 163. Many xenoliths found here. Xenolith types consist of mostly granitoid some as large as 1 meter in diameter, with few small amphibolite samples. Granitoids are variable with leucogranites, gneissic granitoids, garnetiferous granitoids, medium to fine grained pink granite, medium grained biotite granite, and diorite. No metasedimentary, mafic granulite, metagabbro, or mantle xenoliths were found.

Bennett Peak

Located south of Shiprock along highway 666. Xenoliths were rare and small. Most common xenolith types are granitoids that are altered. Some possible mafic and ultramafic fragments found, but very altered and very rare. No metasedimentary xenoliths were found.